P A I R S P E C T R O M E T E R M E A S U R E M E N T S

I N 5 0 0 M E V B R E M S S T R A H L U N G

Thesis by

Duane Herbert Cooper

In Partial Fulfillment of the Requirements

for the Degree of

Doctor of Philosophy

California Institute of Technology

Pasadena, California

1955

ABSTRACT

Experiments are described as performed with a twenty channel pair spectrometer. This instrument uses a 30 ton electromagnet to measure the energies of electron pairs produced by electromagnetic quanta, giving a measurement of the energies of the quanta. These electron pairs are detected by a V shaped array of scintillators located within the magnet gap. A novel network of coincidence circuits, due to Matthew L. Sands, results in a considerable reduction in electronics complexity. With this spectrometer the synchrotron energy was calibrated to better than half a percent. An intensity calibration was obtained with an accuracy of about three percent. The bremsstrahlung spectrum was seen to agree in shape with theoretical predictions to within three or four percent. Relative pair production measurements gave agreement with theory to about two percent for copper and lead relative to aluminum. Absorption measurements in carbon, aluminum, copper, tin, and lead gave agreement with theory within about one percent.

ACKNOWLEDGEMENTS

Work on the pair spectrometer was initiated by Robert L. Walker, and has continued under his supervision. The design and construction of the 30 ton spectrometer magnet was his responsibility. The author has had the benefit of Dr. Walker's close interest and participation during the developmental and experimental work.

The conception of the time delay multiplexing coincidence scheme is due to Matthew Sands. Many discussions with Dr. Sands contributed materially to the development of the electronics. Other electronics consultants have been James C. Keck and Alvin V. Tollestrup.

David C. Oakley grew all of the stilbene scintillation crystals used. Much of the development of the spectrometer detector system was performed by him.

The above named persons contributed their labors and skills to the operation of the synchrotron and to the experimental procedures. Also to be thanked in this connection are Robert V. Langmuir, John G. Teasdale, James I. Vette, and Paul L. Donoho.

Thanks are also due to the many laboratory technicians who constructed the electronic circuits and those who helped with the operation of the synchrotron.

The author wishes to take this opportunity to express his appreciation for the continuing interest of Dr. Robert F. Bacher.

This work was supported in part by the U. S. Atomic Energy Commission.

TABLE OF CONTENTS

I. INTRODUCTION

In that portion of modern physics dealing with the interactions of high energy particles, electromagnetic radiation processes have a unique position. Historically, it was in connection with radiation that the need for quantum concepts first became evident, yet the early successes of Planck and Bohr were obtained mostly through modification of the elementary particle dynamics. Much later, a complete quantum theory was developed, and it was quickly followed by the quantum electrodynamics. Over the recent years, this quantum electrodynamics has been made exact. This being so, one may say that of all the interactions that can occur between high energy particles, only electromagnetic interactions are precisely understood.

The work to be described here is of an experimental nature, and it will not be to our purpose to give a detailed discussion of the radiation theory. The reader will be referred, for example, to Heitler's book (1). It will be useful, however, to comment on some of the characteristics of the two processes with which we shall be most concerned. These are pair production and bremsstrahlung. There is a third process, Compton scattering, which plays such a small part in some of the experiments, that no test of the theory is provided. Accordingly, we will use this theory to make a small correction, but otherwise say no more about it.

The reader is referred to Heitler's book and the original article by Klein and Nishina (2), for treatments of Compton scattering.

Pair production, in which a quantum of electromagnetic radiation (photon) gives up its energy to the creation of a positive and negative electron pair, and bremsstrahlung, in which an electron, suffering a change of momentum, gives up energy by emitting a photon, were first given a thorough treatment, using the relativistic quantum theory of radiation, in the famous paper by Bethe and Heitler, published in 1934 (3).

In this relativistic theory, there is a striking symmetry between pair production and bremsstrahlung. This may be expressed by viewing a positive electron as an ordinary electron moving backwards in time, as explained by Feynman (4). Then, conceptually, these twin processes are inverse cases of one kind of scattering event: either a backwards (in time) moving electron absorbs a photon, and recoils to a forward motion in time (pair production), or a forward moving electron emits a photon, and recoils to a new forward direction in time (bremsstrahlung). The observable process is not so simple; for the conservation of momentum and energy, there must be a third charged particle present, and intermediate steps, involving momentum transfers to this third particle, are involved.

While the theory is correct, exact calculations, as Bethe and Maximon have shown (5), are all but impossible,

and one must resort to mathematical approximations. The first complete treatment used the Born approximation (3). In this approximation, the symmetry between the two processes is not obscured, because the same plane wave functions may be used for both. The resulting formulae may be converted one to the other by simple transformations. In a better approximation, recently given by Bethe, Maximon, Davies, and others (5), (6), the more correct wave functions differ for the two cases, evidently just because the bremsstrahlung wave functions must show symmetry in time, which is not true for pair production. In the mathematics for the new calculations, the inverse-relation between the two processes is somewhat obscured. These calculations give corrections to the Born approximation, and are expected, when the final angle-integrations are published (they are not yet available for bremsstrahlung), to be definitely smaller for bremsstrahlung than for pair production.

Enough symmetry remains, however, so that the characteristics which we shall note for the one process may be seen in the other, for relativistic energies. The presence of the third charged particle (an atomic nucleus, usually) is important to both; the cross sections for the processes go nearly as the square of the nuclear charge. These cross-sections may be expressed in terms of a universal radiation cross section $\bar{\phi} = Z^2(e^2/mc^2)^2\ (e^2/\hbar c)$, in the customary symbols, Z, e, $\hbar$, c, m, being the nuclear charge number, electronic charge, Planck's constant, the velocity of light,

and electronic mass, respectively. We usually write this more compactly as $\bar{\phi} = Z^2 r_o^2/137$, where r_o, the classical radius of the electron, is the combination e^2/mc^2. Numerically, $\bar{\phi} = Z^2 \times 5.793 \times 10^{-28}$ cm^2. Just above the energy threshold, $2mc^2$, pair production cross sections increase rapidly with energy, but at higher energies both processes approach finite limits, of the order 10 $\bar{\phi}$, owing to the increasing importance of screening. At high energies, pair production and bremsstrahlung yields dominate over all known competing processes.

The necessity for the presence of the third particle complicates the kinematics, in the usual manner for three body problems. The energy partitions between the emergent pairs may not be predicted and must be given by a probability distribution like that of Figure 1, for example, in the case of pair production. Similarly, for bremsstrahlung, the energy imparted to the photons must be given by a distribution like the dashed curve in Figure 2.

Some of the energy relationships are simple, however. At the higher energies, and especially where screening is important, most of the contribution to the cross section comes from interactions where the momentum transferred to the nucleus is very small, being near to the minimum value allowed by the conservation laws, and is of the order of $mc(mc^2/E)$, where E is the incident particle energy. This has the consequence that the energies given to even light nuclei may be neglected in any practical calculation, and

we consider that all the incident energy is borne by the emergent particles.

This same small momentum transfer is reflected again in the simplicity of the situation for the angles of emission. These are characteristically small for both processes, and are in a narrowly forward direction, the solid angle being of the order mc^2/E, where E is the incident particle energy.

The experimental utility of betatrons and synchrotrons illustrates a way in which some of these characteristics of high energy radiation are experimentally important. The extreme forward angle for the bremsstrahlung provides a narrow, well-defined, experimental beam, and the high yield allows the use of quite thin foils of metal as radiators. Thus, the narrow beam, obtainable in principle, may be obtained in practice also, because of the small contributions to angular spread coming from scattering in such thin foils.

The operation of the pair spectrometer is another illustration, and it is with this instrument that we shall be principally concerned in this paper. It will be seen that these characteristics combine to make the pair spectrometer a conceptually simple instrument allowing one to make precision measurements of these radiation processes. The range of its capabilities has been well exploited in several laboratories in this country.

Lawson (7) made use of the energy discrimination properties of a pair spectrometer so that he could study photon

absorption cross sections for 88 Mev in a variety of materials. Using only the upper portion of the bremsstrahlung spectrum from a betatron, he was able to avoid problems due to degraded radiation. He was able to show clearly the errors in the theoretical cross sections as a function of Z. The error to be expected in the Born approximation (1) should go as Z^2, and this is what Lawson found. By using various pair converters, he was able to corroborate the pair production cross sections obtained from his absorption measurements. The technique of changing converters allows only relative measurements of pair cross sections.

Confirming many of Lawson's conclusions, Walker made absorption measurements for 17 Mev photons. These were emitted as γ-rays from a nuclear reaction induced by a cyclotron proton beam (8). Again, the energy discrimination properties of the spectrometer were exploited to avoid problems of degraded radiation. Walker also made a study of relative pair production (9) in the manner of Lawson. Together with McDaniel he found the spectrometer useful for the study of the emergent spectrum of p-γ reactions produced by the cyclotron (10).

For higher energies, absorption studies have been made at 280 Mev by DeWire, Ashkin, and Beach (11) in a manner similar to Lawson's, again confirming his conclusion for the trend in error in the Born approximation. In addition to relative pair production, they also studied the bremsstrahlung spectrum (12) from their 310 Mev synchrotron, determining

the maximum energy of the photons and the relative intensity distribution, comparing it with theory. They were also able to study the partition distribution (as in Fig. 1) of pair production on a relative intensity scale, confirming the theory as to shape.

More recently, a pair spectrometer was used to extend the range of absorption measurements down as low as 5.3 Mev. This work was done by Rosenblum, Schrader and Warner (13).

Finally, McDonald, Kenney and Post have constructed a simplified pair spectrometer to monitor that portion of the bremsstrahlung above 300 Mev, as produced by their synchrotron (14).

In one of the papers giving the new more exact radiation calculations, Davies, Bethe, and Maximon (6) review this experimental work, together with some done by other methods, comparing the results with their theory. The agreement was judged to be excellent.

The work to be described here extends most of these experiments to higher energy. Using the 500 Mev bremsstrahlung from the California Institute of Technology Synchrotron, we have measured x-ray absorption in carbon, aluminum, copper, tin, and lead. This work includes measurements of the radiation from the synchrotron, providing an experimental study of the bremsstrahlung process in its spectrum details, and making an energy and intensity calibration available to the laboratory.

II. THE PAIR SPECTROMETER

A description of the pair spectrometer will be in order, before we examine the experiments. This description will not only be useful to the understanding of the experiments, but should prove of value to those who may have occasion to use this instrument in the future.

We shall give our attention principally to details of construction that are of the greater importance to understanding the instrument's operation and adjustment. We will not, for instance, go into any detail concerning the great amount of engineering work that went into the design and construction of the magnet itself. Where some elements of novelty occur, as occasionally, for instance, in the electronics, these may be discussed in some length. In fact, the electronics may be expected to be discussed in considerable detail, for this is fairly complex, and must, in the nature of the electronic art, be subjected to adjustment and maintenance at intervals more frequent than for other sections of the instrument.

A. EXPERIMENTAL ARRANGEMENT

A horizontal section of the 30 ton magnet, showing the disposition of detectors and pair converter, is presented schematically in Figure 3. The magnet is fairly conventional; it has two end yokes which have been bored to allow passage of the x-ray (bremsstrahlung) beam from the synchrotron. It has trapezoidal pole pieces, which allows it to be used as a focussing magnet when it is not being employed in pair spectrometer service. The breadth of the trapezoid is 40 inches.

The water-cooled windings were designed for a maximum load of 50 kilowatts. The power source is an Amplidyne controlled motor generator set. A current of 260 amperes is sufficient to produce an induction of 12.5 kilogauss which allows the measurement of 500 Mev x-ray quanta. This field, and lower ones, have been measured and shown to be uniform within a few tenths of a percent over that portion of the chamber active in analysing pair-energies.

The pair converter is a thin metallic foil. Several of these were mounted in a foil changing mechanism which may be operated without opening the vacuum chamber. Available foils were 0.0005, 0.001, 0.002, 0.005 inch thickness of copper, 0.001 inch of lead, 0.005, 0.001 inch of aluminum, together with one blank space used for studying backgrounds. The one used most often was the 0.005 inch aluminum foil,

since it was felt that the pair production cross sections were best known for this element. This thickness also gave a useful yield relative to the background.

The detectors are scintillators one inch wide, one-half inch thick, and four inches long reaching from top to bottom of the four inch magnet gap. These were stilbene crystals grown by David C. Oakley, except that some showing flaws were replaced by plastic units recently obtained.

The scintillators were cemented to the ends of lucite rods acting as light pipes conducting the scintillations to be detected to photomultiplier tubes mounted on top of the magnet. As will be seen in Figure 4, these light pipes pass through a vacuum seal and through holes bored in the pole piece and top yoke of the magnet. Sheathing the scintillators in aluminum foil shielded each from the light coming from its neighbors.

There were ten detectors on each side of a 60 degree V (fig. 3). Measured from the vertex of the V, the nearest detectors are at a distance of 11.5 inches. The spacing between detectors is 2.80 inches.

The trapezoidal chamber has thin side walls (0.03 inches of Dural) to minimize back-scatter of the pair electrons. The chamber is evacuated to a pressure of a half millimeter, or less, of mercury, to minimize the spurious effects of pairs created in the residual air. The chamber is connected to snouts (also evacuated), so that the entrance and exit windows for the x-ray beam may be located so as not to produce

detectable pairs; in particular, the entrance window of 10 mil aluminum was thus located a few meters in front of the spectrometer magnet, and one meter in front of the "broom" magnet. The use of a "broom" magnet and lead and concrete shielding further served to reduce the background (Fig. 5).

B. OPERATING PRINCIPLES

High energy electromagnetic quanta create positive and negative electron pairs in the converter mounted at the vertex of the V. These electrons, bearing substantially all of the energy of the quanta, as mentioned, start out in the direction of the incident quanta, and are deflected into circular arcs of opposite curvature by the magnetic field. A typical pair of such trajectories is shown as the dotted lines in Figure 3.

The total energy U, of a high energy particle is related to its momentum p by the relativistic formula

$$U^2 = c^2p^2 + m^2c^4,$$

where c is the velocity of light, m is the mass of the particle. This leads to the approximate expression:

$$U = cp\left[1 + \tfrac{1}{2}(mc^2/cp)^2\right],$$

in the case where $cp \gg mc^2$. For cp about 250 Mev, one makes an error of only a few parts per million if he neglects the second term inside the brackets entirely. Thus, the total energy of an electron, for the range of energies under consideration, is almost exactly proportional to its momentum. Thus, it follows that the energy of the incident

quantum is proportional to the sum of the momenta of the electrons it produces. The momentum is proportional, in turn, to the radius of curvature of the path in the magnetic field.

Because of the 60 degree geometry employed, the radius of curvature of an electron's trajectory is equal to the distance between the converter and the detector it strikes. The sum of these distances for a pair is proportional, then, to the energy of the quantum creating them.

Multiple scattering in the converter and the occurance of a finite angle between the pairs can influence the accuracy of the above description. For the 5 mil aluminum converter most often used, one finds that its thickness is only 0.0012 radiation lengths, so that using the approximate formula for the root mean square angle of scattering,

$$\theta_{rms} = \frac{21}{E(Mev)} \sqrt{t},$$

where t is the thickness in units of a radiation length*, one estimates that a 75 Mev electron (half of a 150 Mev pair), travelling an arc of length 24 inches to a middle detector, will suffer a root mean square displacement of a quarter of an inch.

Borsellino (16) has shown that the most probable angle between pairs is given by

$$\theta_p = (4mc^2/k)\phi_z(k,v) \quad ,$$

- -

* The radiation length is a convenient unit in which to express radiation yields, since when this is used these yields are nearly independent of the material considered. Tables and formulae are given in Rossi's book (15).

where $\phi_Z(k,v)$ is only a very slowly varying function of the atomic number Z and the quantum energy k. For a partition of $v = U_+/k = \frac{1}{2}$, where U_+ is the energy of the positive electron, for instance, the value of ϕ_Z is very nearly unity. The angle one computes from this gives a displacement of 0.33 inches, for the above conditions. These will be compared with the one by four inch dimensions of the scintillators, and the effects estimated in a later section.

Further, the incident x-ray beam has a finite width, and some of the pairs may start out at some distance to one side of the vertex of the V. If this causes one electron to go too far, however, the other one will not go far enough, so that the sum of these distances will be measured correctly to first order. (We will give a quantitative study later.) It is clear that this kind of compensation would be exact if this were a 180 degree spectrometer. The beam width is determined by the collimators; the second collimator has a quarter by a half inch hole, the long dimension being vertical. This spreads to a half by one inch at the radiator.

C. ELECTRONICS REQUIREMENTS

In all the detection events, arising ultimately as pulses of electric current from the photomultipliers, that can occur, only those pairs of events arising in opposite sides of the V, and which are coincident in time, are useful events, indicating pair production events from which energy measurements of the incident quanta may be obtained. One

needs, therefore, some provision for selecting only such events, and, to perform the energy measurement, for sorting these into channels characterized by the pair energy, that is, by the sum of the distances between the detectors and the pair radiator. Further, these events must be counted in each channel and the counts displayed in a manner suitable for recording by the operator. These duties are performed by rather elaborate electronic circuits.

We may number the detectors, starting with the ones nearest the vertex of the V, with numbers running one through ten. Then if we designate a coincidence event by a pair of such numbers (i,j), the quantum energy corresponding to this event will be a linear function of the sum, i + j. It is convenient to assign the energy channels with numbers, each of which is the sum of the numbers designating the coincidence events belonging in it. These channel numbers give the energy of the channel by a linear relationship. Channel 4, for instance should receive coincidences of the form (1,3), (3,1), (2,2). In pairs of integers ranging from 1 to m, the number of pairs is m^2; the largest sum is 2m, the smallest 2, and there are 2m-1 different sums in all. Thus, in our case of 10 detectors on each side of the V, there are 19 channels, and 100 different kinds of coincidence events, to be sorted into these 19 channels.

One way in which this sorting may be done is given in a block diagram in Figure 6. Electronic circuits, which

give an output pulse only when the two inputs are coincident pulses, are connected in what may be called a matrix array. Figure 6 is drawn for m = 3. The outputs of all the coincidence circuits with same i + j are joined to feed a common display device or register, one for each channel. The complexity of such an arrangement for m = 10 is clear, yet if the coincidence circuits could be particularly simple such an arrangement might be quite practical. Such matrix arrays have been used (10).

We want to ask ourselves questions regarding the degree of refinement that must be built into the coincidence units used in the matrix array. We will first point out that even if there arise only those kinds of events which we want to count, there are some unfortunate accidents which can occur. As an example, consider a (3,1) coincidence occurring simultaneously with a (1,2) event. These should be recorded in channels 4 and 3 only, but they are also spuriously recorded in channels 2 and 5. To get rid of such accidents we might want to connect some more coincidence circuits, so as to record any coincidences that occur within each side of the V. The data from these, being a record of all such accidents, including others where one member of the pair is lost, would allow one to monitor the "dirt" in the apparatus, as Lawson points out (7), and would provide a basis for removing accidentals of this kind from the data.

There is another approach to this problem of accidental events. With the advent of very fast-acting detectors

(scintillation counters) and equally fast circuitry, one might hope to impose such severely precise timing on these accidents, as to make those capable of being recorded occur very rarely. One would expect that the precision in timing that one should impose should be scaled to the average time between events, in such a way that, if one finds himself limited to the sort of time precision he can impose, he still has the alternative of counting very slowly, i.e., with a very weak x-ray beam. This should not be carried too far, however, not only because of the possibility of encountering extreme operating times, but also because one might encounter severe background troubles.

We proceed to make these ideas more precise. A coincidence circuit may be characterized by a resolving time, t, such that if each of its inputs is excited by pulses occurring within the time interval, t, the circuit will respond to them and not otherwise. For statistically independent inputs, one at an average rate N_1, the other at an average rate N_2, there will be an average accidental rate

$$2N_1N_2t.$$

This relation will be used in deriving the accidental rates that one might expect from an obvious coincidence array like the matrix. In what follows, certain assumptions will be made concerning the distribution of events among the detectors. These assumptions will not be too far from the truth, but a more careful treatment in a later section will reveal them to be incorrect. The treatment to follow will, however,

be a correct consequence of these assumptions, and will have the advantage of being mathematically more transparent.

Suppose, for a particular channel and a particular coincidence circuit, that each of the two inputs has a coincidence (true) rate N per beam pulse and a total rate RN per beam pulse*. The factor R will be derived under spectrometer response from reasonable assumptions for the spectrum, and from the spectrometer geometry. R is to account for the fact that each detector is feeding other coincidence circuits, counting in a manner statistically independent of the one we are considering; for the fact that each detector will see many members of a pair, the other member being lost; and for background radiation from the synchrotron. A good value for R will be shown to be about 50, when it is derived. We neglect N, relative to RN, and have for the accidentals

$$A = 2R^2N^2t$$

per beam pulse, if t is in units of beam pulse duration. The accidental to true ratio is

$$(A/N) = 2R^2N\ t$$

for that coincidence circuit, and hence for the channel, if we make the same assumptions for each counter. This ratio increases with N, so that one may expect to have to restrict his counting rate if the ratio of accidentals to trues is to be restricted. We expected this from our qualitative discussion.

This result will give us the requirements on resolving time, for we must have

* The synchrotron x-ray beam is produced in bursts, or pulses, having a duration of about 10 milliseconds, normally, at a repetition rate of about once a second.

$$t = \frac{(A/N)}{2R^2N} .$$

It would be convenient to be able to obtain 3000 counts in a channel in about 10 minutes. Since there are about 60 beam pulses per minute, this is about 3000/600 = 5 per beam pulse. To ensure this kind of performance in a majority of channels, at least, we shall ask that it occur for a channel being fed by 5 coincidence circuits. Thus, we are asking for N = 1. We demand that accidentals amount to only one percent; (A/N) = 0.01. We recall that R = 50. Using these, we have $t = 2 \times 10^{-6}$, in beam duration units. The duration of the beam pulse may be taken to be 10 milliseconds, so that in ordinary units t = 20 millimicroseconds.

The required resolving time is barely an order of magnitude, or so, slower than that for the fastest coincidence circuits that the electronics art can provide, and the required circuits may not be expected to be unusually simple, or unusually free from troubles. Further, the fast amplifiers required to drive such coincidence circuits are costly, so that the number required (twenty) is almost prohibitive.

Fortunately, one can see that a solution to this problem of complexity should be available. Some of the complexity is due to an uneconomical use of information. The matrix array makes distinctions among the various kinds of coincidences going into a given channel, and then this distinction is thrown away by the parallel output connection. If this distinction were not generated in the first place, one

would expect some simplifications.

Important simplifications of this kind are realized in the more sophisticated Time-Delay Multiplexing Coincidence circuit invented by Matthew Sands (17). This circuit, which is the one that was decided upon, uses only three coincidence circuits per channel, all driven by only four amplifiers.

This circuit, drawn for m = 3, is shown in block diagram in Figure 7. Referring to this figure, it will be noticed that the coincidence circuits are already labelled with channel numbers. The legend describes the symbols used. It will be noticed that there are two coincidence networks connected to the phototube V. The basic idea may be grasped by considering only one of these networks at a time. For definiteness, let us consider the one labelled Primary 1. Now, channel 3 should respond to (1,2) and (2,1). For a (1,2), we have a signal from phototube 1 on the left coincident with one in phototube 2 on the right. The signal reaches the left amplifier with two units of delay and the right amplifier with only one. One more unit must be made up on the right; this is done when the signal reaches the right hand imput of channel 3. Similarly, for a (2,1) there is one unit on the left and none on the right, and we find this deficiency made up at 3. Channel 4 is for equal delays and sees, consequently, (1,3), (2,2), (3,1). For channel 5 and 6, the deficiencies are to be made up on the left, and are one and two units, respectively. The unnumbered channel is looking for the non-existent (3,4) and (4,3)

coincidences. It may be numbered 1, if one's aesthetics so incline. It is the so-called dummy channel, and is intended to record accidentals.

For events randomly distributed in time, the time delays play no role, with the result that, for accidentals, each coincidence circuit is connected to every phototube pair. Thus, the accidental rate is higher than that of the matrix array for equal resolving times*. This can be remedied at the expense of trebling the number of coincidence circuits, which is cheaper still than the matrix, and cheaper than shortening the resolving time by another order of magnitude.

The idea is simple. One installs Primary 2, which works just like Primary 1 for the trues, and installs a third set of slow coincidence circuits. This third set (not shown), the so-called Secondary Coincidence array, merely asks that channel n in Primary 1 be in coincidence with channel n in Primary 2, separately for each channel. The registers are then driven from the Secondaries.

The secondary coincidence has to be slow for the reason which is illustrated by considering channel 3 receiving a (1,2) event. Channel 3 in Primary 1 is excited after two units of delay, but Channel 3 in Primary 2 is excited after only one unit of delay. The reverse is true for a (2,1) event. The secondary resolving time must be as much as m units of delay for some channels. The secondary resolving

---

* The severity of this depends on the channel. In the most favorable case, the multiplexing array would exhibit an accidental-to-true ratio m times larger than that for the matrix.

time is chosen to be uniform for all channels to promote uniform response to accidentals. This resolving time should be kept fairly short compared to the average time between pulses, and, for the parameters chosen, this can be done.

The kind of accidentals not seen by the matrix, and eliminated by the Secondaries, is illustrated by considering events in phototube 1 on the left and 3 on the right, with that in 1 initially delayed by one unit. This will be recorded in channel 3 in Primary 1 and in channel 5 in Primary 2. This is vetoed by the Secondary.

This removes practically every kind of accidental event to which the multiplexing scheme would be subject, and the matrix is not. Only some very rare "triples" events remain. Naturally, the multiplexing arrangement cannot, in principle, be better than the matrix.

For m = 10, we have 40 fast coincidence circuits and 20 slow ones, to be compared with 100 for the matrix, and we have only 4 amplifiers, to be compared with 20 for the matrix. We have equal performance.

The spectrometer uses the counting and register circuits that are incorporated in the Synchrotron Differential Pulse Height Analyser, or Kicksorter. There are twenty registering channels available, and connection is readily made by multiple-coaxial patch-cords.

D. CIRCUIT DETAILS

Reference here will be made to simplified figures for

the purposes of circuit description, but also, so that this section will be useful to those responsible for circuit maintenance and modification, reference will be made to the Standard Synchrotron Electronic Drawings by their drawing numbers, although these are not intended to form a part of this thesis. Thus, the more detailed drawing corresponding to Figure 7 is 10-T-205.

Figure 8 (10-T-213) gives the connections made to the individual photomultipliers. It shows a resistive voltage divider to supply the various dynode potentials, with a capacitive filter to remove any voltage fluctuations due to varying dynode currents. A portion of the high voltage distribution chassis (10-T-183) is shown. In this, the adjustment of the voltage to be applied is made by selecting R's and adjusting the rheostats. The correct voltage must be found for each 1P28.

A provision is made for bringing individual signals out from each tube and for inserting test pulses individually. The test pulser (10-T-187) is a standard mercury relay type and will not be further described. The "singles" amplifier requires a special pre-amplifier (10-T-192), with unusually high gain. This amplifier required some protracted development, because its high gain made stray pick-up problems unusually severe. This development was not completed at the time that the synchrotron was made available for these experiments; thus, since its design is not complete, it will not be described further here.

A pair of stepping switches, operated by a telephone dial, makes it possible to switch the test pulser and singles preamplifier to various phototubes independently on each side of the V. This switching arrangement was designed by David C. Oakley (10-T-184), (10-T-185).

Attention is now directed to the coil connected to the 1P28 anode (Fig. 8). The time delays are all accomplished by means of coaxial cables, so that the strings of delays required should be ideally one long length of cable properly terminated at each end. Yet, it is necessary to connect, at intervals, some capacity in the form of vacuum tube grids and anodes across the coaxial transmission line. These small capacities would give rise to echo pulses which will not be very small in view of the rise-times of the order of millimicroseconds involved. Further, in a periodic structure, these echoes could conspire to give large spurious signals. The center-tapped coil provides an m-derived low pass filter section, using the tube capacity as an element. This section has its characteristic impedance (125 ohms) matched to the line, and sharply reduces the echo magnitudes to tolerable levels.

The design of these coils calls for some comment. The m-derived filter is so-called because of a parameter m, occurring in the design equations, and which is related, in this case, to the mutual inductance, M, between the

halves of the coil. When viewed as a circuit element, M appears as a negative inductance in the capacitor lead, and has the effect of extending the range of frequencies for which the impedance of the section is near its nominal value.

Because of the large role played by distributed reactances, it is a little incorrect to regard these filters as networks, and the design equations, having only qualitative relevance, will not be presented here (18). We will point out that, where these design equations do apply, it is shown that a rather wide range of m is acceptable, giving the best value for M when the length of the coil is about 1.5 times its diameter (19). However, grid lead inductance has the effect of cancelling part of M, the indications being that for very short coils one might have just enough effective M left to do some good. This effect is difficult to estimate, and it was found expedient to proceed empirically, seeking to make the coils "good and short". The coils used here have a length that is definitely less than the diameter. In order that the coils could be uniformly and cheaply fabricated it was decided that they should have a fairly large diameter, consisting of only 3 or 4 turns in 20-per-inch threads cut into half inch lucite rods.

The capacities of the tubes were measured, and one having a capacity near the average was selected, and used in a geometrical duplicate of the intended circuit. The total inductance of the design coil was adjusted to meet

the condition of minimum observed echo. A normal 30% echo could be thus reduced to 1% or so. With the normal variation in tube capacities, the echoes are less than 3 or 4 percent. (The final coil designs are given in 10-T-214.) Much of the success of the execution of the Time-Delay Multiplexing designs is dependent on a proper control of the magnitude of these echoes.

These filter sections introduce small time delays of about 1.25 millimicroseconds for the phototube anode coils and 1.95 millimicroseconds for the coincidence grid coils. The phototube cables can each be shortened to compensate for this, but there is an almost complete automatic compensation in the coincidence delay network (Fig.7). Imagine a small delay at each junction; then, as one follows the signal upwards along either side, one sees that for every small delay added on the left, a comparable one is added on the right. There are two exceptions. For Primary 1, for instance, one must lengthen the left hand input cable, if channel 4 is to be an equal-delay channel (lengthened by m coil-units), and the delays accumulated in getting past channel 2 on the left must be removed from the delay between 2 and 5 on the left, as must the delay added into the left input cable (2m coil-units in all).

The last named effect sets a lower limit to the size of the delay unit. Not only should the delay unit be definitely longer than the resolving time, but they should be

longer than 2m coil-units. Here the unit delay was chosen to be 36 ft. of RG 63/U, which is 40 millimicroseconds. If one subtracts 2m (2m = 20) coil-units from this, one is left with only about 4 feet of cable. The final trimming of these two cables is best done empirically.

Each amplifier (Fig. 7) consists of a Model 30 preamplifier and shaper, driving a Hewlett Packard 460 A amplifier, which in turn feeds a Hewlett Packard 460 B amplifier, which drives the coincidence circuits. These amplifiers are of the distributed type.

The Model 30 preamplifier is shown in Figure 9 (10-T-147). It consists of a "half-clipper" driver T-1, an integrator T-2, and an output clipper-driver T3. The effects of these operations on the pulse shape are shown in Figure 9. The final result is a nearly triangular pulse with the usual asymptotic tail removed by the "half-clipping" operation. The clip-times are each 10 mμ sec, and the final pulse width at half amplitude is this value also.

R_1 can be selected to give varying amounts of "half-clipping" amplitude. As it turned out, the best value for R_1 was very near the characteristic impedance of the clipping line (160 ohms), implying that the exponential decay of the input pulse was faster than expected and needed little or no "half-clipping" to remove its tail. The absence of this tail is important with reference to pile-up problems.

A typical member of the primary coincidence arrays is shown in Figure 10 (10-T-215). This is a Garwin-type circuit,

well known to the art (20). It ought to be observed that both 6AH6's are quiescently conducting, and that an output pulse occurs only when both tubes are simultaneously turned off by coincident negative pulses on the input grids. Larger pulses, than the 6 volts or so necessary to do this, have substantially no further effect. The circuit thus exhibits saturation. The output pulses have been stretched to have a 0.1 microsecond decay, since once the primary coincidences have been performed, pile-up is a much less serious problem. The output pulse has an amplitude of 3 volts when fed into the load presented by the Secondary Coincidence circuit.

A typical section of the Secondary Coincidence circuits is represented in Figure 11 (10-T-216). In this circuit the input pulses are stepped up to 9 volts amplitude by the transformers and used to trigger a multivibrator. The normally conducting sections (shown shaded) are turned off for a half microsecond interval each time the multivibrator is triggered. This time interval is determined by the 2.5 millihenry inductor together with tube and stray circuit capacities. This time interval is, then, the resolving time of another Garwin type coincidence circuit connected in the plate circuit of the normally-on sections. The output pulses are stretched to a one or two microsecond length and are 50 volts high. These are suitable for operating the counting circuits provided in the Kicksorter.

The bias voltage is set by a ten-turn potentiometer (not shown). If this bias is set too near the 50 volt

value of the fixed biases, the multivibrators will free-run. In principle, this bias should be set so as to accept all true pulses from the Primaries but reject all small spurious ones, such as noise and feed-through "singles".

Provision is made for grounding either the 50V-1 line or the 50V-2 line. This has the effect of disabling the coincidence circuits, so that if the 1 line is grounded, pulses only from Primary 2 are fed directly through to the counters. The switch (not shown) which performs this function has the positions labelled S1, N, S2, meaning Singles 1, Normal, and Singles 2. This switching may also be done separately for channel 1, the dummy channel.

Provision is also made for inserting a gate pulse so that the circuits will be operative only during a pre-determined interval, corresponding to the beam on-time. The counting circuits in the Kicksorter also have this provision, and it is the latter that is most often used.

All the coincidence circuits, comprising some 150 tubes and at least as many diodes, together with the associated delay cables, are mounted in one 6 foot rack, together with a small 300 volt power supply, and a power distribution chassis (10-T-202) which meters some of the currents as an aid in trouble-shooting.

The principal power consumption is, aside from filament power, taken at 150 volts dc, the current demanded being about 1.7 amperes, provided by a separate commercially built regulated supply, of 2 ampere capacity.

In view of the large currents involved and the need for protecting the primary coincidence diodes from surges, a special turn-on procedure is required. One first makes sure that all DC switches are off. One then turns on all the AC switches. The filaments of all tubes should light, and the cooling fan should come on above the primary coincidence chassis. One then may turn on the DC switch on the large power supply and those for the primary coincidence circuits, provided the DC supply voltage control is set to zero. One then raises this voltage to 150 volts. Finally, one simultaneously turns on the 150 and 300 volt switches on the secondary coincidence circuits; one may reverse the order of this procedure for a shut-down.

E. SPECTROMETER RESPONSE

It would be well, before going on to describe the experimental procedures, to obtain some idea of the way the data should look for certain conditions.

The x-ray energy in the quantum energy interval dk is written as

$$I(Z,k,E_o)dk\ ,$$

where Z is the atomic number of the synchrotron radiator material, and E_o is the energy of the electrons. This function will be discussed later in more detail, but a plot of it for our case is given as the dashed curve Fig. 2. $I(Z,k,E_o)$ is a slowly varying function of k for $k < E_o$. Near E_o, it drops rapidly to zero, remaining there for larger k. Let us assume that I is everywhere constant at I_o, for

the purposes of this discussion. The number of quanta in the quantum energy interval dk is obtained by dividing by k, thus:

$$I_o dk/k .$$

The pair electron yield is proportional to the cross-section for pair production. This yield may be written as

$$P(Z,k,v)dv ,$$

giving the number of pairs (created by a quantum of energy k) in the partition interval dv, where $v = U_+/k$, for a pair converter material of atomic number Z. This function may be seen plotted in Figure 1. It will be discussed in more detail later also. It is a slowly varying function of k and v for the partitions used by the spectrometer, so let us assume here that it also is a constant, P_o, for all k and $0 \leqslant v \leqslant 1$. We see that the quantum energy interval and the pair energy interval accepted in any channel is the same, so instead of dv we write dk/k. Thus the number of events going into channel n will be

$$P_o I_o (dk/k)_n^2 ,$$

provided each channel had the same multiplicity. The multiplicity is the number of coincidence pairs for a given channel. More abstractly, the multiplicity is the number of positive integer pairs (i,j), such that $i + j = n$. Here, for $m = 10$, we have the multiplicity as

$$m_n = 10 - |n-11| , \quad 2 \leqslant n \leqslant 20 ,$$

We also have, using the geometrical parameters of the spectrometer,

$$(\Delta k/k)_n^2 = 1/(8.70 + 1.40\ n)^2,$$

which will be derived below. The product of this with m_n gives the variation of counts with n, the channel number. This is plotted to a normalized vertical scale as the dashed curve in Figure 12. The reciprocal is given in Table 1 (along with the channel energies), both as described, and for the case when one of the Number 10 detectors is not operative, as was the actual case. Multiplying the counts by these tabular entries is one of the first steps in data reduction. The subsequent corrections are much smaller.

Referring to Figure 13, we derive the channel energies $k_n = U_n$ and resolution $(\Delta U/k)_n = (\Delta k/k)_n$. For channel n, one sees that

$$\rho_i + \rho_j = \rho_n = (2 \times 11.5 - 2 \times 2.80 + 2.80n) \text{ inches}$$

or

$$\rho_n = (17.4 + 2.80n) \text{ inches},$$

which gives an energy of

$$k_n = (13.26 + 2.134\ n)B,$$

where appropriate conversion factors have been used so that B may be expressed in kilogauss for k_n being in Mev.

The channel resolution is

$$(\Delta k/k)_n = \Delta\rho/\rho_n$$

a numerical ratio, not involving B. It is seen from Figure 13 that $\Delta\rho = 2.00$ inches, so that one has

$$(\Delta k/k)_n = 2.00/(17.4 + 2.80n) = 1/(8.70 + 1.40n).$$

From these one computes Table 1.

We will now derive the resolution function giving the response of a channel as a function of energy. The average value of its width is what was just computed. If we consider the trajectory of one member of a pair as varying over a detector width, while the other is held fixed, we get a rectangular resolution function. This is to be integrated, varying the second member of the pair. The result is simply the fold of two rectangles, which is a triangle of average width $(\Delta k/k)_n$.

This resolution function needs to be folded with a displacement distribution function, arising from multiple scattering in the converter and from Borsellino's probable angle between pairs (16). We compute these for channel 12 operating at an energy of 500 Mev, and assume a gaussian form. Using a path length of 26 inches, we estimate 0.15 inches root mean square displacement from these two effects. The result of folding this with the triangular resolution function is shown in Figure 14. In any uses that we make of the resolution function, we will always assume the triangular form, since the effect from the fold is so small in channel 12, one of the few channels important in tracing out the upper end of the bremsstrahlung spectrum.

One might expect a finite beam width to affect the resolution function. Let us examine this. Consider a trajectory with center of curvature in the plane of the

converter foil, but at a distance x from the vertex of the V. We will assign a radius ρ to this trajectory, and, for x near ρ, this trajectory will intersect the line of detectors giving an apparent radius ρ'. The relation between these quantities is

$$\rho'^2 - \rho' x = \rho^2 - x^2.$$

From this, one may readily write a Taylor's series expansion:

$$\delta\rho' = -\delta x - 3(\delta x)^2/\rho + \ldots .$$

For one member of the pair, δx is positive, and for the other member δx is negative. The result is, for a pair of detectors (i,j), that

$$\delta\rho_i + \delta\rho_j = (\delta\rho)_n = -3(\delta x)^2\, \rho_n/\rho_i\rho_j .$$

Thus, the pair spectrometer records the energy as too small by the amount

$$-(\delta k/k)_n = 12(\rho x)^2/4\rho_i\rho_j.$$

For equipartition, one has $4\rho_i\rho_j = \rho_n^2$. For channel 12, $\rho_n = 51.0$ inches, and $2\sqrt{\rho_i\rho_j} = 45.8$ inches for the most extreme partition. The hole in the second collimator has a half-width of 0.125 inches, which spreads to $\delta x = 0.25$ inches at the pair converter. Using this, we have for the range of energy depressions in channel 12, 0.027% to 0.036%.

We next proceed to study the accidentals. For detector i, the counting rate will be

$$S_i = \int_{U_i}^{E_o} I_o P_o (dk/k)(\Delta U_i/k) = I_o P_o (\Delta U)_i\, (1/U_i - 1/E_o),$$

where the integration is done over all energies k that can produce pairs one of whose members has energy U_i in the interval ΔU_i, and where E_o is the synchrotron energy. This

does not include background, which will be examined shortly.

From this one may write the accidentals coming from each detector pair into channel n = i + j as

$$A = 2S_iS_jt = 2I_o^2P_o^2(\Delta U)_i\,(\Delta U)_j\,(1/U_i - 1/E_o)(1/U_j - 1/E_o)t$$

The true rate in channel n is, per detector pair,

$$N = I_oP_o(\Delta k/k)_n^2,$$

so that the ratio of accidentals to trues is

$$(A/N) = 2I_oP_o\,\frac{(\Delta U)_i(\Delta U)_j}{(\Delta k/k)_n^2}\,(\frac{1}{U_i} - \frac{1}{E_o})(\frac{1}{U_j} - \frac{1}{E_o}),$$

which is

$$(A/N) = 2I_oP_o\,k_n^2(\frac{1}{U_i} - \frac{1}{E_o})(\frac{1}{U_i} - \frac{1}{E_o}),$$

and which is

$$(A/N) = 2N\,k_n^2\,(k/\Delta k)_n^2(\frac{1}{U_i} - \frac{1}{E_o})(\frac{1}{U_j} - \frac{1}{E_o}).$$

For a pessimistic evaluation we neglect $1/E_o$, then we have

$$(A/N) = 2N(k/\Delta k)_n^2\,\frac{k_n^2}{U_iU_j}\,t$$

For equipartion we have $4U_iU_j = k_n^2$ (this is very nearly the same thing as $U_i + U_j = k_n$, from the properties of the geometric mean). Thus, we have

$$(A/N) = 2N\,(k/\Delta k)_n^2\,4t.$$

From Table 1, a central channel (12, say) has a $(k/\Delta k)$ of about 25, so that we have

$$(A/N) = 2(50)^2Nt = 2R^2Nt$$

with 50 being the value for R used previously.

The above result, R = 50, assumes no stray radiation from the synchrotron. This assumption is justified in the experiments. We performed what we called background runs

by operating the spectrometer with no pair converter in the beam. The observed counts are then such as arise from pairs created in the residual gas in the vacuum system together with such radiation as reaches the counter by other means. These background counts were seen to be sharply dependent on the magnet current, decreasing by two orders of magnitude as one increased the magnet current from 50 amperes to 260 amperes. Further, at the higher currents, the background was one order of magnitude below the measured accidentals that occur with a converter in the beam. The conclusion is that stray radiation plays no significant role in generating accidentals, and that the accidental and background measurements may be treated as mutually independent.

F. INITIAL EXPERIMENTAL PROCEDURES

It will be useful to give a brief history of the problems encountered in getting the spectrometer into operation, so that many of our difficulties may be avoided by those persons who may have occasion to use this equipment in the future.

The first major problem was assembly. Almost all of the electronic equipment had been fabricated and tested synthetically in the electronics shop some time before the synchrotron was available. The fabrication of the few long signal and service cables to run from the spectrometer magnet to the electronic gear remained.

As soon as the spectrometer magnet was released from its other duties, the work of mounting the equipment to be

associated with it was begun. This included mounting the phototube housings, the high voltage distribution chassis, the stepping-switch chassis, the 60 interconnecting cables between these, and the 18 signal delay cables. Tape markers were affixed to the interconnecting cables. These were marked with a letter followed by a number. Numbers 1 through 10 were used for the left side of the V, viewed from above at the vertex, and 11 through 20 for the right side. The letter X was used for high voltage supply leads, the letter S for the singles leads, and the letter T for the test pulse input leads. Numbers above 20 were used for the few long corresponding cables that lead to the assembly of electronic gear.

The magnet was then moved into position and lined up with the synchrotron beam. While the foil changing mechanism was being installed, the broom magnet was moved into place, the long snout was installed, etc.

One of the first tests was undertaken to determine the influence that the small magnetic field on top of the magnet had on the operation of photomultipliers. This was done with a small scintillation counter and a radioactive source. It was found that a rather elaborate system of shields was required for the photomultiplier. A workable arrangement is shown in Figure 15.

While the detectors and light pipes were being installed (many of the very fragile stilbene crystals were broken and replaced with plastic), and the vacuum system was being

assembled and tested, electronics systems tests were begun. In these tests, the test pulser was to supply pulses to the phototube anodes via the stepping switches, all the various pairs to be tested in sequence. Here, capacitative feed-through in the stepping switch made these tests all but impossible. After exploring many peculiar effects that were not understood, in view of the myriads of other paths these spurious pulses seemed to take, the feed-through was sharply reduced by supplying capacitative loading of 20μμfd to each of the switch contacts. The tests could then proceed. (It is possible to re-build these stepping switches to provide a simple shielding arrangement, and this should be done.)

Of the nearly 60 1P28 photomultipliers available, 20 were selected on the basis of some synthetic tests, the criteria included low noise, large signal outputs, and small spreads of output pulse sizes. These tests were conducted by David C. Oakley. In spite of every reasonable precaution, it seemed that these tests were not pertinent; practically none of the selected phototubes were useful, nor did the recommended operating voltages have any meaning.

With the synchrotron operating, and presumably with the scintillators being excited by pair electrons, the photomultiplier outputs were observed at the inputs to the coincidence circuits, this being done visually with a very fast oscilloscope (Tektronix 517), and with high voltage supplied to only one photomultiplier at a time. One sought to determine the required high voltage (and hence the R's in the H.V. Distribution chassis) and amplifier gain settings,

so that the bursts of pulses, that came with the synchrotron beam pulse, would be sufficient, in amplitude, for all of them to saturate the coincidence circuits, but with the spurious noise pulses (present all the time) being too small to do so. There were only two tubes where the signal pulses could be distinguished from the noise, and, for these, the spread in amplitude was such that it was suspected that a large fraction of the pulses were lost in the noise.

It was guessed that some of the 1P28's had been spoiled by being permanently magnetized through careless handlihg. A check showed that they were indeed rather strongly magnetized, but after demagnetization their performance was very little better.

David C. Oakley recalled having seen the following effect (21). If the photocathode of a tube like the 1P28 is operated at a high negative potential with the envelope at zero potential, then at normal operating potentials the noise pulses are so large and numerous that only with exceptional specimens may the signal pulse be discerned.

Apparently the mechanism involves positive ions liberated in the residual gas, these bombarding the dynode structure, and actually entering the structure, bombarding the photocathode, where they eject secondary electrons. The electric fields are too small within the dynode structure, evidently, to have this effect, except in the region between the last few dynodes and the photocathode, where the manufacturers have provided a large barrier. Even then, the

positive-ion feed back effect is observed at unusual operating potentials. Ordinarily, one operates these tubes such that zero-potential structures are rather far removed from the tube envelope, as was not the case with our close fitting magnetic shields.

One cures this by elevating the inner magnetic shields also to a potential near that of the photocathode. When this was done, the improvement was so great, that 20 "good" tubes could be selected and suitable operating voltages determined. Actually, only 19 were good, but this was considered to be a satisfactory state of affairs. We refrained from applying high voltage to the offending tube. (Much later, we discovered that the stilbene crystal for this tube had become uncemented. Indeed, on inspecting the scintillators after the experimental arrangement had been finally dismantled, it was discovered that large voids existed in the cemented joints for some of the plastic scintillators. Evidently, the cemented joints had not been allowed to age sufficiently before being placed in the vacuum.)

For a final determination of the correct high voltage to be applied, one plots counting rate versus the applied high voltage. One expects this curve to rise sharply, and then level off as the coincidence circuits saturate. One then expects to see a quite flat plateau indicating 100% counting efficiency, followed, at higher voltages, by another rise as the coincidence circuits begin to respond to noise pulses and exhibit a large accidental rate.

Figure 16 shows some of the "High Voltage Plateau" curves obtained. These were not considered satisfactory. The installation of one more amplifying unit in each signal line produced some improvement (Figure 17). The conclusion drawn from these is that the pulse height spread from the 1P28's was too great. This is presumed due to the poor optical coupling to the photocathode, an almost unavoidable effect, since the photocathode is located quite deeply within the dynode structure of the tube. This was confirmed when we tried using 5819's for the beam calibration. We had time to try only one pair of these tubes, which have the photocathode coated on the inside of the envelope, and the various plateau-curves were excellent (Figures 18 and 19).

We next tried to determine the proper setting of the Secondary Coincidence bias controls. Plots of counting rate versus setting should show a plateau for small settings, and the counting rate should be small for large settings. Figure 20 shows some of these curves; there are not many conspicuously flat places.

Clearly the pulse height spread was too great for saturation effects to save us, and even the pulse height spread for the output of the Primaries was too large. This last named defect could have been avoided if a larger overall output from the Primaries had been provided, but it was judged that there was not sufficient time available to attempt any modifications to this end.

In view of these difficulties, considerable doubt was entertained as to whether the coincidence circuits were working at all, as such. Accordingly, it was decided to take data with the intention of plotting counts versus lengths of delay inserted in the signal leads. Some of these curves are displayed in Figure 21. These have an entirely normal appearance, and this one doubt, at least, was dispelled.

It was clear that 100% counting could not be guaranteed, and that the counting efficiency and accidental rates could be expected to fluctuate from one channel to the next. There was grave doubt as to whether one should attempt to use the spectrometer under these circumstances. It did seem, however, that absorption experiments could at least be performed, and since the synchrotron time was available, the decision was made to proceed.

G. EQUIPMENT EVALUATION

Here, we summarize the things we learned about the spectrometer characteristics with reference to what one might do in future uses of the instrument.

Much of the power of a multiple channel instrument of this kind depends on a uniformity of characteristics among the channels. For the deficiency in this regard, as it occurred here, the blame must be principally levied against the unfortunate choice of photomultiplier tube type. Future uses of this instrument will most certainly involve the use

of the end-window type tubes, so popular (and justly so) in other scintillation applications. This blame may be partly shared by the defects that were observed in the joints where the plastic scintillators were cemented to the Lucite light pipes, and, in the future, due precautions should be taken to ensure proper aging of these joints, before they are installed in a vacuum system.

These things notwithstanding, defects in the electronics design must carry a large burden of blame, for it seems likely that even with better phototubes, fairly large variations in pulse height will still be encountered, both because of limitations of even the end-window types, and because of the large number of these in operation. With the present electronics, these variations may, it seems, be expected to be near the maximum that this electronics can handle reliably. It would appear, then, that some modification of the electronics should be undertaken.

Some caution must be observed in proposing modifications, however. Increased reliability of individual circuits is usually obtained at the expense of increasing complexity, which may lead to a decrease in overall system reliability, due to the increased rate of component failure. Further, a small modification applied to one section can become a formidable modification, when it must be applied to all sections.

Our experience indicates that an increased pulse size, applied to the inputs of the Secondary Coincidence multivibrators (Figure 11), would be the only major modification

required. It is possible that this could be achieved by the use of a pulse transformer with a larger turns-ratio, if such could be obtained compatible with its other characteristics. Sample transformers, with this end in view, were obtained from PCA Electronics of Santa Monica, California. Although tests on these are not complete, it appears that their primary impedance is too low to allow them to be driven properly by the Primary Coincidence Circuits. It may be that transformers can be supplied that have this characteristic improved.

Failing this, one would reluctantly turn, perhaps, to replacing these transformers each with a section of the double-triode tube type 12AV7 operated as a grounded-grid amplifier. There is ample reserve power available from the 150 volt line, but some of the fuses and metering provisions would have to be changed. Additional or larger filament transformers would have to be installed.

More modest modifications are also considered to make the multivibrators themselves more reliable. The 12AV7's may be replaced by the triode-pentode type 6U8 (which has identical characteristics to the 12AV7 if operated as a double triode), with the pentode section in the normally-on position, its screen power being taken from the 150 volt line, and the cathode resistor changed to perhaps 8200 ohms. This should have the effect of providing a more sharply defined resolving time, through improved shape of the output pulse, and increasing the ease with which this circuit may be triggered.

It will be noticed that the 2.5 millihenry inductors (Figure 11) are each shunted with a damping-diode and damping-resistor combination. More reliable and uniform triggering characteristics also might be obtained by providing a small back-bias to the diode by connecting a 0.68 megohm resistor from ground to the junction of the damping-diode and the damping-resistor. If a larger resolving time were needed, it may be obtained by shunting this diode with 10 μμfd, say.

Finally, the stop-bus should derive its power from a cathode-follower, so that it may not be severely loaded by the backward currents in the stop-diodes.

With these modifications, the performance of the electronics should be vastly improved, while maintaining comfortable operating times between component failures, on the average. Indeed, one should expect that the full capabilities of such a multi-channel instrument will be realized.

III. EXPERIMENTS

In this section will be presented the manner in which the data for the various measurements were obtained. A later section will be devoted to the analysis of the data and comparison with theory. These measurements are the energy distribution of the synchrotron bremsstrahlung, total absorption x-ray coefficients in carbon, aluminum, copper, tin, and lead, relative pair production cross sections in aluminum, copper, and lead, and the intensity calibration of the synchrotron bremsstrahlung.

A. BREMSSTRAHLUNG

In this series of experiments, the spectrometer magnet was operated at currents of 50, 100, 160, 200, and 261 amperes, corresponding to magnetic fields of 2.8, 5.41, 8.50, 10.4, and 12.61 kilogauss, so that channels 2 through 14 (the ones having satisfactory statistics) covered energy intervals of 49 to 121, 95 to 233, 149 to 367, 182 to 449, and 221 to 544 in Mev. Except for the highest current, the magnetic field values were obtained from the magnet calibration curve (Figure 22), since the counting rate varies quite slowly with field, for the lower fields. The values of fields corresponding to currents greater than 220 amperes were measured with the aid of a proton resonance magnetometer. One run each was also made at currents of 228, 232, 240, 243, 251, and 261 amperes, so that closely spaced data points might be obtained in the region of the

high energy limit. The 0.005 inch aluminum foil was used for the pair converter.

The synchrotron beam was monitored during these runs by three methods. Monitor M_1 was an ionization chamber with thick walls of copper*, originally designed at Cornell University (23). This monitor was located behind the spectrometer and was placed directly in the beam (Figure 5). Monitor M_2 was a gas-filled Cerenkov detector located between the first and second collimators. Monitor M_3 was identical to M_1, except that it was located before the first collimator, and, so as not to degrade the spectrum obtained by the spectrometer, it was placed with the accepted portion of the beam passing a fraction of an inch above it. This monitor responded, then, to the "stray" radiation from the synchrotron, in particular, that portion of the bremsstrahlung emitted at the fairly large angles of one or two degrees. For the spectrum measurements, only M_1 was actually used. Data were taken from the others as corroboration. M_2 might have been useful, except that the dark-currents in its photomultiplier proved difficult to measure reliably. M_3 was used in the later absorption measurements.

The total electric charge collected from these monitors in any one run was measured by electronic current integrators. One integrator unit of charge is called a "bip" in the jargon

---

* One inch for each. The one inch air space between contains a centered 0.062 inch thick copper plate serving as a collection electrode. This wall thickness allows a cascade shower to come near to its maximum development (22).

of the Synchrotron Laboratory. The size of this unit needs to be determined for each integrator by calibration procedures. The number of bips is recorded on a mechanical register, with interpolation of fractional bips being read on a panel meter.

A set of runs consisted of those at the magnet currents of 50, 100, 160, 200, and 261 amperes, each set being performed three times. This was done so that small changes with time in counting efficiency could be averaged out for any particular magnet current. No such changes were observable, however, probably because these data were obtained in the space of one afternoon. Finally, the six closely spaced high-current runs were taken to obtain the data on the upper end of the spectrum.

While this was being done, the synchrotron energy was monitored. This makes use of a flux coil and electronic integrator combination. The peak output voltage of the integrator is proportional to the peak magnetic field in the Synchrotron, and hence, is a measure of the machine energy. This voltage is compared with a "standard" voltage by a potentiometer arrangement, and this "standard"voltage may again be compared against a standard cell of the Weston type. This "standard" voltage varied by at most 0.2% during the above runs. The variations in machine energy covered a range of 1.6%, and, in particular, the machine energy was lowest when the end runs were taken. During the end runs the variation covered a range of only 0.05%.

For those runs where the proton resonance magnetometer was employed, the magnetometer was used to maintain the field to a constant value by manual adjustment. The

precision with which this may be done exceeds, it is judged, the precision with which the magnetometer frequency was measured. This latter measurement was made with an Army Signal Corps frequency meter model BC 221. The magnetometer oscillator was subject to some frequency-pulling by this instrument, but by varying the coupling between them, one could judge that this produced an error of less than 0.1%. Flip-coil measurements verified that the field at the magnetometer probe agreed with that of the center of the vacuum chamber to an accuracy of 0.04%.

By turning the foil changer control, so that no foil was present to produce pairs, we were able to make background measurements. These were smallest for the high energy runs, being only about 4 per channel per 10 bips for 261 amperes, and they increased to about 300 per channel per 10 bips for the 50 ampere runs. The number of data counts was about 3000 per channel per 10 bips in runs approximating 8 minutes in length.

Qualitative monitoring of the accidental rate was possible with the Dummy Channel (Channel 1), but to measure these for the individual channels, one needs to insert a delay in each of the two lines for one side of the V, of a length longer than the multiplexing unit delay. These accidentals were of the order of 40 per channel per 10 bips for running times comparable to the above. These were measured much later in the experimental series, but the channel fluctuations corresponded to what was observed in

the bremsstrahlung data, and, in any event, the accidental counts were few.

B. ABSORPTION MEASUREMENTS

These measurements of absorption coefficients for carbon, aluminum, copper, tin, and lead required a more elaborate treatment of the monitoring problem. Monitor M_3 or monitor M_2 were clearly the ones to use, but M_2 was not useful because of instrumental difficulties. M_3, however, was subject to some error, since the portion of the beam it intercepted was suspected of being very sensitive to small changes in machine parameters. Checking it against M_1, and against the Pair Spectrometer, showed that this was indeed the case.

However, if one operated the synchrotron at constant intensity, the change of the M_3/M_1 ratio with no absorber was quite slow with time, with perhaps a 2% change over a span of a couple of hours, but if one made large changes in beam intensity (a factor of 4, say), one could expect changes in the M_3/M_1 ratio of as much as 8%.

The procedure adopted will now be described. With no absorber present, a run would be made recording the spectrometer and monitor data. The absorber would be put into place, and a run at a higher beam intensity (higher, so that the spectrometer would count at its proper rate) would be made, again recording the monitor and spectrometer data. Then the absorber would be removed, and a run would be made at as near the same beam intensity as possible, recording

only the monitor data, there being no need to record the spectrometer data. (The counting rate was always excessive for the spectrometer on this run.) Such a trio of runs was always made for every measurement of absorption. For the normalization, the observed M_3/M_1 ratio would be used as follows:

$$(C_n/M_3)_A(M_3/M_1)_o,$$

where C_n stands for the counts in channel n, the subscript A is to denote the presence of an absorber, and o its absence.

While the runs were being made, the ratio M_3/M_1 was computed for each trio, so that difficulties could be detected as soon as they occurred (except for the thicker piece of lead; see below).

For each element measured, we used two different thicknesses of absorber, and we usually made four measurements on each thickness. The larger thicknesses were capable of giving greater statistical accuracy, but to guard against other errors we used the thinner thicknesses also.

Background measurements, as previously described, were made, both with and without the absorbers, immediately at the end of the series for that particular material. Data on the accidentals were the same as used for the spectrum measurements, since the insertion of a lead absorber made substantially no change in the accidental-to-true-ratios.

While the absorption measurements were properly done for the thinner of the two lead absorbers, the measurements were not so carefully done for the thick lead absorber. Lead was the material first treated, before some of the

necessary precautions were fully appreciated. It was usually necessary to change integrator scales for taking the monitor run, when an unusually thick absorber had been used, for then the bips would come through very fast. Under these circumstances the register-driving relay would remain operated for such short intervals that the electrical impulse delivered to the register was observed to be too small to operate it reliably. Consequently, some of the bips would appear to be lost, though the current integrator would be operating properly. Fortunately, where necessary (only for the thicker lead absorber), it was possible to "guess" how many bips had failed to record by assuming that M_3/M_1 ratio changed by less than 14% since the proper register number was about 7. Intentions of repeating the measurements with the thick lead absorber were not fulfilled because of the lack of time. It developed later that this method, despite its inelegance, gave results that were in excellent agreement with those for the thin lead absorber, for which the measurements were properly performed.

In all the absorption measurements, the magnet current was maintained at 261 amperes. Measurements at lower fields were not considered, since the presence of degraded radiation from the absorbers would vitiate any attempts at absorption measurements at any energy except in a small interval near the upper limit of the bremsstrahlung.

Considerable care was taken to obtain pure materials for the absorbers. The materials used were finally obtained

from A.D. Mackay, Inc., 198 Broadway, New York 38, New York. Although we have not conducted tests for chemical purity, some information on this matter was obtained from the supplier. The carbon absorbers were in the form of graphite rods and were each cut from the same rod. These are quoted as a high purity grade for nuclear research. More specific information is available concerning the aluminum, the quotation being 99.9% pure. The grade of copper obtained is known as OFHC (Oxygen Free High Conductivity Copper). Copper of this grade usually has a purity exceeding 99.9%. For tin, we have the quotation 99.9%, or better, and the same is to apply for lead.

The dimensions of the absorbers were measured, using micrometer calipers for all dimensions less than 5 inches. There were none less than about ½ inch. Larger dimensions were measured, reading to the nearest 64th of an inch, using a metal scale. Averages of several tries were made so that these dimensions are presumed known to 0.1%. In the case of the aluminum absorbers, which were cut from castings, some of the cast surfaces were still in evidence around the sides, and, near these, small voids could be observed. These cast surfaces were milled away, enough material being removed so that no more voids could be seen, but no changes were made in thickness.

The absorbers were weighed, such precautions being observed as to assure 0.2% accuracy at worst. As a final check the volume density was computed and compared among the various samples of each absorber. For lead the agreement

was 0.2%, for copper 0.8%, for tin 0.3%, for aluminum 0.6%, and for carbon 2.2%. The worst case was carbon which was in the form of graphite, and for which uniform density is difficult to assure.

C. RELATIVE PAIR PRODUCTION

For this experiment, the available converters were those mounted in the pair spectrometer foil-changing mechanism. These were 0.0005, 0.001, 0.002, 0.005 inch of copper, 0.001 inch of lead, and 0.001 and 0.005 inch of aluminum.

The runs were made with M_1 as a monitor and at a fixed magnet current of 261 amperes. As a check, the counts normalized for 10.00 bips on M_1 were computed for 3 selected channels, and compared as each series was obtained.

Three complete series were made, together with one background run. The accidentals that apply were those that were also used for the preceding.

These foils were also obtained from A. D. Mackay, Inc.. Again, chemical tests for purity have not been performed. The quotations on these is 99.3% for aluminum, 99.9% for copper, 99.9%, or better, for lead. These foils were weighed by James I. Vette, and their weights and areas are believed known to better than 1%. On account of the uncertainty about the impurities, we shall assume a 1% error from both sources.

D. INTENSITY CALIBRATION

For this last experiment, all the 1P28's were removed and their light pipes replaced with iron rods except for

position 6 on each side of the V. For these, two of our best-looking plastic scintillators were chosen; their widths measured 0.983 and 0.982 inch. Two 5819 photo-multipliers, shielded with iron and mu-metal, were installed for these, and connected to the two signal cables for Primary 1.

It was found that the extra amplifiers that were needed for the 1P28's could be removed, and that a normal value of high voltage (1000 volts) would give 10 volt signals at the coincidence inputs with a pulse height spread estimated at only 25%.

While it was found that the magnetic shielding for the 5819 was inadequate, counts from a radio-active source decreasing for magnet currents above 200 amperes, it was possible to run with the magnet at 150 amperes and take the data at 311 Mev, which was satisfactory.

Only the equal-delay channel (channel 11) should count, except for accidentals, but to have a check, a "jumper" was installed so that 10 was disabled and channel 9 would also count. The secondary coincidence was disabled by switching to Singles 1 operation.

Since channels 9 and 11 were on separate chassis for the Secondary multivibrator, their biases were independent, and it was possible to take bias plateau curves with high statistical accuracy. These circuits should now count identically, pulse for pulse, except for the relative losses occurring in one due to changing only one of the biases. In the ratio of counts, one to the other, the errors

are due only to the statistics of the difference. Figure 18 shows such a curve. The dashed line is the result of an attempt to explain the plateau slope as being due to accidentals, since the level, at which the Secondary accepts pulses from the Primary, controls, to some extent, the Primary resolving time. This attempt appears to be successful up to a bias setting of about 17. The jumper was removed for measuring accidentals in channel 9, which was considered the data channel.

Data for a high voltage plateau curve were also taken. This may be seen in Figure 19. The points were mistakenly obtained with some lead absorber, that had been used to check the effect of absorbers on accidentals, and which was still in place. Nevertheless, over the range of 1000 to 1150 volts the data seem to be consistent with a genuine plateau, or, at least, one with very little slope. The criteria for 100% counting seem to be fulfilled.

After the lead had been removed, 10 runs were made to get good statistics (only one pair of counters meant a lower-than-normal counting rate by a factor of ten). A background and an accidental run were made. For 9661 counts one had to subtract 245 background and 67 accidental counts*. For these 10 runs the high voltage was varied over the range of 1000 to 1150 volts.

---

* Approximately one of these accidental counts was found to be due to the background. This confirms our previously mentioned discovery that the accidental and background data could be regarded as independent.

Since this calibration is properly one of the standard ion chamber, the temperature and barometric pressure were recorded so that the data could be reduced to conditions of standard temperature and pressure. Also, the machine energy was monitored, the dial setting pertinent to this being "895".

Finally, the number 1 scale of the M_1 current integrator (as used) was calibrated by connecting a known voltage source to the input of the integrator via a calibrated 940 megohm series resistor. This source supplied 0.4592 volts. One has to know, however, the voltage at the input of the current integrator to know the current being integrated. One may establish this to be zero at the start of the integrating cycle by substituting a short circuit for the voltage source, leaving the 940 meghom resistor in place, and making circuit adjustments so that no drift (or a very small one which may be measured and subtracted from the integrated current) is observed. The input is the grid of an electrometer tube, operating in a feed back circuit, and one may see, from assumptions about the feed back gain and the maximum output voltage, 20 volts, that this grid is made to rise to 0.01 volts during the integration cycle, having an average potential of 0.005 volts. Thus the applied voltage should be taken to be 0.4542 volts. The time required to produce 25 integration cycles (about 1.88 minutes) was measured several times, so that the time per cycle (bip) could be accurately determined. Using this procedure, we determined that 2.185×10^{-9} coulombs was equivalent to one bip. The overall error is estimated to be one percent.

At the conclusion of the entire experimental series, the line-up of the magnet with the beam was checked. It was found that over a period of a month and a half, the beam had shifted to such an extent that the collimators pointed to a place on the exit port of the synchrotron which was ½ inch off beam-center. This will be seen to have no bad effects, as will be explained when we examine the bremsstrahlung angular distribution in the section to follow.

IV DATA ANALYSIS AND DISCUSSION

A. BREMSSTRAHLUNG DATA

The individual channel data, for channels 2 through 14, after the background and accidentals were removed, were normalized to 10.00 bips on M_1, and were averaged for each of 3, and in one case 4, runs that were made at each magnet current. Finally, the individual channel corrections were applied using the entries in Table 1 .

Figure 23 shows the results, excluding the data taken for the end-runs, and excluding all data for energies above 430 Mev. The variation of pair cross section with energy has not yet been taken into account, although the partition correction, which will be discussed later, has been applied.

The statistical deviations for these points are nowhere greater than 1% and are not large enough to explain the fluctuations observable in the figure. These fluctuations are to be interpreted largely as a reflection of the variation in counting efficiency among the channels. It will be observed that since the data for each different magnet current are plotted with a different symbol, one can discern a system in the fluctuations. Channel 11, for instance, is always that lowest point in each of the sets of points. Each channel has been tracing out a separate bremsstrahlung curve, to a scale peculiar to itself, as the magnet current was changed.

To extract the maximum information from these data, one should make such scale adjustments as to make these curves coincide. It was observed that if one multiplies the theoretical pair-production cross section (for equipartition, $v = \frac{1}{2}$, say) by the theoretical bremsstrahlung intensity distribution, then in the region of 50 to 450 Mev the product is quite constant, much resembling the curve in Figure 23, except of course, in that it has a continuous slope. Thus, for reasons shortly to be apparent, this region is particularly suited for the data adjustments undertaken to achieve the above goal.

If one mentally makes corrections for fluctuations that can be clearly seen to occur systematically, by channel number, then one will draw a curve much like that shown in Figure 23. Actually, when initial attempts were made to carry out this adjustment, it was observed that one could almost as well draw a single straight line, arriving at the same adjustments after a little more labor. Then, selecting a particular channel, channel 11, for example, one computes the ratio of the value for the curve for that channel, at that energy where it happens to lie, to the data for that channel. One does this for each magnet current setting, for that channel, provided the energy lies within the prescribed range, averages these ratios for that channel, and regards the result as a correction factor to be applied to that channel only. One then proceeds similarly for all other channels whose energies lie within the prescribed

range of 50 to 430 Mev. In so doing, the end-run data were also taken into account for the cases whose energy lay within this prescribed range. The results were then taken to be the appropriate corrections wherever the energy of the channel happened to lie.

When these corrections were applied, even when the adjustments were computed relative to a single straight line, the points collapsed strikingly about a curve very much like that shown in Figure 23. If one had started with a straight line, he would then feel strongly compelled to draw a better curve and run through the adjustment procedure again. The use of such a curve as in the figure, initially, then, is seen to be an innocuous shortcut.

Finally, one multiplies these data by the reciprocal of the pair production cross section, shown plotted as the reciprocal in Figure 24. The results are shown in Figure 25. In this figure, the curve shown is a theoretical one, whose derivation is shortly to be discussed.

For the pair production cross sections, the Bethe-Heitler formulae (3) were used for aluminum, including the recently derived corrections to the Born approximation (5), (6), and integrated over angles including screening for a Fermi-Thomas model of the atom. To this one must add the cross section for pair production in the field of the atomic electrons. Some of the many papers on this have been reviewed by Bethe and Ashkin in their article in Segre's book (24). For us, the conclusion is that the same general properties, such as

those resulting from small momentum transfers to the third particle (electron) obtain as if the third particle were an atomic nucleus, except that the cross sections, instead of going as Z^2, go only as Z, for atomic electrons. (These things are true of bremsstrahlung, also.) The calculations of Wheeler and Lamb (25) were used, since their treatment included screening. All this was done for equipartition, $v = U_+/k = \frac{1}{2}$, since the partition corrections had already been applied.

These partition corrections will now be discussed. The partition, v, being that fraction of the incident quantum energy borne by one of the electrons in the pair process (the remainder is borne by the other) is, in general, different for each detector pair. Thus, a spectrum of partition values is to be associated with each channel. Now, the pair cross sections are not independent of the partition. In Figure 26, for example, are plotted the pair cross sections for aluminum, divided by that for $v = \frac{1}{2}$, for the range of partitions pertinent to the spectrometer, and for several incident quantum energies, k. These are derived from the same sources cited above. It should be mentioned that these functions are symmetric in v, about the value $v = \frac{1}{2}$, so that they needed to be computed only for values of partition less than, or equal, to this. (This is true even when the corrections to the Born approximation are applied.) Figure 26 was plotted, with as much precision as seemed warranted, to serve as a means of interpolation for deriving the partition corrections.

A table was prepared (Table 2), entering for each channel the partitions for the detector pairs belonging in each channel. From the geometry of Figure 13, one may readily derive that for an (i,j) coincidence belonging in channel n, the partition is*

$$v = (4.35 + 1.40\ i)\ (\Delta k/k)_n.$$

Noting that all partitions except v = 0.5 are to be considered twice, one averages the values obtained from Figure 26, separately for each channel, and as a function of energy. These partition corrections, derived for the special case of one of the number 10 detectors being inoperative, are shown plotted in Figure 27. The points marked are for the particular energies for which data were taken.

Much of the fluctuations in data due to partition variations are automatically removed by the method of data adjustment previously described. It is sufficient, then, to normalize the marked points in Figure 27 against the partition corrections for the highest energy run, and use such reduced corrections. When this is done, it is seen that the corrections to be applied amount to nowhere more than a percent. (This is an upward correction.) This conclusion is rather disappointing, in view of the labor involved, but it should be mentioned that the full amount of partition correction would be applied under normal circumstances, where the data were taken to represent 100% counting efficiencies.

---

* This is a convenient algebraic combination. The factors $\Delta k/k$ have no special physical significance.

For the purpose of comparison with theory, the curve shown in Figure 25 was derived, and this derivation will now be discussed. Its principal features are those of the bremsstrahlung cross section, derived by Bethe and Heitler (3). This derivation is also presented in Heitler's book (1). Any numerical results that are given, however, result from the use of the Born approximation, except that recently Bethe, Maximon, and Davies (5), (6) have calculated corrections to be applied to the Born approximation for bremsstrahlung, and its related process, pair production. For the bremsstrahlung, however, these corrections, as published have not yet been integrated over angles, nor has screening been taken into account. The result is that one must still be content with the Born approximation. The work done thus far, however, indicates that there may occur a very small correction, which will always apply so as to decrease the radiation cross sections (5).

For screening, the Fermi-Thomas statistical model of the atom is nearly always used. This approximation is to be expected to be poorest for the atoms of smallest atomic number Z, but Wheeler and Lamb (25) have shown that even in the case of nitrogen (Z = 7), the error due to using this model may be expected to be less than one percent. For the calculation of the radiation cross section in the cases where screening is important, one must use certain numerical results presented either in the form of graphs or numerical tables.

These have been reproduced in various places (15), (26), but usually in a form quite unsuited to the purposes of accurate calculation. These functions may be found, however, plotted to rather finely divided scales, in the article by Wheeler and Lamb (25), and in the article by Bethe and Ashkin appearing in Segre's book, "Experimental Nuclear Physics" (24). The latter curves, while easier to read, are probably no more accurate than the original source, the curves given in the Bethe and Heitler article.

Wheeler and Lamb, in their article, referred to above, have presented their calculations of the radiation cross sections for processes occurring in the field of the atomic electrons, as integrated over all angles and with screening taken into account. This cross section must be added to that for bremsstrahlung in the screened nuclear field.

The result is a function of Z, E_o, and $u = k/E_o$, and is only a slowly varying function of E_o, the incident electron energy, for E_o near 500 Mev. This function was then computed for Z = 29, since we used a copper radiator in the synchrotron, and for E_o = 500 Mev. A plot of this function may be seen as the dashed curve in Figure 2.

Before the theory may be compared with experiment, however, there are a few corrections to be applied. One must take account of the fact that the electrons which produce the radiation are not mono-energetic, but are supplied to the radiator by the synchrotron over a band of energies beginning in the neighborhood of 96 to 97% of E_o and extending up to

the machine energy, E_o. Another group of corrections must be made to take account of the finite thickness of the synchrotron target which is made of copper, having a thickness of 0.016 inches.

The above are all corrections that must be made because of the properties of the synchrotron. Finally, one must make corrections to take account of spectrometer properties. Most of these have been applied to the data, but there is one outstanding important correction which is most easily applied to the theory. It is to be expected that the spectrometer would not reveal as sharp a decrease as may be seen near E_o in the theoretical bremsstrahlung curves, because of the finite resolution of the spectrometer. This correction, then, will also be applied to the theoretical curves, for the purpose of comparison with experiment. We consider first the radiator corrections.

Powell, Hartsough, and Hill (27) have carried through such radiator (target) thickness corrections for their case of a platinum target of 0.020 inch thickness and a machine energy of 322 Mev. They describe their procedure in the following words:

> "This spectrum is modified by the thickness of the target as the result of the following process. First, the electrons lose energy by radiation, so that their original energy is lowered, and the x-rays produced by them farther along in the target will show a lower average energy. This lowering in energy would be more marked were it not for another effect which reduces this considerably. The electrons which have been multiply scattered are no longer pointing in their original direction. Using the multiple scattering formulae of E. J. Williams, it may be shown that after traversing the first 4 mils of the target, the electrons are sufficiently out of line as to make

> most of them miss the cloud chamber completely. This effect was pointed out by McMillan, and its result is to give a spectrum more like that for an infinitely thin target. The spectrum comes almost entirely from the first fifth or quarter of the target, and, therefore, these quanta will be absorbed in passing through the remaining three-quarters of target. Only about 10% of the quanta are absorbed in the target, and the absorption coefficient changes only by about 12% from 40 Mev on up. The correction is practically a constant one and reduces the intensity almost uniformly by about 10%."

They give the result of all these corrections in a table in their paper. Rossi has plotted their tabular data, comparing the corrected and uncorrected spectrum, in a figure on page 302 of his book (15).

These corrections may be expected to be quite different in our case, since our target is much thinner in radiation lengths. Their target of 0.020 inch of platinum has a thickness of 0.18 radiation length, whereas our target of 0.016 inch of copper has a thickness of 0.028 radiation length. For instance, the x-ray absorption in the full thickness of our radiator amounts to only 1.5 percent, and varies over the range from 50 Mev on up by perhaps 0.3 percent. Variations this small will be neglected.

We will now consider the effects of electron energy loss in the radiator. The effect will be to introduce a spread in the energy limit of the bremsstrahlung, and is equivalent to introducing a spread in the machine energy. Since there already exists a spread in the machine energy, which will be taken into account, it will be interesting to compare these two. Bethe and Heitler in their original

paper (3), give a distribution function specifying the fraction of the emergent electrons in an energy interval dE, after having passed through material of thickness t in radiation lengths, and with initial energy E_o. This function is

$$w(E_o,E,t)dE = (dE/E_o)\left[\Gamma(t/\ln 2)\right]^{-1}\left[\ln(E_o/E)\right]^{(t/\ln 2)-1}$$

In this, all the loss is assumed to be due to radiation, which is a good assumption above 50 Mev. This formula, which has also been derived by Eyges (28) by a different method, is based on an approximation to the radiation formulae which tends to favor, somewhat, the electrons suffering the smaller losses. This function may be seen plotted for the full thickness of our radiator in Figure 28, where it is compared with the electron energy distribution (each normalized to unit area) characteristic of the synchrotron. The synchrotron electron energy distribution is calculated below on the basis of some assumptions, which if modified by any reasonable amount, will still leave us with the following conclusion: the energy spread introduced by energy losses suffered by the electrons in passing through the radiator may be neglected in comparison with the synchrotron energy spread.

Thus, according to the correction program of Powell, Hartsough, and Hill, our radiator is ideally thin. If our radiator were ideally thin in every sense, however, there would be one other correction that one would have to make. We used the formula for the bremsstrahlung that had been

integrated over all angles of the emergent electron, and all angles of the emergent quanta. The usual justification that is given for this (29) goes something like the following: for targets which are not too thin, the angular width of multiple scattering will be considerably larger than the natural angular width of the radiation; this has the effect of performing an integration over the angles of emergent radiation. Schiff (30) has given the angular distribution of the bremsstrahlung for ideally thin targets in a calculation including a screening approximation. This distribution has been calculated for the case of copper with an electron energy of 500 Mev and for two different quantum energies, 100 Mev and 400 Mev. The results are displayed in Figure 29, where the curves have been normalized to unit area. It is clear from the figure that if this represented the radiation from our target, i.e., if our target were ideally thin, one should expect the radiation passing through the collimator to be somewhat less, than the integrated bremsstrahlung formula gives, for the low energies relative to the higher energies. In passing, it might be mentioned that the distribution shown would be finite at the orgin if it gave the radiation per unit solid angle; for the distribution as shown, however, an integration has been performed over the azimuthal angles, so that what appears is the radiation going into a zone of width given by the differential polar angle. Thus, areas may be directly compared.

We turn, then, to an examination of multiple-scattering, as it occurs in our synchrotron radiator. Bethe, following Molière, has given a thorough treatment of the problem of multiple-scattering including the so-called plural scattering (31). He has given his results in a form well adapted to computation, and has shown that good agreement exists with experimental results. Since radiation is coming from all depths of the radiator, the distribution that is pertinent to the discussion of the angular distribution, is that distribution which results when the multiple scattering formulae have been integrated over the radiator thickness, as has been pointed out by Schiff (29). The distributions given by the Molière calculations, as performed by Bethe, were integrated by numerical methods, for the whole radiator thickness, excluding the first 0.002 inch. For this first portion of the radiator, the method of numerical integration in use was not applicable, so a gaussian fit was resorted to, and integrated analytically for this portion. The result so closely resembles the exponential integral function that Schiff derived (29), integrating a gaussian function for the whole thickness, that one might have done almost as well by proceeding as he did. The result, normalized to unit area, and shown in Figure 30, is interesting in that it gives some idea of the portion of the radiation, accepted by the collimator, that comes from various depths of the target. The important conclusion to be drawn is that if

this contribution to angular spread were combined with that of Figure 29, one would be unable to distinguish the resultant angular distribution for 100 Mev quanta, from that for 400 Mev quanta. Further, the spectrum will be so much the same at moderate angles off the beam axis, that the half inch drift of the beam at the collimators should not have noticeable effects.

Thus we contend, finally, that our x-ray radiator is thin enough, considering the machine energy spread, and x-ray absorption in the target, and thick enough, considering multiple scattering, so that no radiator corrections need be made.

There remains, for synchrotron corrections, only the effect of the machine energy spread. The manner in which the electron energy distribution, shown in Figure 28, was derived, will now be discussed. The peculiar wave-form of the voltage supplied to the synchrotron magnet, by the Ignitron rectifier-inverter set, is rather well known to the synchrotron personnel. If one integrates a slightly idealized version of this wave form with respect to time, the result is a representation of the magnetic field, which, in turn, gives one a representation of the electron energy as function of time. The result of this integration is shown in Figure 31. The rounded top of this curve is a portion of a sinusoid, and the sloping sides are also made up of pieces of sinusoids, joining where the arrows indicate the location of the "ripples" that appear in the voltage-wave. The effect of these ripples is barely discernible in

the current wave. The interval of time between ripples is a convenient unit of time, since many of the synchrotron functions are synchronized with these. The ripple interval is about 1/6 of a 60 cycle-per-second period. The interval of time over which the radiation is produced is usually adjusted and specified relative to the ripples. This time interval, as adjusted for the spectrum-runs, was so specified and is represented in Figure 31. The intensity was not uniform over this interval, but its actual distribution fluctuated from one burst to the next, keeping within limits something like these. We will assume that the radiation was uniform in time, however, and within these limits. We shall see that we can tolerate quite a large error in these assumptions. Incidentally, it should be pointed out that the scales for this figure were obtained by assuming that the magnet current reached its peak value in 71 ripples, as is the way the synchrotron is adjusted for 500 Mev operation.

One has, then, the functions dB/dt and hence dE/dt and also dn/dt, where B is the instantaneous magnetic field value, E is the instantaneous synchrotron energy, and n is the number of electrons striking the x-ray target. One can then eliminate the time parameter, and have dn/dE, the electron energy distribution. The result is that which has been presented in Figure 28.

Without going into the mathematical details, which are of little moment, one may be permitted to observe that

dn/dE is made up of pieces of simple algebraic functions whose integrals are elementary. The integral distribution is shown in Figure 32. Inspecting this, one can see that a reasonable simplification of this distribution, dn/dE, would be a rectangle of width 3.4% and integral weight 80%, together with a delta-function, of an integral weight 20%, located at E_o. Such a simplification is of considerable value, since the machine energy spread has to be combined with the bremsstrahlung curve by a process of numerical integration.

If one writes the spectrum intensity function as I(u), where $u = k/E_o$, then the form of this machine-energy spread correction integral is

$$\int_{1-\Delta}^{1} I(u/u') \left[dn(u')/du' \right] du'$$

where Δ gives the amount of machine energy spread, and $u' = E/E_o$. The resulting function differs from I(u) only where one is near places of rather large slope. In particular, the only discernible effect of the machine energy-spread is seen for the region very near to E_o, whereas for the low energy region the effect is less than 0.2%. Rather simple numerical methods will suffice for the evaluation of this integral if one does not plan to plot the result in close detail, as is the case for Figure 2, which was computed for a machine energy spread of 4% of E_o, i.e., 20 Mev. If one plans a plot on an expanded scale, then one must go to considerable trouble to get a smooth curve. It was found convenient, for some of these integrals, to separate the functions involved into the sum of two parts,

an analytic fit, and a residual portion. If the residual portion can be made small, very simple-minded numerical techniques will serve for it, and the rest may be integrated by analytic means.

The last major correction that must be made for the comparison of theory and experiment, is that for the spectrometer resolution. The resolution function has been described previously (Figure 14). If one expresses this resolution function as r(x), being symmetrical in x, and normalized to unit area, and vanishing when $|x| \geq k/E_o$, one would write the integral that takes account of the spectrometer resolution as,

$$\int_{u-\Delta u}^{u+\Delta u} I(u')r(u-u')du' \ ,$$

in which u and u' are the energy nominally measured by the spectrometer, and the spectrum energy, respectively, in units of E_o. The integration is performed over the spectrum energies accepted by the spectrometer when it is nominally measuring u. From the way r(x) was defined, one could just as well take infinite limits. Since $\Delta k/k$ is a constant for a given channel it will be noted that $\Delta u = (\Delta k/k)u$. As in the case of the machine energy spread integral, the result is appreciably different from I(u) only when one is near regions of large slope in I(u). The low energy part of the spectrum, then, is not affected, especially since Δu is smaller there. The value of $\Delta k/k$ used, 3.77% (which we will quote as 3.8%), was obtained by averaging the six

different values for the channels most important in obtaining data near E_o. The assumptions regarding shape are not too important, since both the machine energy spread function and the resolution function have the effect of smearing each other out, so that fine details of shape would be lost. We assume a triangular shape. For some notion of the effects of these integrals one is referred to Figure 33. The tails on the resolution function are almost negligible, as may be seen by examining the data for energies above 500 Mev in Figure 25, and Figure 34.

The curve plotted in Figure 25, where the spectrum data points are also plotted, has had both the machine energy spread and spectrometer resolution corrections applied to it. This was done for a machine energy of 500 Mev, an energy spread of 3% (15 Mev) and a spectrometer resolution of 3.8% at the maximum energy.

In this figure, one observes that below about 300 Mev, the experimental points seem to show a definite tendency to lie below the theoretical curve. This effect seems to be about 4% at 150 Mev. The question naturally arises as to whether this effect is real. The answer must be in the negative, at least in the sense of representing an effect in the radiation. No, the effect is probably due to a process occurring in the spectrometer, and is purely instrumental. We will now examine this.

As was pointed out before, Borsellino (16) has computed the probable angles between pairs as

$$\theta_p = (4mc/k)\ \phi_Z\ (k,v)$$

where v is the partition and ϕ_Z is very nearly unity for v = 0.5. He also calculated the pair angle distribution, $d\phi$, and shows a curve, done for tin, for energies of k = 50, 100, 1000 Mev, and infinite energy, with θ/θ_o ranging over 0 to 6, the vertical scale being plotted in units of $\bar{\phi} = Z^2 r_o^2/"137"$. For v = 0.5 the angle θ_o is defined as $\theta_o = 4mc^2/k$. For k = 150 Mev, one finds that

$$\theta_p = \theta_o = 0.0136,$$

and, for a 24 inch path-length to a central detector, one finds a displacement corresponding to this of 0.33 inches. Now, a 2 inch displacement vertically is enough to lose the electron; the angles corresponding to this are $6\theta_o$ at 150 Mev and $18\theta_o$ at 450 Mev. We shall attempt to estimate what fraction of pairs might be lost because of these angular spreads. For large $x = \theta/\theta_o$, one can see that Borsellino's distribution goes as $1/x^3$. We shall assume, as seems quite plausible, that these distributions are only slowly changing with Z. Then, from this distribution, plotted for tin, one sees that for x = 6 the value of the distribution function should be $\bar{\phi}/5$, approximately. Thus one writes

$$d\phi = A\bar{\phi}\, dx/x^3 \qquad \text{where } A = 63/5.$$

Making the transformation $x^2 = \xi^2 + \eta^2$ and $2\pi x\, dx = d\xi\, d\eta$, the above becomes

$$d\phi = \frac{A\bar{\phi}}{2\pi} \frac{d\xi\, d\eta}{(\xi^2+\eta^2)^2}\ .$$

Now, the laterally deflected electrons are not lost, so one

integrates over all ξ , say. This integration is elementary, and one is left with

$$(A\,\overline{\emptyset}/4)\quad d\eta\,/\,\eta^3$$

The loss, then is to be given by twice the integral of this, going from $\eta = 6$ to $\eta = \infty$. The result is

$$A\,\overline{\emptyset}/4.6^3 = 3\,\overline{\emptyset}/10.$$

Since the cross section for all angles is approximately $10\,\overline{\emptyset}$, one has 0.03 = 3%, for our estimated loss; further, we observe that this loss should go roughly as $1/k^2$ for k above 100 Mev, say. We also notice that the multiple scattering angles are almost as large as for the pair production, for the 5 mil aluminum foil, that large-angle scattering goes as $1/\theta^3$ also, and that the energy dependence should also be about the same as for the angles in pair-production. Thus one would guess that scattering might contribute 1 or 1.5% loss, as well. This brings our estimated loss up to about 4 or 4.5%, while the loss at 450 Mev would only be 0.5%. A variation of this size is just about what is needed to explain the observed effect.

One could use these equations of Borsellino in their more exact form, together with Bethe's treatment of multiple scattering (31), especially for the larger angles, to derive more exact channel corrections for this loss-effect. One would have to integrate the scattering formulae over converter thickness, and perform a fold-integral of it with the pair angular distribution. One would, of course, convert to projected angles before performing the fold, which would

otherwise be two dimensional, and projected angles are what are pertinent, anyway. One final integration would give the percentage loss. One would do this for each counter pair, as a function of energy, and combine these results into channels. Since practically every integration would have to be done numerically, this is an extremely ambitious program to undertake for such small corrections. Short-cuts would have to be found (The most useful, that one might think of, would be to dispose of the multiple scattering problem through the use of a thinner foil, for then the integrals are only two, and these might be done analytically. This, of course, is for the future, for practically all our data were taken with this thicker foil.), but even then the program might not be short. Here, most of the individual channel variations due to this effect have been "washed out" by the method of data adjustment used, and only a kind of an average effect is left.

One concludes that the theoretical curve is justified in every respect so far, except as to the absolute magnitude, of course.

From time-to-time, there has been some speculation as to what form the corrections to the Born approximation would take when applied to the bremsstrahlung. The non-relativistic, but otherwise exact, formulae of Sommerfeld (32) show a real discontinuity at the high energy limit. It is clear that the condition for the Born approximation to be valid,

namely that the velocity of the electron, both before and after the radiative process, should be large (in units of the velocity of light) compared to Z/"137", cannot possibly be maintained sufficiently near the high energy limit. Elsewhere, in fact, it would seem rather surprising that the Born approximation is as good as it has appeared to be in the instances of large Z. The presence of screening, reducing the effective Z, may account for part of this accuracy. Even screening won't help for the high energy end, for, classically, close impacts with the nucleus are involved, and the velocity of the emergent electron is hopelessly small. Heitler (1) has proposed a correction factor, analogous to a factor occurring in Sommerfeld's formulae. The new corrections to the Born approximation (5) are not expected to correct the end of the spectrum, for these new calculations are supposed to still contain an error going as the reciprocal of the electron energy, and anyway these corrections are expected to be small, and always downward, with stronger effect where large momentum transfers to the nucleus are involved. Unfortunately, it is just in this end region, where the mathematical approximations are poorest, that the greater theoretical interest lies, for it is these "close impact" situations which could provide the strongest tests for the Quantum Electrodynamics, in the area of high energy radiation processes. We will, therefore, examine closely the upper end of the measured spectrum. The dashed curve in Figure 34 was computed using a discontinuity at the high energy limit,

the jump going to the value of the intensity at 425 Mev, and the distribution assumed constant down to that energy. The fit was obtained for E_o = 497.6 Mev, and corrections for a machine energy spread of 4% (this time) and resolution of 3.8% were used.

Now, the channel adjustments used here are those derived at lower energies, where the consistency seems to justify (as will be discussed shortly) the marked errors as probable ones. The resolution of this experiment would seem to be just about good enough to tempt one to decide against this kind of a discontinuity. Other kinds of discontinuties are clearly not ruled against, however. For instance, a behavior like a continuous fall-off to, say, half value, then dropping discontinuously to zero at E_o, could easily be consistent with the data. Further, one would be inclined to resist this temptation if he felt that there was a rather large long tail to the electron energy distribution, dn/dE, at the lower energies. This could be the case, for instance if the electron energy straggling computation (Figure 28) were in serious error, but the fraction computed for those which had lost 20 Mev, say, would have to be in error by perhaps a factor of 10, which is not compatible with the overall justification of the bremsstrahlung at low energies.

An error in our estimate of the machine energy spread, Δ , will give rise to an error in our estimate of E_o, the machine energy. We have remarked that the x-ray intensity

spectrum, regarded as a function of u, E_o, and Z, is only slightly dependent on E_o. This fact was used in the integral giving the effect of the spread in machine energy. For the "spectrum", into which we have put both the effects of the machine energy spread and the spectrometer resolution, we choose the notation $J(u,\Delta)$. In this, we have supressed the E_o dependence and the dependence on the resolution. We assume that the resolution has already been accounted for in a fixed manner. $J(u,0)$ is intended to give the "spectrum" for no machine energy spread. $J(u,\Delta)$ and $J(u,0)$ are connected by the integral indicated earlier:

$$J(u,\Delta) = (0.8/\Delta)\int_{1-\Delta}^{1} J(u/u';0)du' + 0.2J(u,0),$$

in which we have displayed the explicit form taken for the electron energy distribution dn/du'.

With the aid of this integral, we can readily find the connection between errors in machine energy and errors in machine energy spread. We may write

$$d\left[J(u,\Delta)\right] = (\partial J/\partial u)_\Delta\, du + (\partial J/\partial \Delta)_u d\Delta .$$

Then, regarding J as fixed in value, we find

$$(\partial u/\partial \Delta)_J = -(\partial J/\partial \Delta)_u/(\partial J/\partial u)_\Delta .$$

One may see from Figure 33, that if one holds the value of J fixed, at say J = 7.5, then an increase in Δ will decrease the value of u for this value of J, and, to get a good fit to the data points, one will have to assume a larger value for E_o. Thus, $(\partial u/\partial \Delta)_J$ gives the connection we are seeking.

From our integral expression, we have

$$(\partial J/\partial \Delta)_u = -(1/\Delta)\left[J(u,\Delta) - 0.2J(u,0) - 0.8J(u+u\Delta,0)\right] ,$$

by the usual rules for differentiation, and making use of

$$(0.8/\Delta)\int_{1-\Delta}^{1} J(u/u',0)du' = J(u,\Delta) - 0.2J(u,0)$$

and $u/(1-\Delta) \approx u + u\Delta$. In Figure 33, we select $J(u,\Delta) = 7.5$. For $\Delta = 0.03$, this gives $u = 0.977$. For these values of u and Δ, we read that $J(u,0) = 10.8$, and $J(u+u\Delta,0) = 2.7$. Thus we find that

$$(\partial J/\partial \Delta)_u = -3.2/0.03 .$$

Again from Figure 33, we determine the slope of the $J(u,\Delta)$ curve for $\Delta = 0.03$ and J near 7.5, and find

$$(\partial J/\partial u)_\Delta = -2.3/0.01 .$$

Putting these together, we have

$$(\partial u/\partial \Delta)_J = -0.46 .$$

From this, we see that if we wanted to change our estimate of the machine energy spread from 3% to 4% of E_o, we would have to change our estimate of E_o by something like 0.46% upwards. We are not contending that an actual change in the machine energy spread produces a change in machine energy, for the machine energy is defined for us by the upper edge of the electron energy distribution. The estimates, however, are connected.

Looking at Figure 34, one gets the impression that a somewhat better fit would have been obtained, for the points near 470 Mev, if a larger machine energy spread had been used. Perhaps 3.4% should have been used, according to our original estimate, instead of the 3% taken for this figure. Consulting the rather crude sketch in our notebook,

as drawn from an oscilloscope trace, and referring to Figure 31 again, we decide that 4% is too much. We finally settle on $(3.5 \pm 0.8)\%$. The error we attach may seem a little large, but we shall make it carry the burden of errors in the shapes of the resolution function and electron energy distribution.

The curve in Figure 34 was drawn for E_o = 500 Mev. We have taken an increase of 0.46 x 0.5% to 501.2 Mev, and attached an error of 0.46 x 0.8% = 0.37%. The statistical standard deviations are what are marked on Figures 25 and 34. If one looks only at the end-run data (the crosses) of Figure 25, and asks what fraction of the points lie farther than this error, of about 2.5%, from the curve, for energies between 200 Mev and 460 Mev, one counts about 21/51, or about half. From this, we conclude that because of intensity monitoring errors, adjustment errors, and possible changes in channel efficiencies with time, the computed standard deviation errors ought to be interpreted as probable errors everywhere in these data. We make this interpretation, and turn our attention to Figure 34, scrutinizing the curve in the range of 475 to 505 Mev for the accuracy of its fit to the points. We see that if we increased E_o by 0.5 Mev, about half the points would lie within their errors, and about half not. Because of the slope, the marked errors give rise to an error in E_o of 0.5 Mev, or 0.1%. We accept this increase in energy to 501.7 Mev. Another source of error is

in the range of the energy monitor, 0.05%. The error in knowing the spectrometer field is 0.1%, as is also the error due to inhomogeneity. The fractional energy lost by the pairs, in going through half the converter thickness, is about equal to the thickness in radiation lengths; this is about 0.1%, which we take both as an increase in energy and as an error. Combining all this we have, finally, 0.42% for the errors, and we quote the synchrotron energy as

$$E_0 = (502.2 \pm 2.1) \text{ Mev.}$$

This is, in effect, a calibration of the synchrotron energy monitor, the flux coil electronic integrating arrangement which measures the peak synchrotron field. The energy is proportional to V/(2-D), where V is the standard voltage with which the integrator output is compared, and D is the setting of the ten turn potentiometer dial ($0<D<1$) for the null. The quantity V/(2-D) averaged 6.879 during the end runs, for which the average value of V was 7.675 millivolts. For this value of reference voltage, then, the dial setting that belongs with the above energy quotation is 0.884, or, as we more usually write,

$$D = \text{"884"} .$$

B. ABSORPTION MEASUREMENTS

For these data, one first subtracted the background and accidentals, proportioned according to the values recorded for the monitor indication M_1. Then, as discussed

before, the counts in channel n, C_n, were normalized according to

$$(C_n/M_3)_A \, (M_3/M_1)_o \quad ,$$

where the subscript A refers to the situation with the absorber, and the subscript O refers to the no-absorber monitor check taken immediately afterwards. This being done, one could then divide, channel for channel, the results for no absorber by those where the absorber was used, to get what we call the opacity of the absorber. The average of the opacities for a particular channel and absorber was then computed, and the logarithm of this average obtained. Then, from the data on the weights of the absorbers per square centimeter, one computes the number of atoms per square centimeter, and dividing this into the logarithm of the average opacities, one has the total absorption cross sections, as measured.

For comparison with theory, the most important process contributing to absorption, at energies of the order considered, is pair production. Compton scattering contributes significantly, and the total compton cross section is included in calculations using the Klein-Nishina formula (2). The maxima in the photo disintegration cross sections occur at much lower energies, and should not play the role here that was encountered with another pair spectrometer experiment (8). The process of the photo production of pions is much more important here, than at some lower energies, but

even its cross section may be systematically neglected. For instance, in aluminum, if one considers the cross section for pion production to increase as $A^{2/3}$, where A is the atomic mass number, one finds that it is less than 4.0×10^{-27} cm^2, (33), at 300 Mev, decreasing rapidly at higher energies, whereas the Compton cross section is 3.2×10^{-26} cm^2, and that for pair production 1.2×10^{-24} cm^2. For heavier elements, since the pair cross section goes as Z^2, whereas the Compton cross section goes as Z, and that for the photo production of pions may go as $A^{2/3}$, which is about as $Z^{2/3}$, one sees that these smaller cross sections make even smaller contributions, the Compton cross section accounting for less than a percent of the total for lead.

For the nuclear component of pair production one uses the BetheHeitler calculations (3), together with the recent corrections to the Born approximation as cited earlier. Screening is important practically everywhere, so that one starts from the differential cross sections which, integrated over all angles may be expressed as

$$\phi(Z,k,v)dv = \overline{\phi}\left\{g(v,\gamma_o) - (1-4v/3 - 4v^2/3)\left[(4/3)\ln Z - 4f(Z)\right]\right\} dv,$$

where

$$\overline{\phi} = Z^2 r_o^2/"137",$$

and

$$g(v,\gamma_o) = \begin{cases} 4(1-4v/3 - 4v^2/3)\ \ln \frac{200}{\gamma e^{\frac{1}{2}}}, & \gamma \gg 1 \\ 4(1-4v/3 - 4v^2/3)\left[\ln \frac{200}{\gamma e^{\frac{1}{2}}} - C(\gamma)\right], & 2 \leq \gamma \leq 15 \\ (2v^2 - 2v + 1)\,\phi_1(\gamma) + (2v/3 - 2v^2/3)\phi_2(\gamma), & 0 \leq \gamma \leq 2 \end{cases}$$

in which

$$\delta = \frac{\delta_o}{v(1 - v)} ,$$

with

$$\delta_o = \frac{100\ mc^2}{Z^{1/3}\ k} .$$

The function f(Z) supplies the mentioned correction to the Born approximation, for energies large compared to mc^2, and has the structure

$$f(Z) = a^2 \sum_{\nu=1}^{\nu=\infty} \frac{1}{\nu(\nu^2 + a^2)^2} ,$$

where a = Z/"137". That part given by the summation may be seen plotted in an article by Jackson and Blatt (34) for $0 \leqslant a \leqslant 0.4$ (Z up to about 54), and for Z = 82 (lead), Bethe, Davies and Maximon (6) give $f(82) = 0.9250a^2$. The leading terms in the summation give $f(Z) = 1.2021\ a^2$ for small a. The functions $C(\delta)$, $\phi_1(\delta)$, $\phi_2(\delta)$, occurring also for the bremsstrahlung calculations, are functions involving screening. As already mentioned, these may be found in the form of graphs for ϕ_1 and ϕ_2 and usually as a table for $C(\delta)$.

As pointed out by Bethe and Ashkin (24), when one writes the differential cross section in the above form, it is seen that considerable labor may be saved in the numerical integration. In particular, one sees that it is not necessary to perform the integrations as a function of k for each Z separately, but one may write

$$\int_0^1 \phi\, dv = \overline{\phi} \left\{ G(\delta_o) - (28/9)\left[(1/3)\ln Z + f(Z)\right] \right\} ,$$

where

$$G(\gamma_o) = \int_o^1 g(v, \gamma_o)dv,$$

a numerical integration which may be performed once and for all, as a function of γ_o, with sufficient range to cover all the applications one may have in mind. The function $g(v, \gamma_o)$ was plotted versus v for several values of γ_o in the interval $0.02 \leq \gamma_o \leq 0.15$, a range adequate for the treatment of all elements with $6 \leq Z \leq 82$, and 200 Mev $\leq k \leq 500$ Mev. These were then integrated over the range $0 \leq v \leq 1$, using a planimeter, sufficient precautions being observed to assure an accuracy of 0.1%. The resulting function, $G(\gamma_o)$, may be seen in graphical form in Figure 35.

Some error arises from the use of this method for another reason; it is not $v = U_+/k$ which should be integrated from 0 to 1, but rather, the variable should be $(U_+ - mc^2)/(k - 2mc^2)$, so that the first order effect is that the range of integration is 0.2% too long at 500 Mev. Fortunately, $g(v, \gamma_o)$ is always very small near the ends of the proper range of integration, so that most of the error (negative) is due to the $(1/3)\ln Z - f(Z)$ term, at the ends of the integration range. This last part varies from 13% to 59% of the average value of the integrand, so that the error from this source (multiplying by 0.2%) is at most 0.03% for carbon up to no more than 0.12% for lead, these errors leading to an under-estimate of the cross section. These limits on the error should be doubled for 250 Mev.

The accuracy is probably better than the accuracy with which one may calculate $g(v, \gamma_0)$ from its numerical sources.

These numerical sources are not to be trusted to high accuracy. Commenting on the difficulty with which the original curves of the Bethe and Heitler article (3) may be read, Lawson (7) expresses doubt as to the accuracy with which they were plotted, expecting errors of 1%. Everywhere that these curves are reproduced (15), (26), they appear to be direct copies from this original source. Even in the Wheeler and Lamb article (25), where these curves may be easily read on a more finely divided scale, the source is given as the Bethe and Heitler article. (Lawson had access to the Wheeler and Lamb article.) A possible exception may be the curves given in Segre's book (24), a more finely divided scale being used also. Though no source is quoted, these curves are not distinguishable from those of Wheeler and Lamb, being even plotted over the same restricted range. Lawson's theoretical total cross sections for absorption were also obtained by a numerical integration over these screening functions. Though he believes the integrations to be quite accurately done, he finds a 2% discrepancy with independent calculations by Hough. Thus a one, or perhaps even two, percent error may be present in our values of $G(\gamma_0)$, despite our precautions.

A similar treatment may be accorded the pair production in the field of the electron, which must be added to the

nuclear pair production. The result is, for the total electronic cross section,

$$\int_0^1 \phi_e dv = (\bar{\phi}/Z)\left[E(\varepsilon_0) - (56/27)\ln Z \right],$$

where $\varepsilon_0 = \gamma_0/Z^{1/3}$, and where the function $E(\varepsilon_0)$ has been obtained from similar integrals involving v and the function $\psi_1(\varepsilon)$ and $\psi_2(\varepsilon)$ of Wheeler and Lamb (25). Presumably, one should also subtract from this $(14\bar{\phi}/9Z)f(1)$, to correct for the Born approximation, but this makes a change of only one part in 10,000, which is negligible. The error described for $G(\gamma_0)$ concerning the range of integration also applies here to a larger extent, since the functions ψ_1 and ψ_2 may not be plotted with much accuracy near the ends of the range of integration. Fortunately, the electronic contribution is less than 20% of the nuclear, for carbon, and less than 2% for lead, so that not so much accuracy is needed for the electronic contribution. The function $E(\varepsilon_0)$ is plotted in Figure 36, over a suitable range.

Off hand, one would not expect the cross sections as measured for, say, 220 Mev to have much meaning if the measurement were performed in 500 Mev bremsstrahlung, since one would expect to find additional 220 Mev radiation emitted from the absorber as radiation degraded from the higher energy portion of the spectrum. One would wonder how near to the upper limit of the spectrum one ought to conduct the measurement if errors due to degraded radiation are to be negligible. It was decided, since data are available down to

about 220 Mev, to reduce the lower energy data also to the form of cross sections, and compare these with theory, to learn if such effects were serious near the energy where a good measurement was intended. It was felt that this ought to be done for atleast two elements, one of fairly high Z, and one of fairly low Z, say tin and aluminum.

A theoretical calculation may be performed, giving the percentage of degraded radiation to be expected. We will not aim for great accuracy in this calculation. We will consider that we have an absorber of thickness equal to three radiation lengths. We shall ask first for the intensity of degraded radiation that is thrown into the interval of width 19.1 Mev at 220 Mev (the conditions for channel 2 as the experiments were conducted), by all parts of a 500 Mev bremsstrahlung spectrum having greater energy, as a fraction of that portion of the incident spectrum for this channel.

Under the assumption that only radiation processes are involved, and that the lateral spread plays no role in the longitudinal development of a shower, Rossi (15) explains that the appropriate diffusion equations may be solved through the use of the Mellin transform. Upon solution, the inverse Mellin transforms are integrals which may be evaluated by the saddle-point method. He gives the result that for an incident photon of energy k, the number of photons of energy k' in dk' emerging in a shower from a material of thickness t radiation lengths is

$$\gamma^{(\gamma)}(k,k',t)dk' = \frac{H_\gamma^{(\gamma)}(s)}{\sqrt{2\pi\lambda_1''(s)t}} \left(\frac{k}{k'}\right)^s e^{\lambda_1(s)t} \frac{dk'}{k'},$$

where s is the value of the Mellin transform variable at the saddle-point, and is to be obtained by solving

$$\lambda_1'(s) = -(1/t)\ln(k/k').$$

Rossi also gives all the functions $\lambda_1(s)$, $\lambda'_1(s)$, $\lambda''_1(s)$, and $H_\gamma^{(\gamma)}(s)$ in tabular form, suitable for quick calculations.

Writing the bremsstrahlung spectrum briefly as $I(k)dk/k$, what we are asking for is

$$(I(k')\,\Delta k'/k')^{-1}\left[\Delta k' \int_{k'+\frac{1}{2}\Delta k'}^{E_0} \gamma^{(\gamma)}(k,k',t)I(k)dk/k\right].$$

We calculated this integral in the following manner. We plotted $\gamma^{(\gamma)}(k\,k',t)$ for k' = 220 Mev and k at 230, 240, 260, 300, 400 and 500 Mev. It turned out to be a slowly changing function except near 220 Mev where it becomes unboundedly large. Fortunately, we need it down to only 230 Mev, where it still had a modest value, the upturn beginning fairly suddenly at about 250 Mev. From previously plotted spectra the whole integrand was plotted. The result, because of a gentle rise beginning above 250 Mev in $\gamma^{(\gamma)}$, was almost constant, except for the drop-off near the bremsstralung limit and the sharp rise at the lower end of the range. The extra area under the rise and the area lost by the drop-off could be judged visually to be almost exactly equal, so that the integral was evaluated at a glance. The square brackets had the value, then, of 0.010 x 270 = 2.7, in certain units, whereas the incident radiation in the channel had the value 0.88 x 19.1 = 16.8, in the same units. Now the direct radiation transmitted in the channel is obtained by dividing 16.8 by the opacity of 7.0 appropriate to 3

radiation lengths at this energy. The fraction of emergent degraded radiation, then, is 2.7/2.4, compared to the emergent direct radiation, and thus is 110% of the emergent direct radiation.

There is hardly any need to point out that this would be really serious if it developed that an appreciable fraction of the degraded radiation were accepted by the pair spectrometer. To determine this acceptance, we ask about the angular spread of showers. Now Rossi does not treat this in his book, but together with Greisen, in their review article (26), the subject is discussed briefly. The argument they make is that radiation angles are always much smaller than scattering angles for electrons, and hence the angular spread of a shower is determined principally by the multiple scattering of its electronic component. Assuming that the mean square scattering angle occurring in a thickness dt radiation lengths is $(E_S/E)^2$ dt, where E_S is 21 Mev, and using the function $\pi(E_o,E,t)$, playing the role for electrons that $\gamma(k,k',t)$ does for radiation quanta, they set up an integral expression giving the effect of the cascade shower-scatter-shower-.... process on the mean square angles. They evaluate this expression and quote for the root-mean-square angle.

$$\theta_{rms} = 0.55\ (E_S/E)\sqrt{t}\ ,$$

where E is the emergent energy, for the electronic component. Now, the angular spread for the quanta should be the

same as that for the electrons, so one puts k' = 220 Mev for E and 3 for t and has θ_{rms} = 0.09 radians. Since the pair converter is about 200 inches away, one finds a root mean square displacement of about 18 inches at the converter. The converter has an average acceptance radius of perhaps 1.2 inches. Now, for a two-dimensional gaussian distribution, which we assume, the fraction accepted in θ_1 is

$$(2/\theta^2_{rms})\int_0^{\theta_1} \exp(-\theta^2/\theta^2_{rms})\,\theta d\theta = 1 - \exp(-\theta^2_1/\theta^2_{rms}).$$

Putting θ_1/θ_{rms} = 1.2/18 = 0.067, we have for the argument of the exponential -0.0044, and we have for the fraction of the degraded radiation accepted as 0.0044; using this, then, the fraction of the degraded radiation accepted, relative to the directly transmitted radiation in the given channel, is 0.5%.

As will be seen, this is of the same order of magnitude as our statistical error, and might show up if our estimate is not too large. Further, from some formulae that Rossi gives, concerning the longitudinal spread in showers, one may compute that, for this case, the maximum of the development should be at a depth near 3 radiation lengths. Thus, for thicker absorbers one would expect less degraded radiation. From these estimates, one feels that the errors due to degraded radiation should be unimportant.

To see if any effects from degraded radiation are revealed in the data, we divide the experimental cross sections by the theoretical ones, and plot the results against energy for the channels 2 through 12. These may be seen in

Figure 37, for aluminum, and Figure 38, for tin. The errors marked are the probable errors, as computed either from the statistics or from the observed fluctuations, whichever is greater. Also, for comparison, the data from DeWire, Ashkin, and Beach at 280 Mev are given (11).

These figures seem to show some hint of a systematic trend away from a theoretical horizontal line at unity. This trend is probably a reflection of the error in computing $G(\gamma_0)$. Any trend from this source is guaranteed to be systematic, since a smooth curve was obtained for $G(\gamma_0)$. Further, since the ranges of the variable γ_0 are considerably different for aluminum and for tin, one could easily expect the trend to take a different direction in each case. We have already estimated the magnitude of this error, citing Lawson's experience.

The agreement with the data of DeWire, Ashkin, and Beach is satisfactory and tends to confirm our low estimate for the effect due to degraded radiation.

There is no evidence for a systematic difference between the two absorber thicknesses. The data from the thick absorber will therefore be averaged with those for the thin, weighting these with regard for the errors. Channel 12 shows large errors, because its nominal energy of 490 Mev places it well down on the drop-off at the upper limit of the spectrum. It is therefore very sensitive to machine energy fluctuations, also having poorer statistics because of a low counting rate.

Channel 11 is not so badly off, but it too is fairly sensitive to machine energy fluctuations. Accordingly, data from these two channels will not be quoted in the final results as given in table 3, for all elements measured.

Agreement with theory is seen to be satisfactory.

C. RELATIVE PAIR PRODUCTION

The data were treated in the following manner. The background runs were first subtracted, proportioned according to the monitor reading M_1. The accidentals, proportioned according to the counting rate and the channel counts, were then subtracted. The resulting data were then divided by the monitor readings M_1, and averaged, within each channel, and for each converter foil separately. Experimental relative yields were then obtained by dividing the resulting data by that for the 5 mil aluminum foil, which was taken as the standard converter foil.

For the purpose of comparison to theory, one needs to compute the theoretical cross section for these elements. In computing this, one must remember that the partition corrections are not functions of channel number and channel energy alone; they are also functions of Z, the atomic number, although the variation with Z is quite slight. Advantage was taken of this fact by the following procedure. The partition corrections, as computed for aluminum, at the energies and channel numbers under consideration (Figure 27), were divided by the ratio of the total pair cross section

to that for equipartition ($v = \frac{1}{2}$), for aluminum. The resulting numbers, when multiplied by the ratio of the total pair cross section to that for equipartition for the element in question, were regarded as the proper partition corrections to be applied to the equipartition cross section for that element. The result is approximately correct, certainly adjusting the aluminum partition corrections in the right direction for application to other elements. Since these corrections never amount to more than about three or four percent, the error incurred by this shortcut treatment is negligible, being some small fraction of a percent.

The cross sections thus obtained, computed for the proper partitions, were next multiplied by the foil thicknesses in grams per square centimeter, as measured, and divided by the atomic weights. The results of these operations are divided by that for the 5 mil aluminum foil to give the theoretical relative yields.

The results, expressed as the ratio of experimental results to theory are given in Table 4. The errors given there are probable ones, computed from the statistics or from the fluctuations, whichever are larger. These errors include the estimated error due to the mass determination of the converter foils, and their impurities.

It is interesting to compare the two aluminum foils. The comparison shows that the thinner (1 mil) foil shows a higher yield, per thickness unit, than the 5 mil foil, by an amount larger than the probable error. Comparison among

the copper foils shows a similar, but not so striking, trend. This may be explained by the greater loss of pairs resulting when the thicker foil is used, this loss being due to multiple scattering in the vertical direction. This tends to confirm our conclusions explaining the behavior of the data for the low energy portion of the bremsstrahlung spectrum. If we are right, the need for using quite thin foils, in future uses of the spectrometer, is clearly indicated. We shall use these data to make a correction to the beam calibration.

Table 4 shows the data to be in satisfactory agreement with the theory, for relative pair production cross sections.

D. INTENSITY CALIBRATION

This calibration will be interpreted as a calibration of the thick-walled ionization chamber used as a standard monitor by the Synchrotron Laboratory (23). When one wants to know how many photons have been put out by the synchrotron, in a given energy interval, one must refer to the monitor record. The response of this ionization chamber is proportional to the energy intercepted by it (22), and for a given spectrum shape, its response is proportional to the energy carried by the incident beam. Thus if one writes $N(k)dk$ as being the number of photons emitted by the synchrotron, these photons having energy k in the interval dk,

the monitor response will be

$$q = (1/Q)\int_0^{E_o} kN(k)dk,$$

where E_o is the machine energy, q is the monitor response in coulombs, $1/Q$ is the monitor sensitivity in coulombs per Mev, and the integral clearly represents the energy carried by the beam, in units of Mev. It is the constant Q which is to be determined by the beam calibration.

We write, in accordance with the above,

$$N(k)dk = (qQ/E_o)I(\tfrac{k}{E_o})dk/k,$$

where $I(\frac{k}{E_o})$ is the intensity spectrum, so normalized that

$$\frac{1}{E_o}\int_0^{E_o} I(\tfrac{k}{E_o})\ dk = \int_0^1 I(u)du = 1,$$

where $u = k/E_o$. I(u) is plotted in Figure 2. This is the theoretical curve, justified by the spectrometer measurements, modified only by being computed for a 4% machine energy spread. The normalization means that its average height is unity. The dashed curve is drawn for no machine energy spread, and is not normalized, but is drawn to the same scale. This spectrum was computed for E_o = 500 Mev, but is such a slow function of E_o that it may be used for neighboring values of machine energy.

The spectrometer response will be, for the number of counts,

$$C_{12} = N(k)(\Delta k)_{12} T\ \sigma(k,v)(\Delta k/k)_{12}$$

where T is the thickness of the converter foil in atoms per square centimeter, and $\sigma(k,v)$ is the cross section for pair

creation. Here, the partition v = 0.5 applies.

Putting in the expressions for $N(k)\Delta k$, we can solve for qQ, and have

$$qQ = \frac{E_o C_{12}}{I(u)\ T\ \sigma(k,v)} \left(\frac{k}{\Delta k}\right)^2_{12}.$$

Now C_{12}, when background and accidentals were subtracted, came out to be 21.05 per bip. We increase this by 1.5% as being the loss due to multiple scattering as indicated by comparison among the converter foils, examining the Cu and Al data in Table 4. Thus, for C_{12} we use 21.37 per bip. Referring to Table 1, for channel 12, we find that for $(k/\Delta k)^2_{12}$ we have 674.3, allowing for the fact that the detector width is 0.982 inch instead of exactly one inch. The machine energy is E_o = 507.2 Mev, corresponding to "895" on the dial, as recorded. For this, and k = 311 Mev, I(u) = 0.906. We compute $\sigma(k,\frac{1}{2})$ = 1.152 barns, using the Bethe-Heitler formulae, as corrected for the Born approximation, and the Wheeler and Lamb formulae for the electronic contribution. For the 5 mil aluminum foil we have T = 6.548×10^{20} atoms per square centimeter. Putting all these things together, we find

$$qQ = 1.069 \times 10^{10} \text{ Mev per bip.}$$

The charge q collected per bip was determined to be 2.185×10^{-9} coulomb. Thus we determine for Q

$$Q_{exp} = 4.894 \times 10^{18} \text{ Mev per coulomb.}$$

This is, of course, for the temperature and pressure at which the experiment was performed: 74.58 centimeters of mercury and 24.0 degrees centigrade. The sensitivity of the ionization chamber increases with the density of the gas in the chamber; this gas is air, the interior of the chamber communicating with the atmosphere. To adjust Q to conditions of standard temperature and pressure, we multiply by (273/297) x (74.58/76.00) and obtain

$$Q_{stp} = 4.414 \times 10^{18} \text{ Mev per coulomb.}$$

For this determination, one source of error is in the integrator calibration; this comes principally from uncertainty regarding the current applied, because of the possibility of not having established the bias on the electrometer tube properly. The error estimated for this calibration is 1%. For the counts, nearly 10^4 counts were collected so that the statistical root mean square error is 1%, or a probable error of 0.7%. Also for the counts is some uncertainty about the bias setting. Referring to Figure 18, we see a variation, not accounted for by the accidental rate variation, of 4%; we take half of this, as a probable error of 2%, from this source. The error in determining scattering loss is 0.5%. We have not allowed for loss due to angles between pairs, and we take a 0.5% shift and error from this source. For converter thickness and possible impurities we allow another 1%. From our comments about the pair cross section calculations, we see that we ought to allow 1% error. We do not assume any error for the shape of the spectrum, since we are taking this as a standard, and we

are not concerned with errors in the absolute value of the bremsstrahlung cross section, in any event. The error in machine energy we take as 0.5%. Putting all these together, we quote an error of 2.9%. Thus we have

$$Q_{stp} = (4.44 \pm 0.13) \times 10^{18} \text{ Mev per coulomb.}$$

This ionization chamber had been calibrated previously by means of experimental studies of cascade showers, in the manner of Blocker, Kenney, and Panofsky (22). This calibration was performed by James C. Keck and others. The value they obtained (35) for Q was $(4.12 \pm 0.20) \times 10^{18}$ Mev per coulomb, at standard temperature and pressure. The disagreement, of nearly 3 probable error units, may not be too distressing in view of the quite different methods used.

V. CONCLUSION

The pair spectrometer has proven itself to be a powerful instrument, capable of obtaining large amounts of precision data in rather short operating times. We were able to obtain all of the data for the bremsstrahlung spectrum in less than one day.

The overall spectrum shape has been verified, using these data, with an accuracy of three or four percent; this represents a greater precision for this than for previous measurements of such spectra (12), (27), (36), (37), (38). Sufficient energy resolution was available to allow us to raise some questions concerning the detailed shape of the spectrum near its high energy limit.

This same resolution made possible a synchrotron energy calibration with a probable error of less than half a percent. In another experiment, we were able to provide an intensity calibration of the synchrotron x-ray beam, the probable error being a little less than three percent.

We have compared pair production yields in aluminum, copper and lead. The ratios of these yields compare with theory to within the probable error of about two percent in almost every instance. Assuming the theoretical pair production cross section for aluminum, we are able to give experimental cross sections for copper and lead over the range of from 221 Mev to 436 Mev.

Total absorption measurements have been made for carbon, aluminum, copper, tin, and lead. These are quoted over the range of from 383 Mev to 436 Mev. The experimental probable

errors are all near half a percent. Agreement with theory is obtained with an accuracy of about one percent, an error which is as large as the error expected to occur in the screening calculations used.

REFERENCES

1. W. Heitler, The Quantum Theory of Radiation, (1944), Oxford University Press.

2. O. Klein and Y. Nishina, Zeits. f. Physik, (1929), Vol. 52, p. 853.

3. H. A. Bethe and W. Heitler, Proc. Roy. Soc. (London), (1934), Vol. A146, P. 83.

4. R. P. Feynman, Phys. Rev., (1949), Vol. 76, P. 749.

5. H. A. Bethe and L. C. Maximon, Phys. Rev., (1954), Vol. 93, p. 768.

6. H. Davies, H. A. Bethe, and L. C. Maximon, Phys. Rev., (1954), Vol. 93, P. 788.

7. J. L. Lawson, Phys. Rev., (1949), Vol. 75, P. 433.

8. R. L. Walker, Phys. Rev., (1949), Vol. 76, p. 527.

9. R. L. Walker, Phys. Rev. (1949), Vol. 76, p. 1440.

10. R. L. Walker and B. D. McDaniel, Phys. Rev., (1948), Vol. 74, p. 315.

11. DeWire, Ashkin, and Beach, Phys. Rev. (1951), Vol. 83, p. 505.

12. J. W. DeWire and L. A. Beach, Phys. Rev., (1951), Vol. 83, p. 476(L).

13. Rosenblum, Schrader, and Warner, Phys. Rev., (1952), Vol. 88, p. 612.

14. McDonald, Kenney, and Post, Phys. Rev. (1954), Vol. 93, p. 951(A).

15. Bruno Rossi, High Energy Particles, (1952), Prentice Hall, Inc.

16. A. Borsellino, Phys. Rev., (1953), Vol. 89, p. 1023.

17. Matthew L. Sands, Private Communication, (July 10, 1951).

18. William R. Smythe, Static and Dynamic Electricity (1939), p. 372, McGraw-Hill Book Company, Inc.

19. J. F. Blackburn (Ed.), H. E. Kallmann, Components Handbook, Radiation Laboratory Series, (1949), Vol. 19, p. 211, McGraw-Hill Book Company, Inc.

20. R. L. Garwin, Rev. Sci. Inst., (1950), Vol. 21, p. 526(L).

21. G. A. Morton and J. A. Mitchell, R.C.A. Review, (1948), Vol. 9, p. 632.

22. W. Blocker, R. W. Kenney, and W. K. H. Panofsky, Phys. Rev., (1950), Vol. 79, p. 419.

23. California Institute of Technology, Synchrotron Laboratory drawing number 13-M-249, and Cornell University Laboratory of Nuclear Studies, drawing number CSD-345 (1951).

24. E. Segre (Ed.), H. Bethe and J. Ashkin, Experimental Nuclear Physics, (1953), Vol. I, p. 166, John Wiley and Sons, Inc.

25. J. A. Wheeler and W. E. Lamb, Phys. Rev., (1939), Vol. 55, p. 858.

26. B. Rossi and K. Greisen, Rev. Mod. Phys., (1941), Vol. 13, p. 240.

27. W. M. Powell, W. Hartsough, and M. Hill, Phys. Rev., (1951), Vol. 81, p. 213.

28. L. Eyges, Phys. Rev., (1949), Vol. 76, p. 264.

29. L. I. Schiff, Phys. Rev., (1946), Vol. 70, p. 87.

30. L. I. Schiff, Phys. Rev., (1951), Vol. 83, p. 252.

31. H. A. Bethe, Phys. Rev., (1953), Vol. 89, p. 1256.

32 A. Sommerfeld, Ann. Physik, (1931), Vol. 11, p. 257.

33 R. F. Bacher, J. C. Keck, V. Z. Peterson, J. G. Teasdale, A. V. Tollestrup, R. L. Walker, and R. M. Worlock, Phys. Rev., (1953), Vol. 92, p. 1090(A).

34. J. D. Jackson and J. M. Blatt, Revs. Modern Phys., (1950), Vol. 22, p. 77.

35. James C. Keck, Private Communication, (1954). (Also see C.I.T. Synch. Lab. Ntbk. no. 63 issued to Wm. Buchman, Dec. 1952.)

36. P. C. Fisher, Phys. Rev., (1953), Vol. 92, p. 420.

37. C. R. Emigh, Phys. Rev., (1952), Vol. 86, p. 1028.

38. R. H. Stokes, Phys. Rev., (1951), Vol. 84, p. 991.

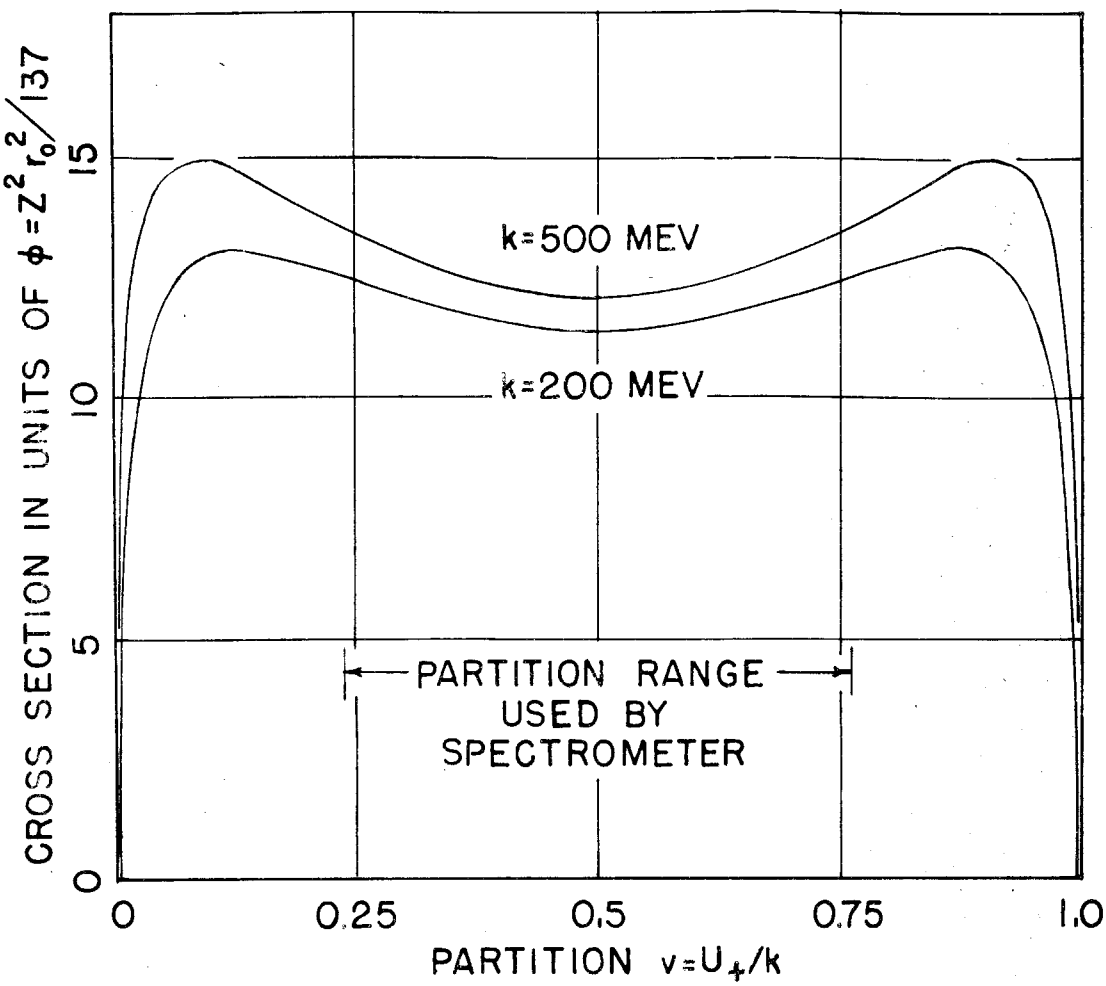

FIGURE 1. PAIR PRODUCTION CROSS SECTIONS IN ALUMINUM
The labels on the curves give the incident photon energies. The partition is the fraction of the incident photon energy borne by one member of the pair. The computation includes screening, pair production in the field of the atomic electrons, and the recent corrections to the Born approximation.

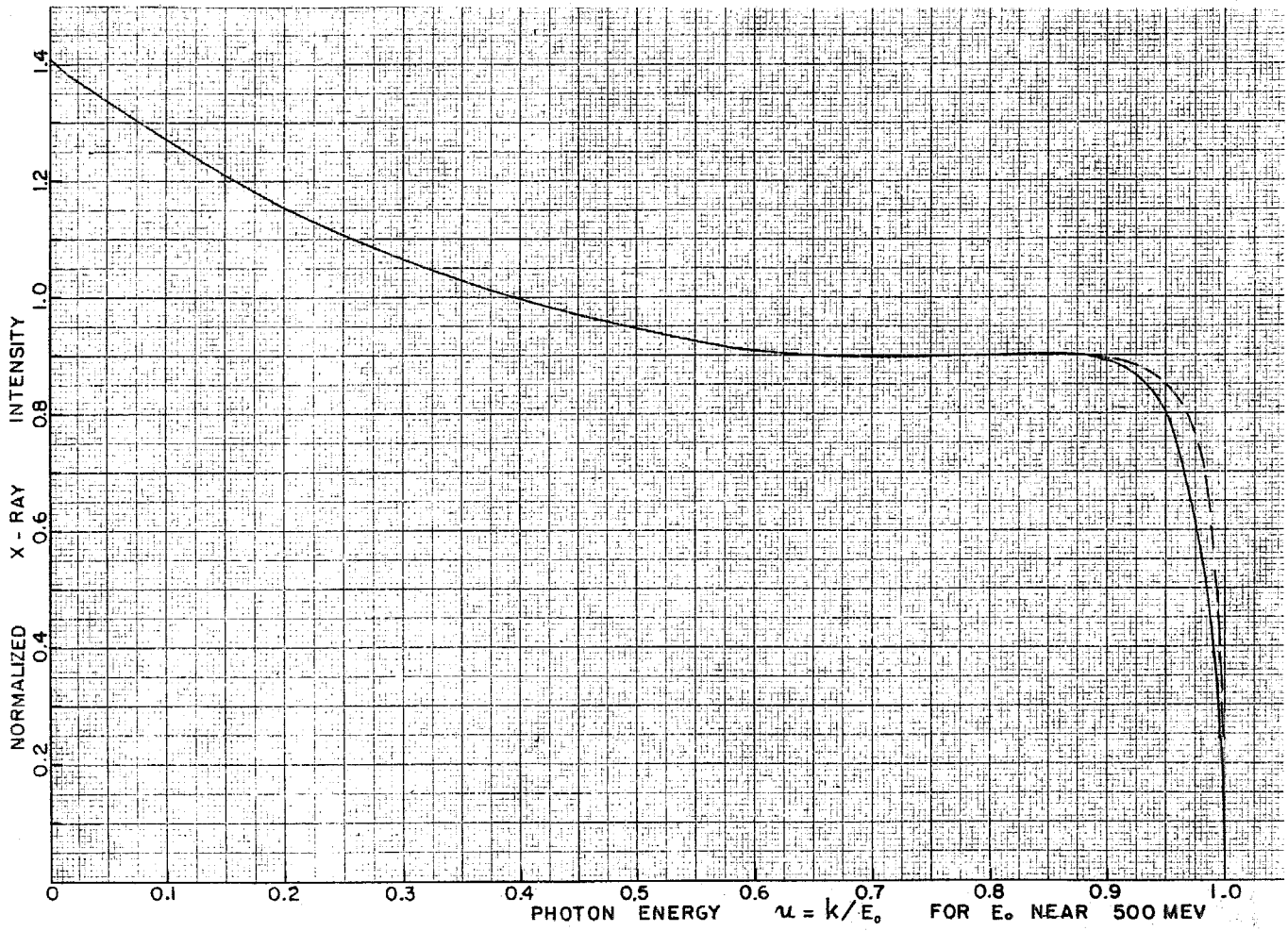

FIGURE 2. BREMSSTRAHLUNG SPECTRUM

The solid curve was computed for copper at E_o = 500 Mev and for a 4% spread in E_o. This curve has average height 1.000. The dashed curve is for no machine energy spread, and has somewhat greater average height.

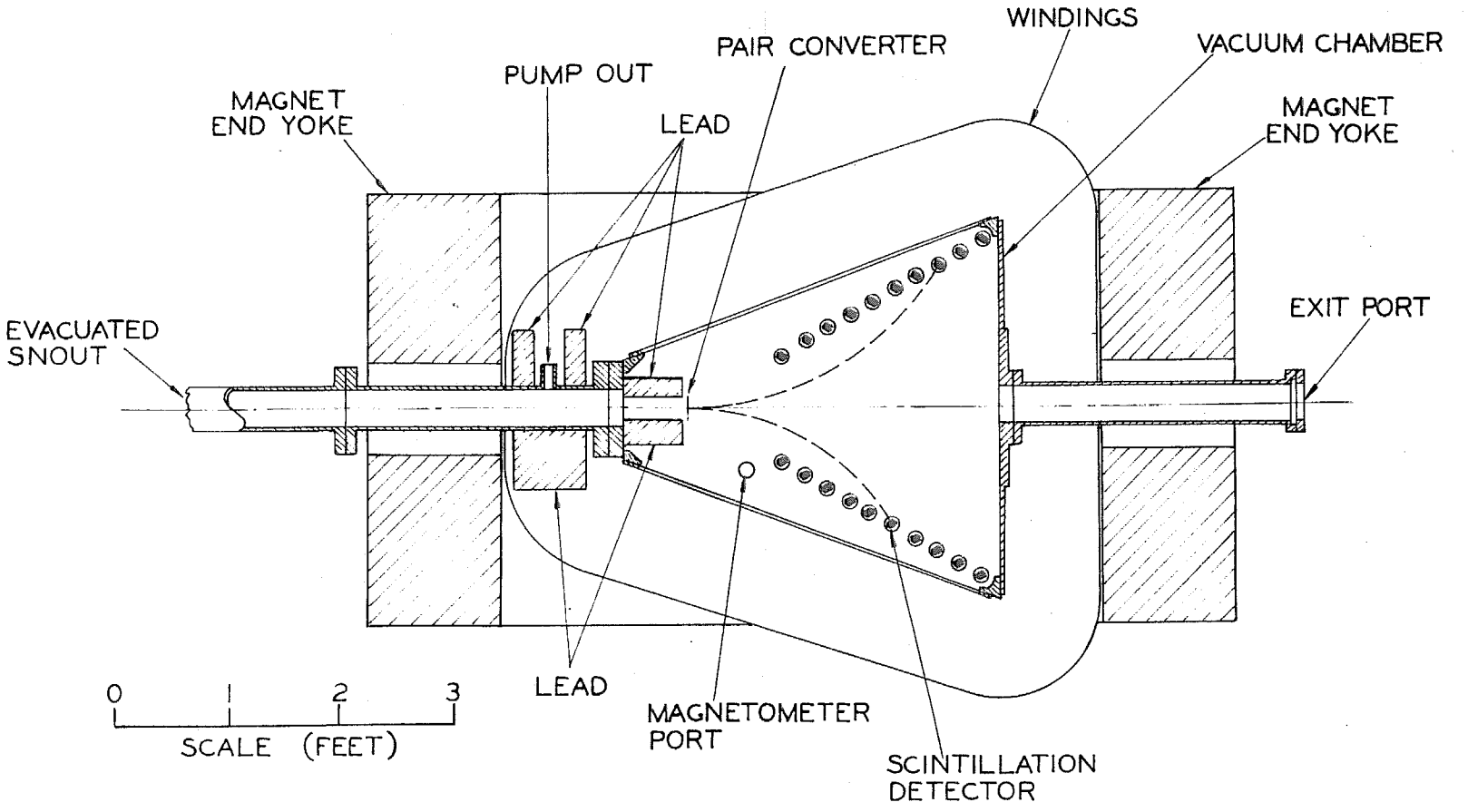

FIGURE 3. HORIZONTAL SECTION THROUGH MAGNET GAP

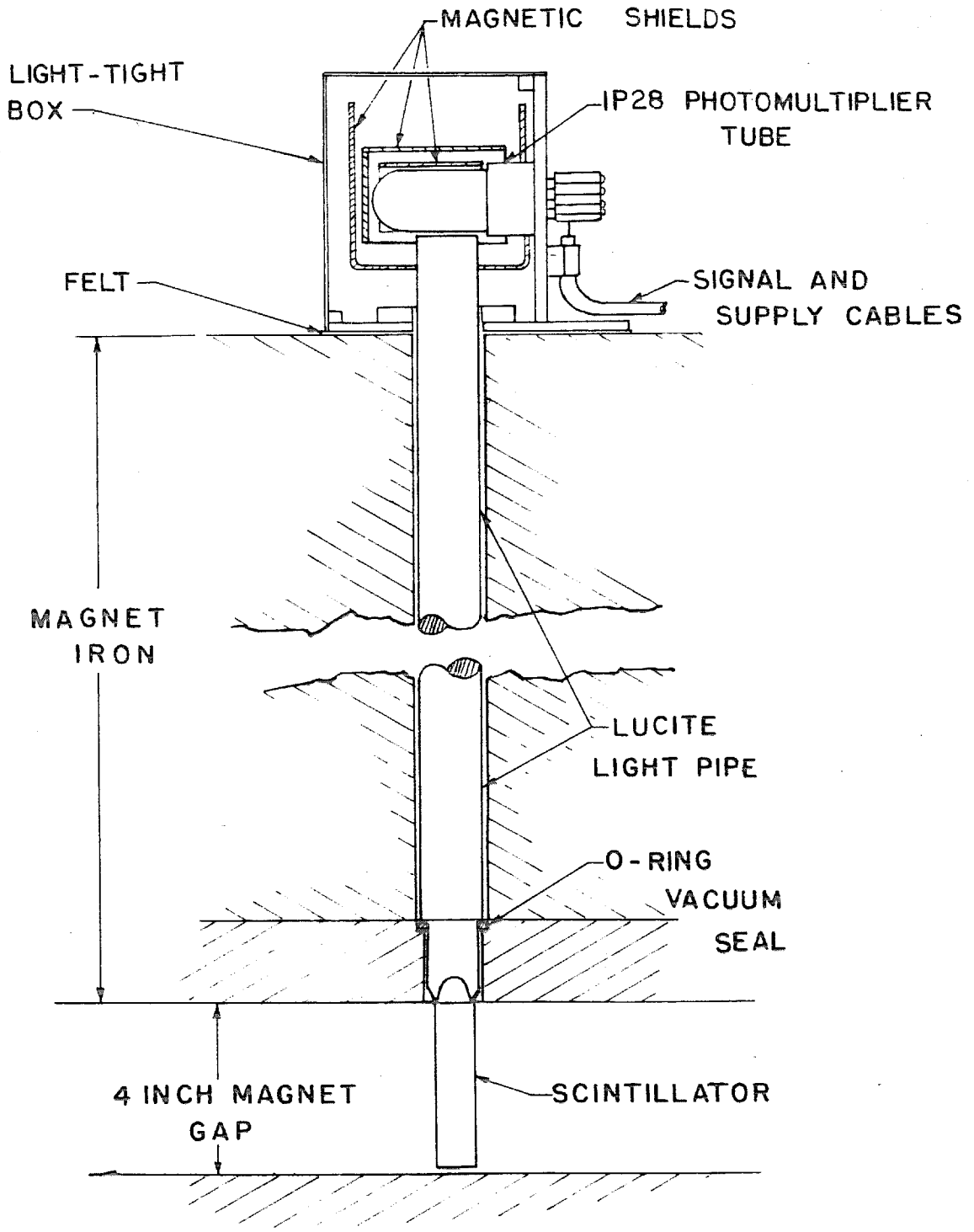

FIGURE 4. VERTICAL SECTION OF MAGNET
This is shown for one of the detector sites.

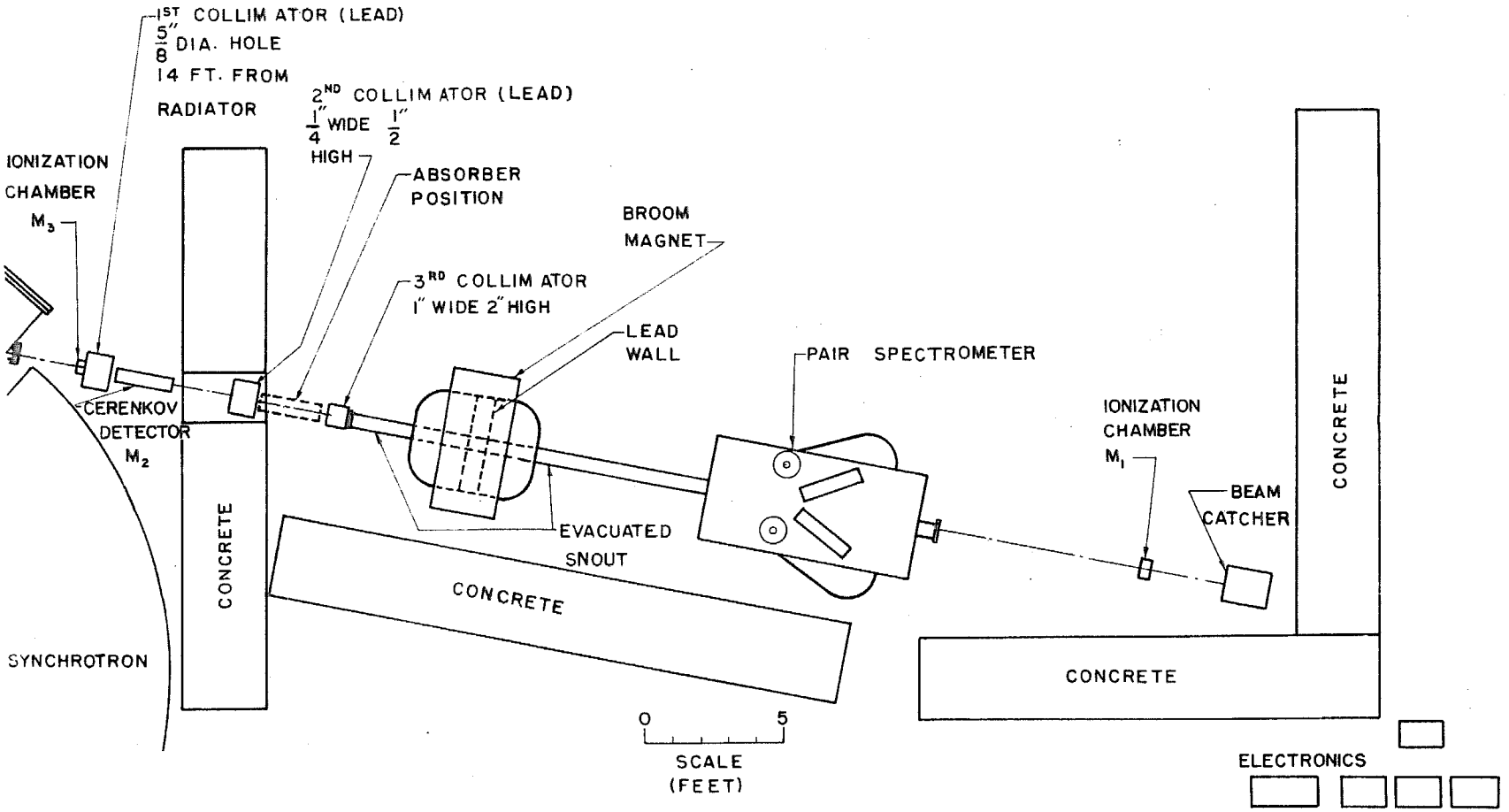

FIGURE 4. PLAN OF EXPERIMENTAL LAYOUT

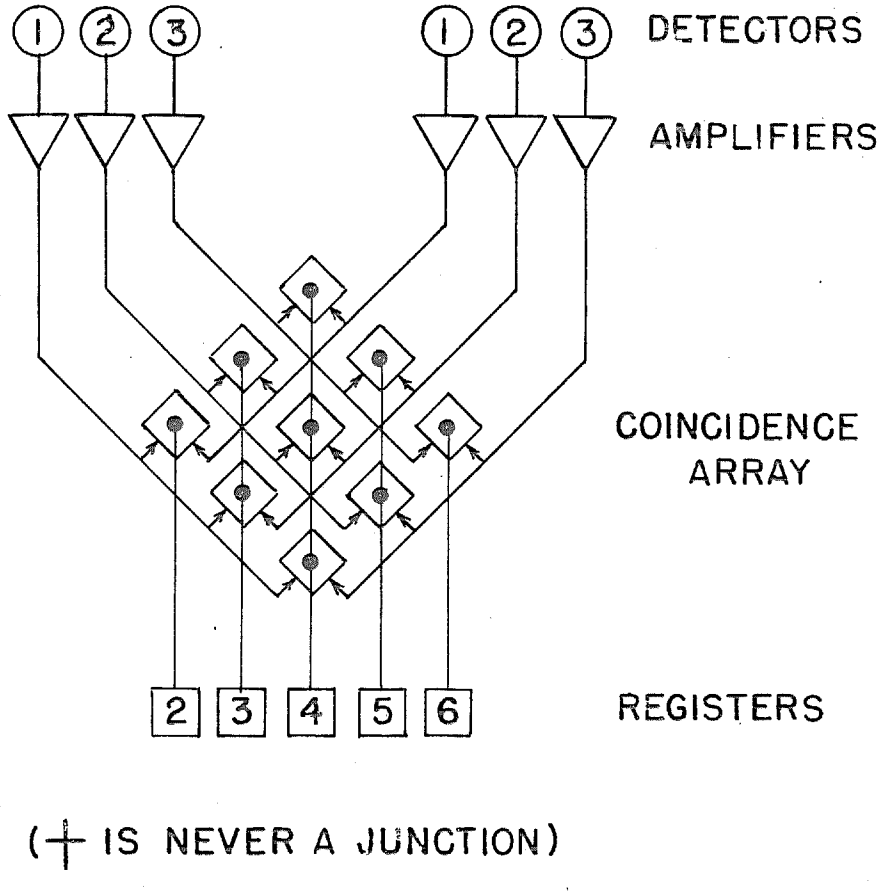

FIGURE 6. MATRIX COINCIDENCE ARRAY
A block diagram drawn for 3 detectors on each side of the V (n=3). The generalization to n=10 is obvious.

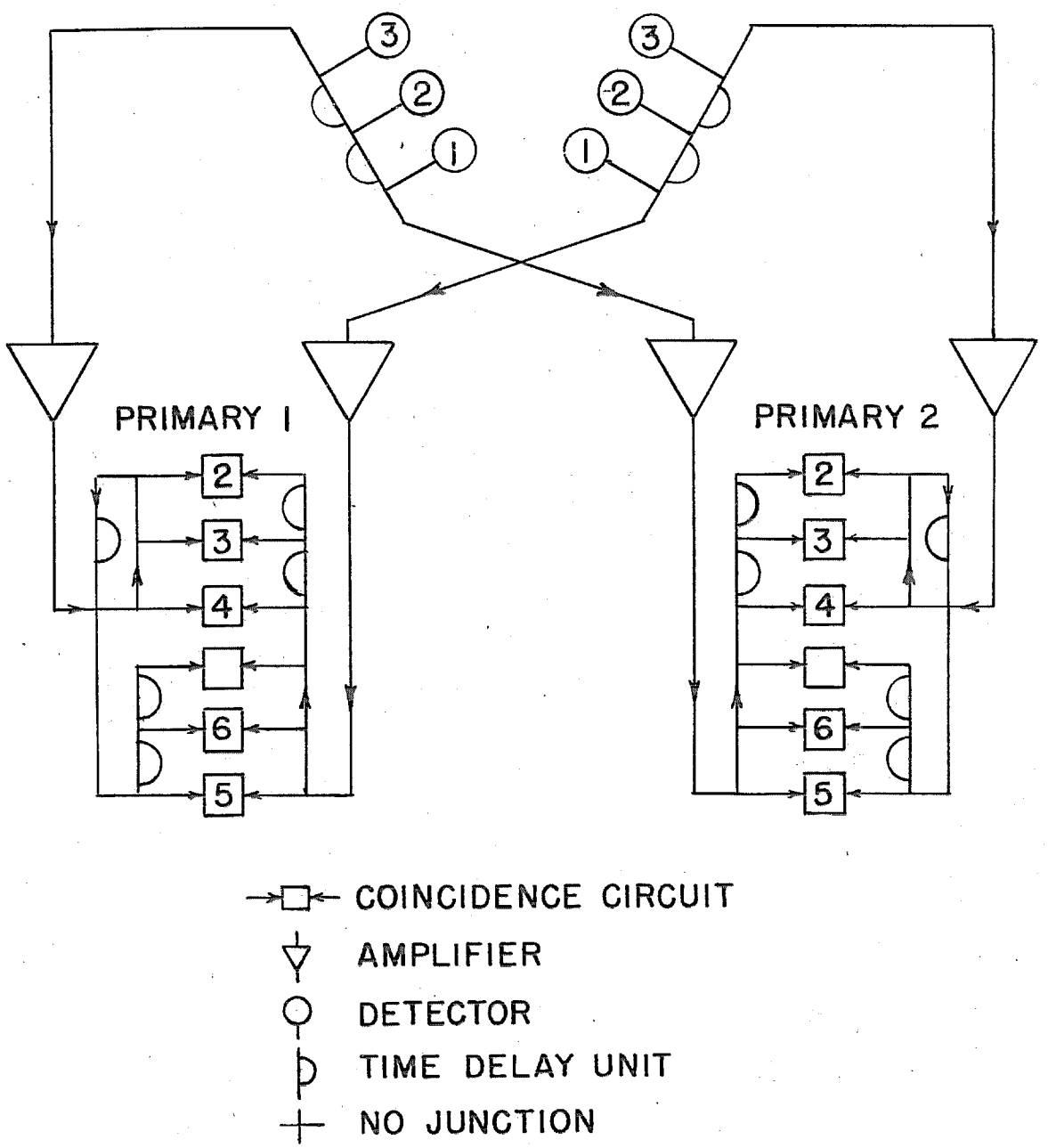

FIGURE 7. TIME DELAY MULTIPLEXING ARRAY
A block diagram drawn for 3 detectors on each side of the V (m=3). For operating principles refer to text.

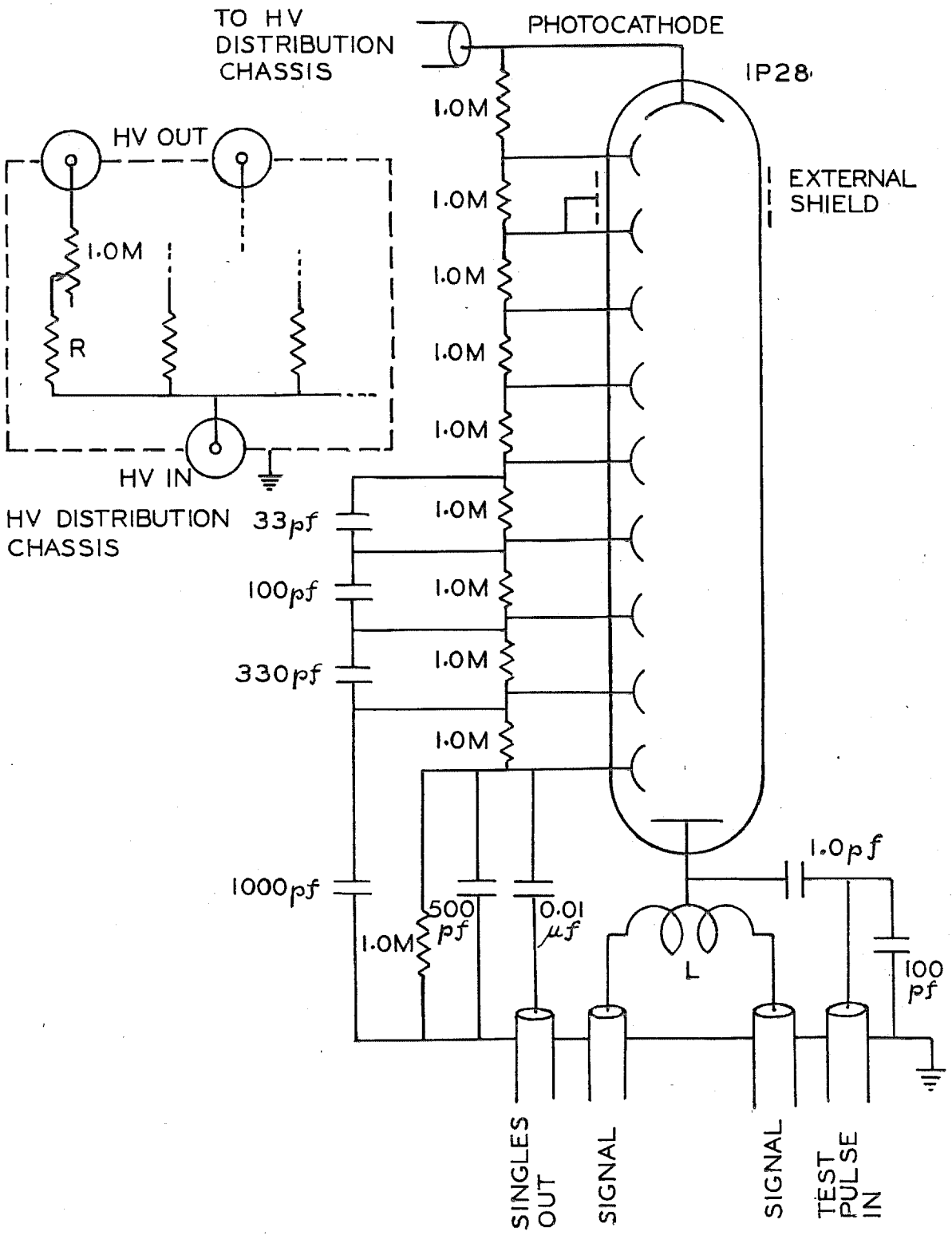

FIGURE 8. PHOTOMULTIPLIER BASE WIRING
A portion of the HV Distribution Chassis is also shown.

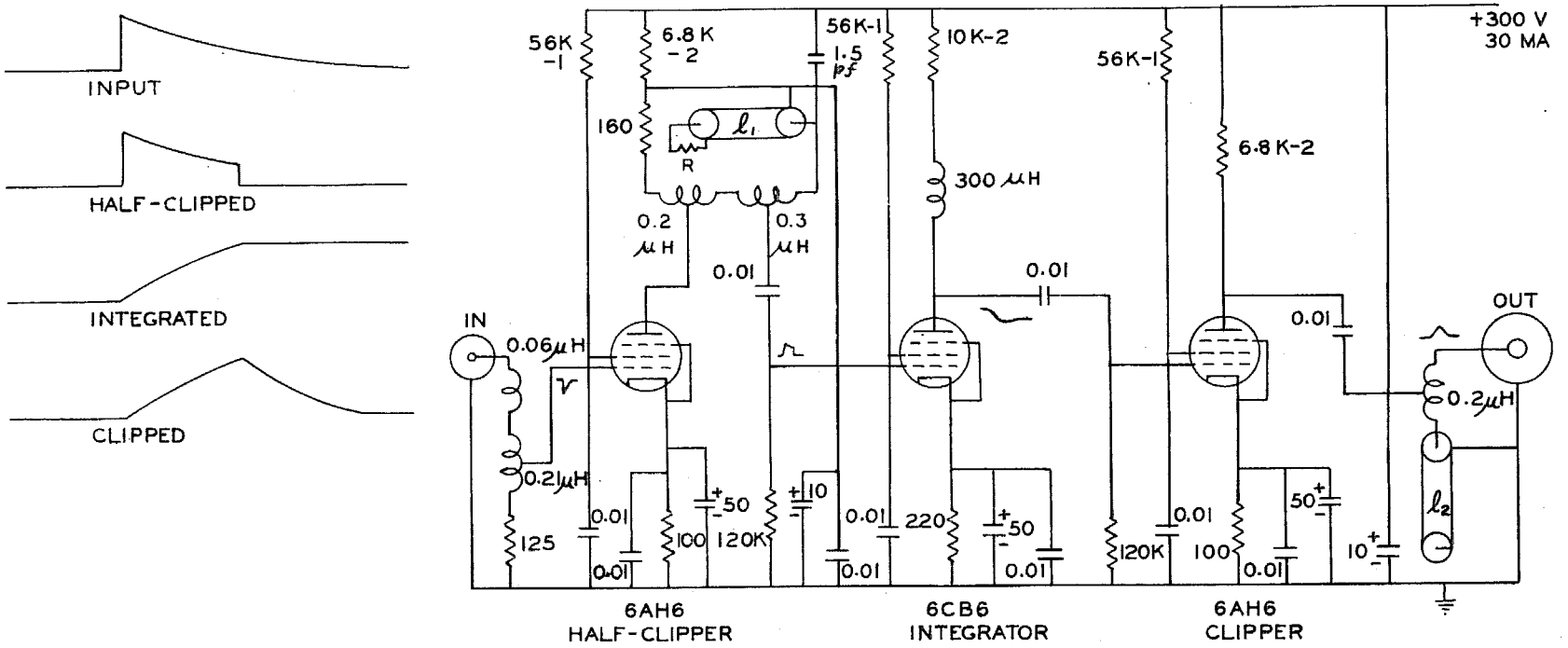

ℓ_1 = 1.05 M K 109

ℓ_2 = 1.14 M K 109

FIGURE 9. MODEL 30 PRE-AMPLIFIER

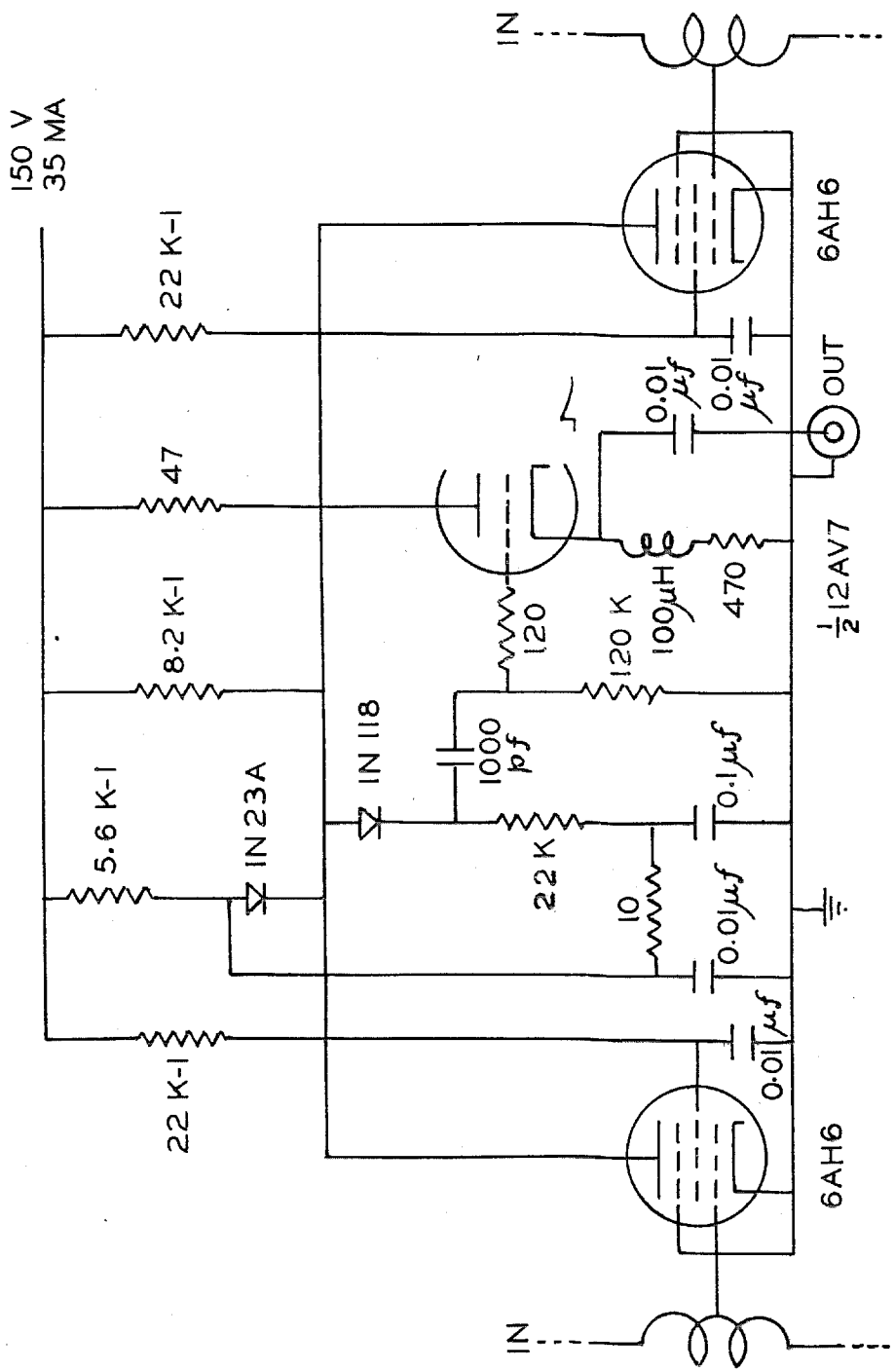

FIGURE 10. TYPICAL SECTION - PRIMARY COINCIDENCE
This is a Garmin circuit; the coincidence diode is marked IN23A.

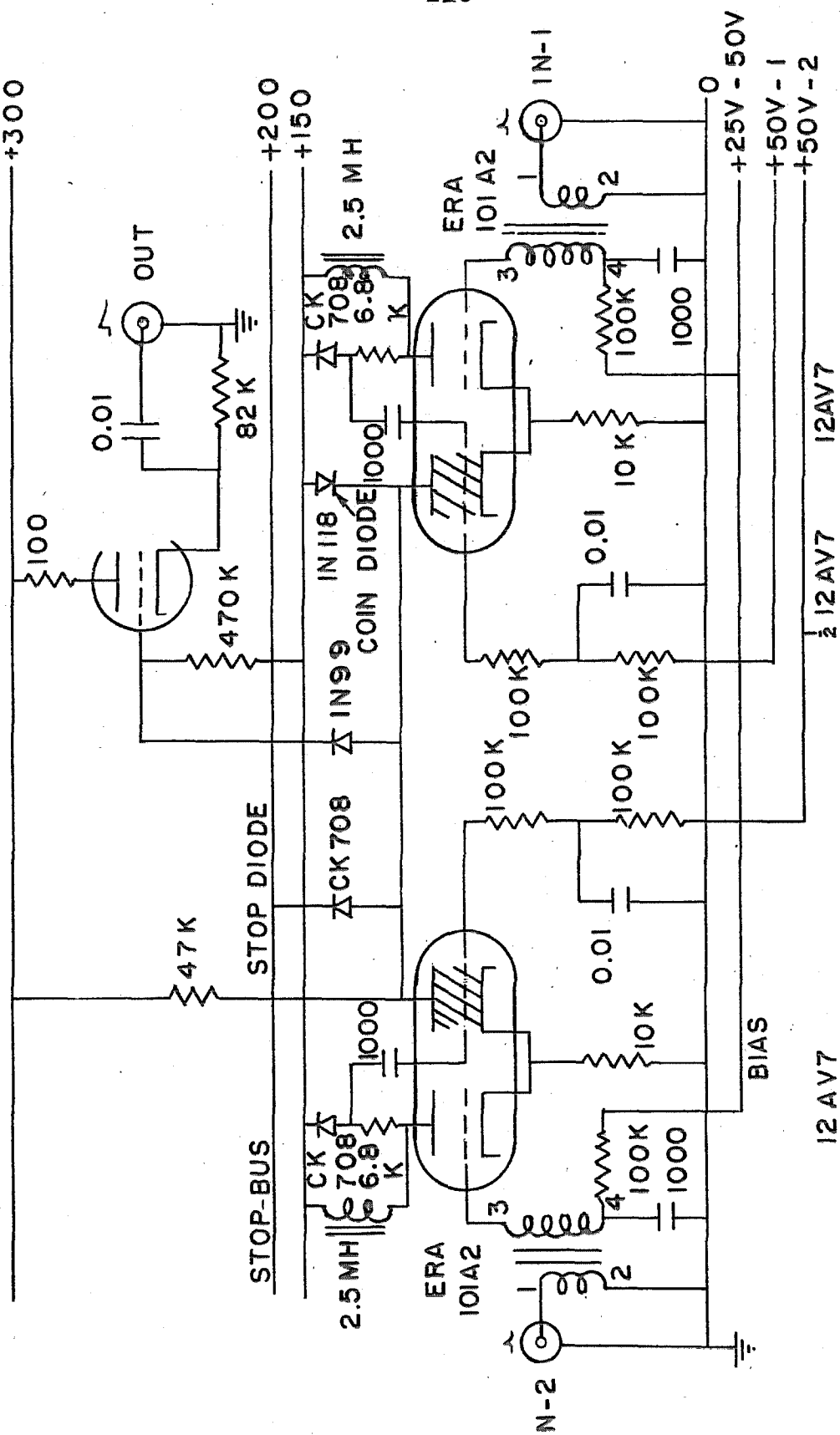

FIGURE 11. TYPICAL SECTION - SECONDARY COINCIDENCE

The diode marked IN118 is in a Garwin coincidence circuit in the anode circuits of the "on" halves of the 12AV7 multivibrators.

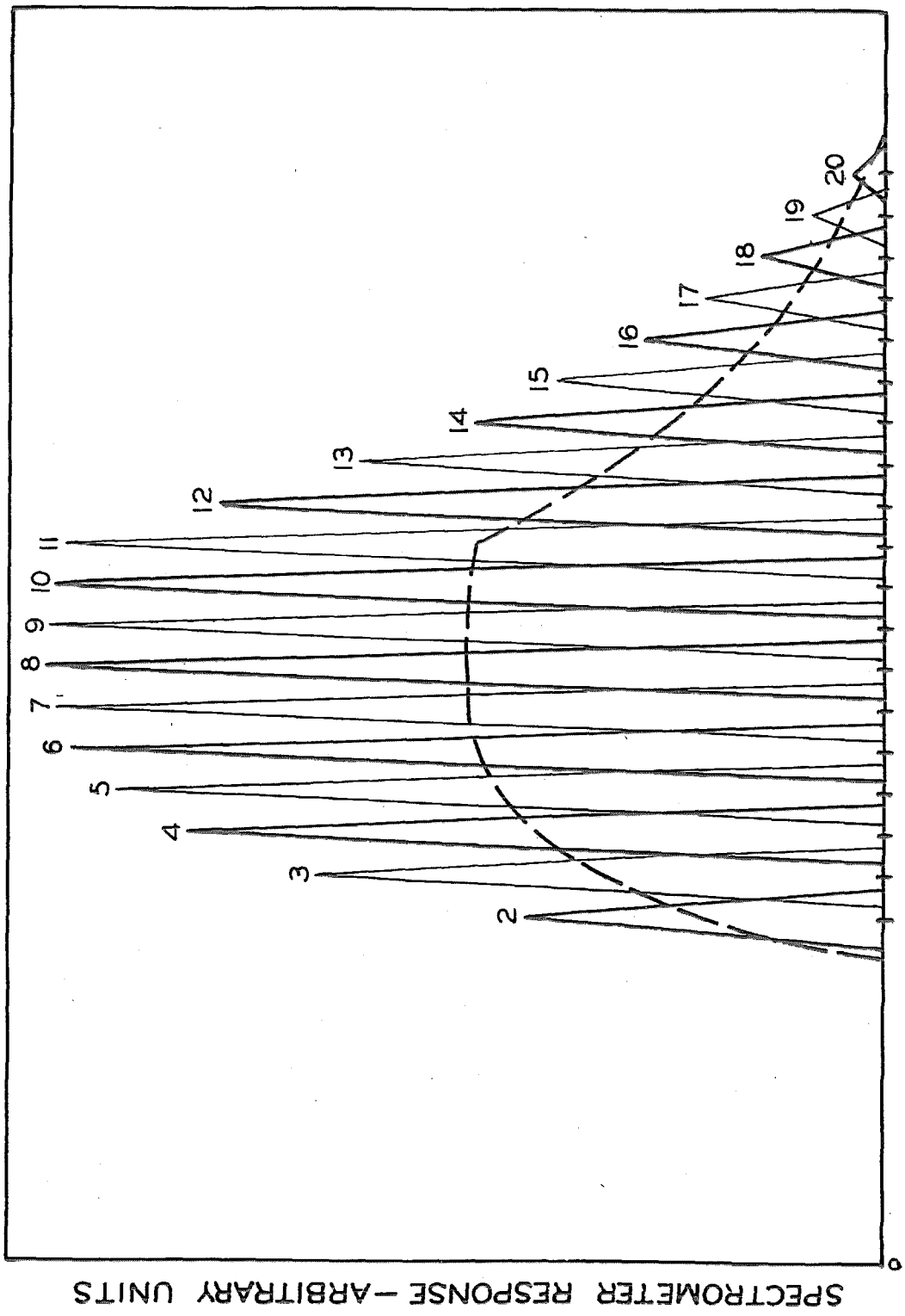

FIGURE 12. SPECTROMETER CHANNEL RESPONSE
This is for a uniform intensity spectrum. The dashed curve passes through the midpoint of the altitudes of the triangles. The triangles indicate the individual channel resolution functions (See Fig. 14).

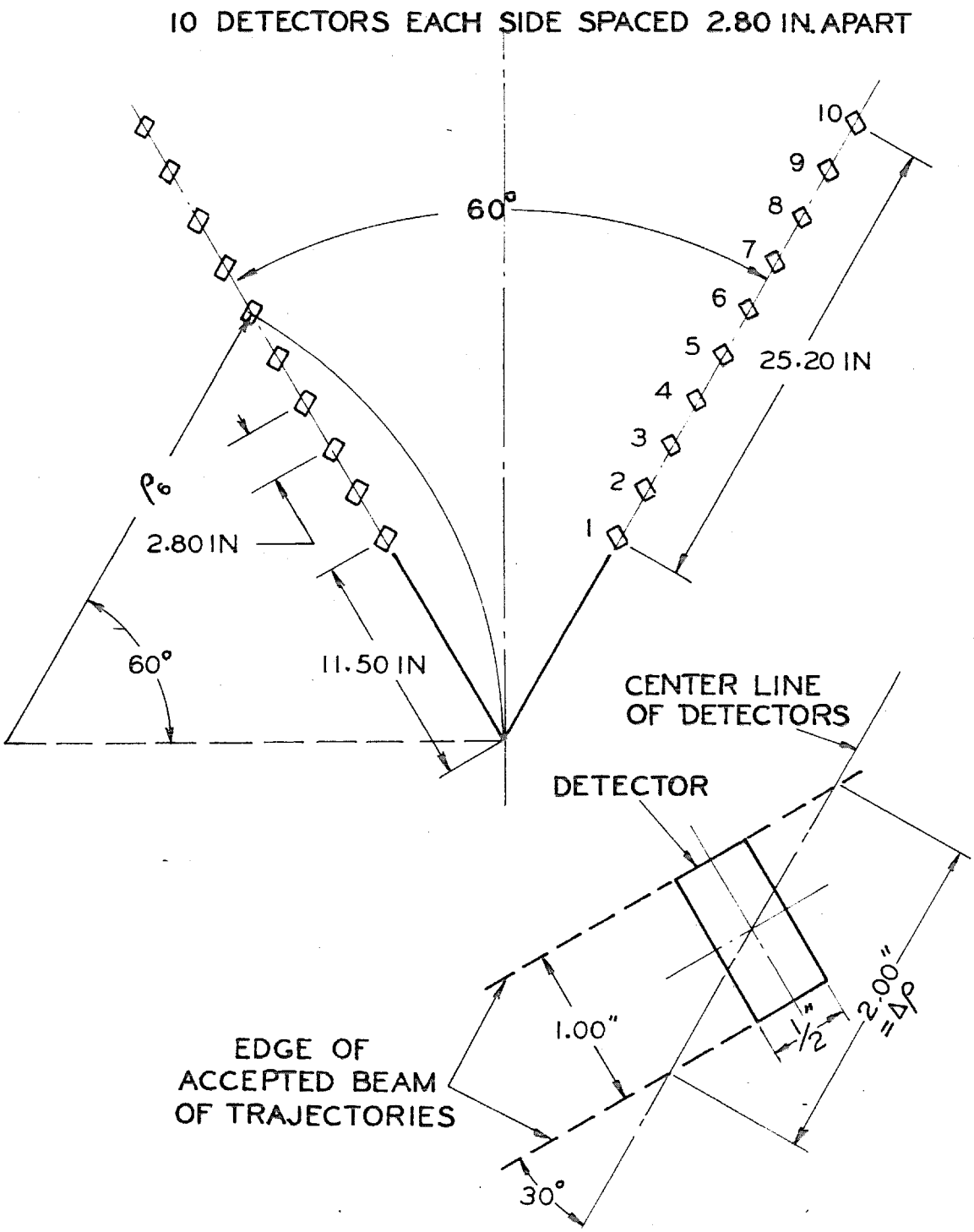

FIGURE 13. GEOMETRY OF DETECTOR CONFIGURATION

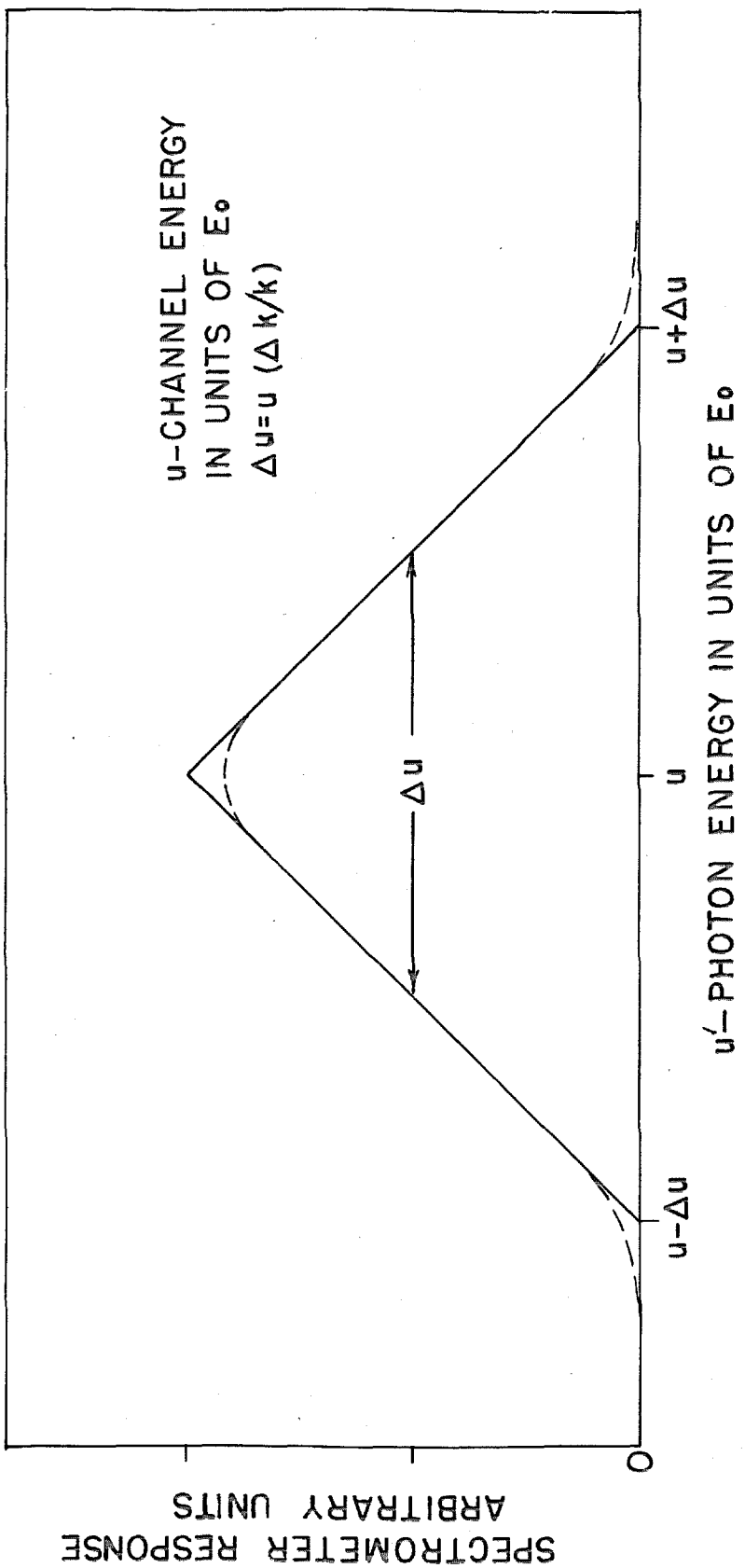

FIGURE 14. RESOLUTION FUNCTION
The dashed curves indicate the effects of a finite angular distribution for the electrons emerging from the converter for Channel 12 at 500 Mev.

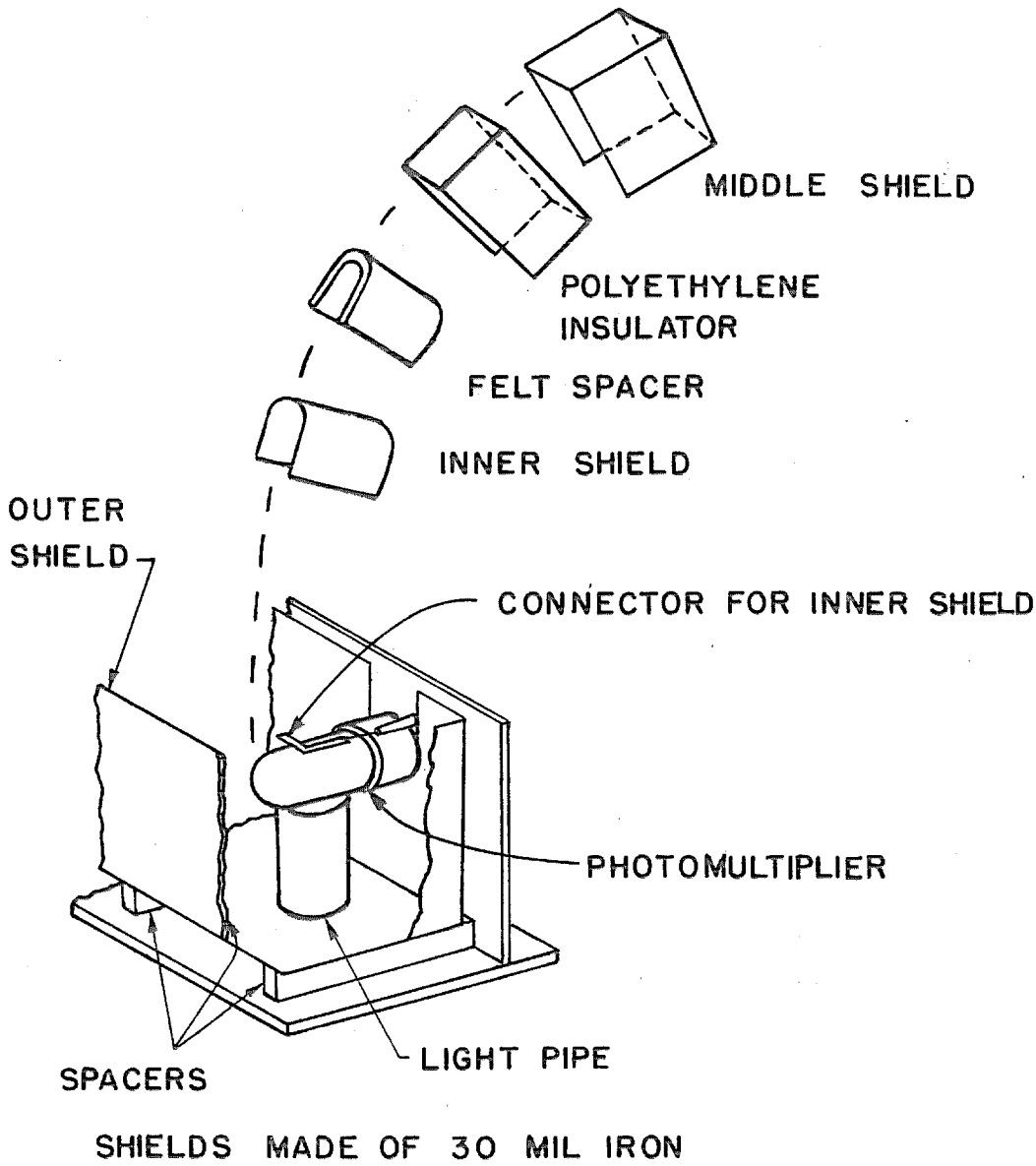

FIGURE 15. MAGNETIC SHIELDING FOR PHOTOMULTIPLIERS

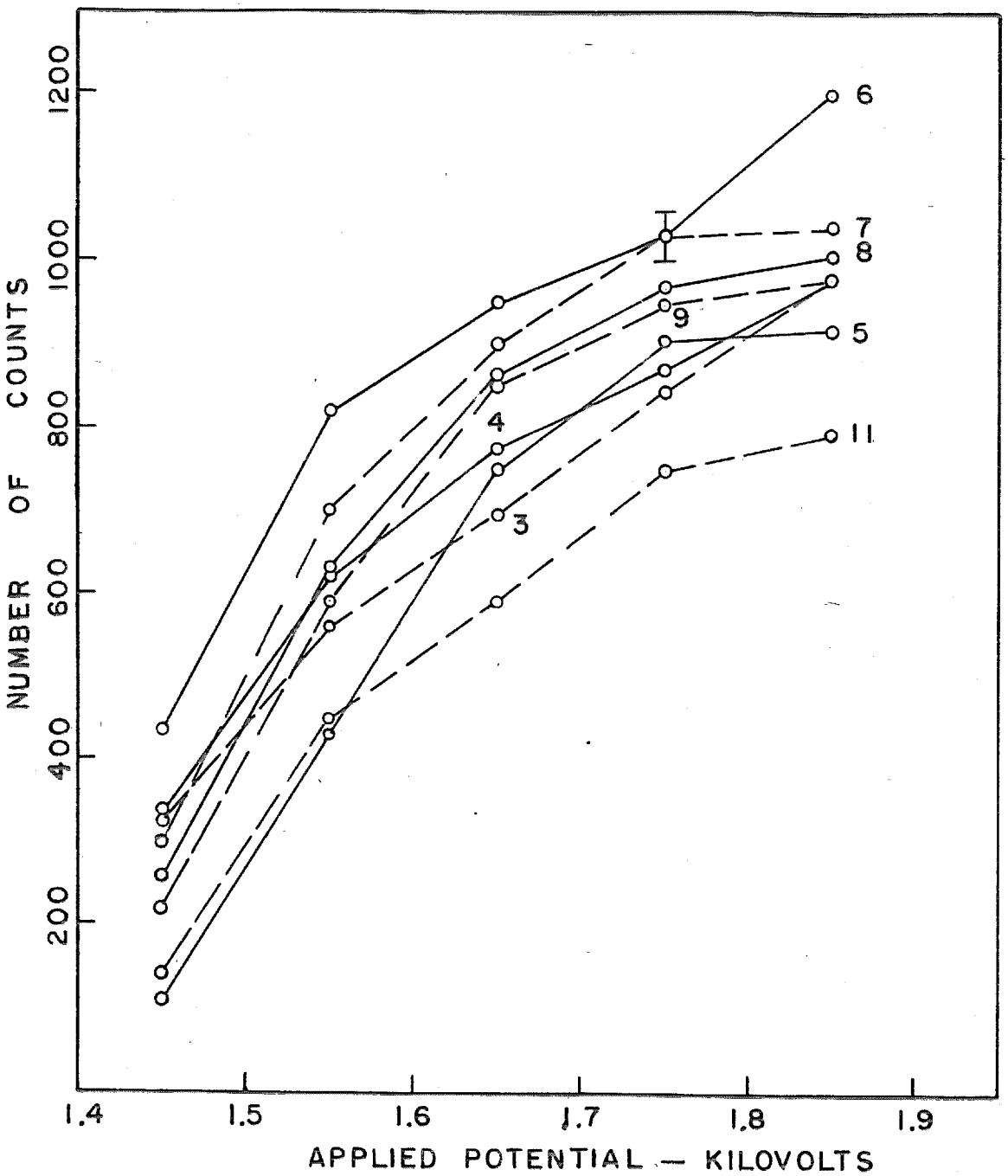

FIGURE 16. 1P28 HIGH VOLTAGE "PLATEAU" CURVES

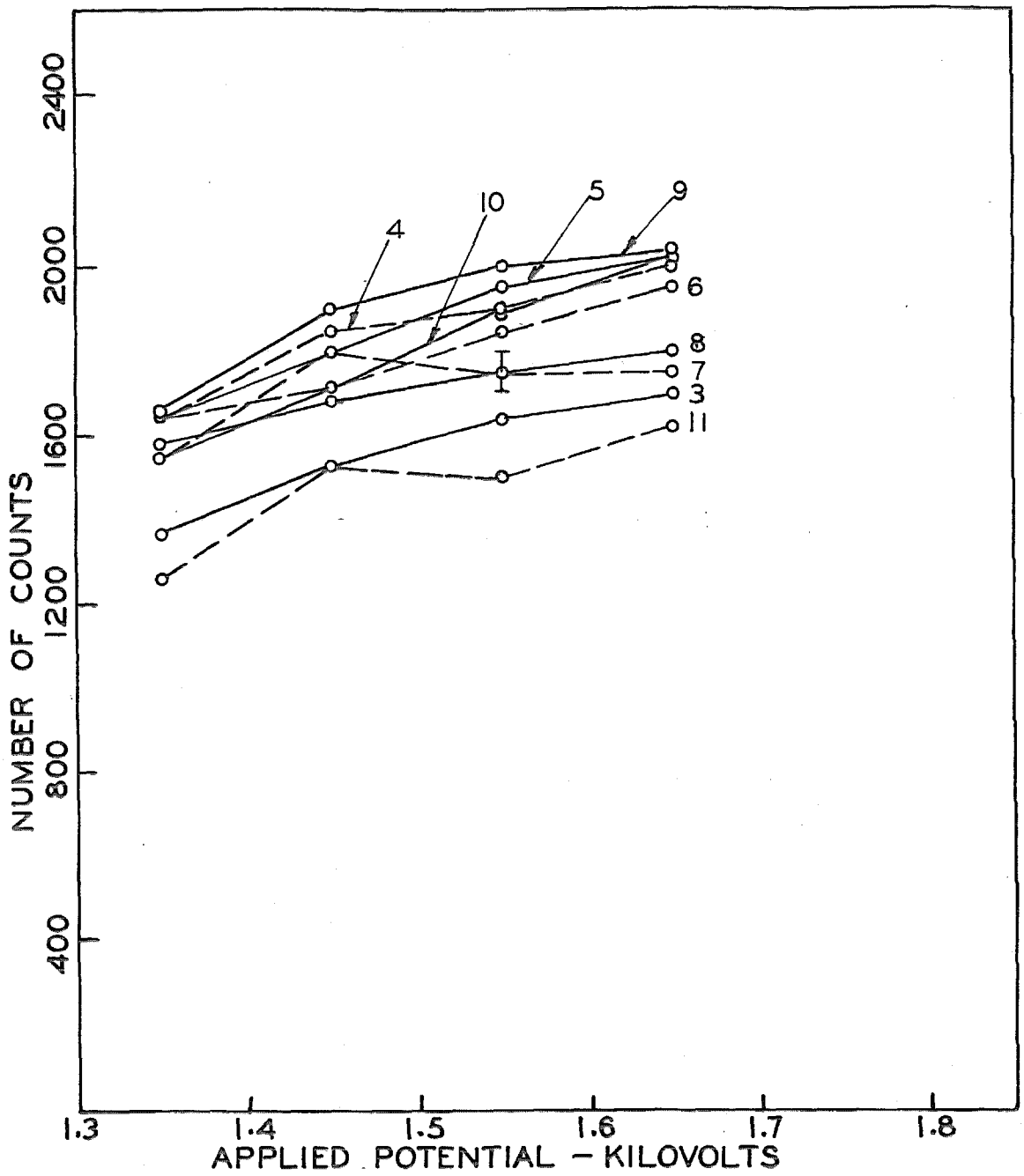

FIGURE 17. 1P28 HIGH VOLTAGE "PLATEAU" CURVES
An extra HP 460 A amplifier was used. Compare with Fig. 16.

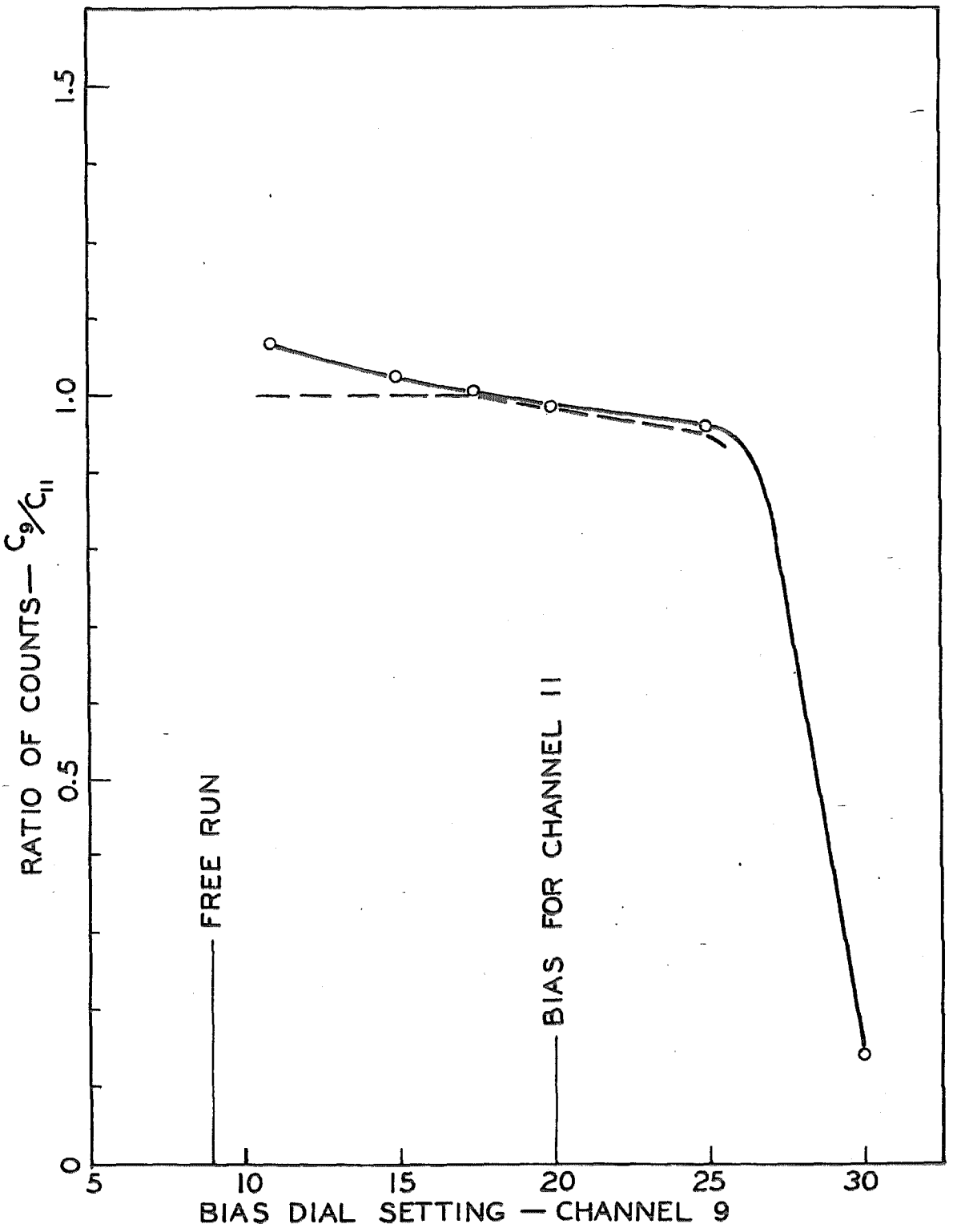

FIGURE 18. 5819 BIAS "PLATEAU" CURVE
The dashed curve shows the effect of subtracting accidentals.

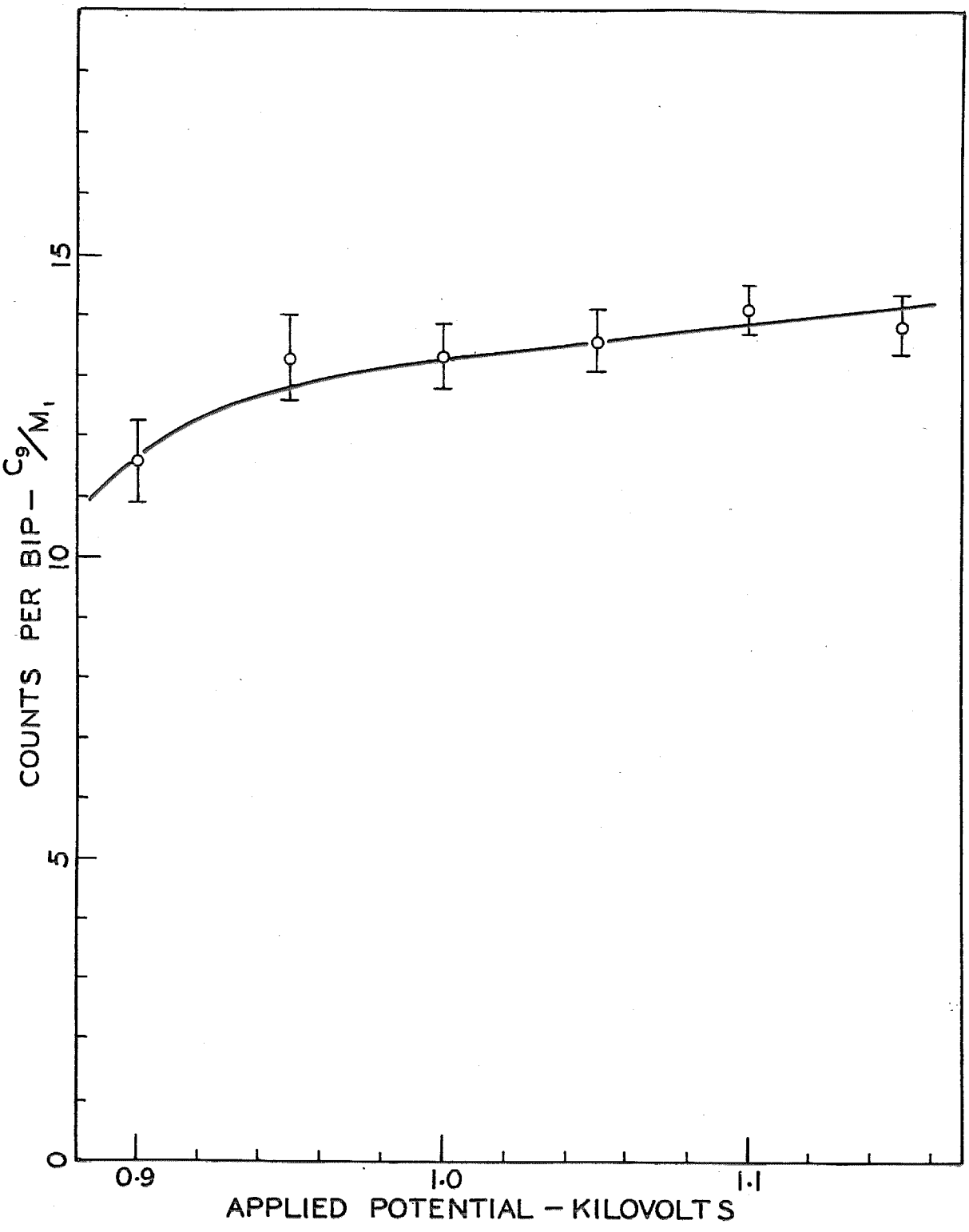

FIGURE 19. 5819 HIGH VOLTAGE "PLATEAU" CURVE

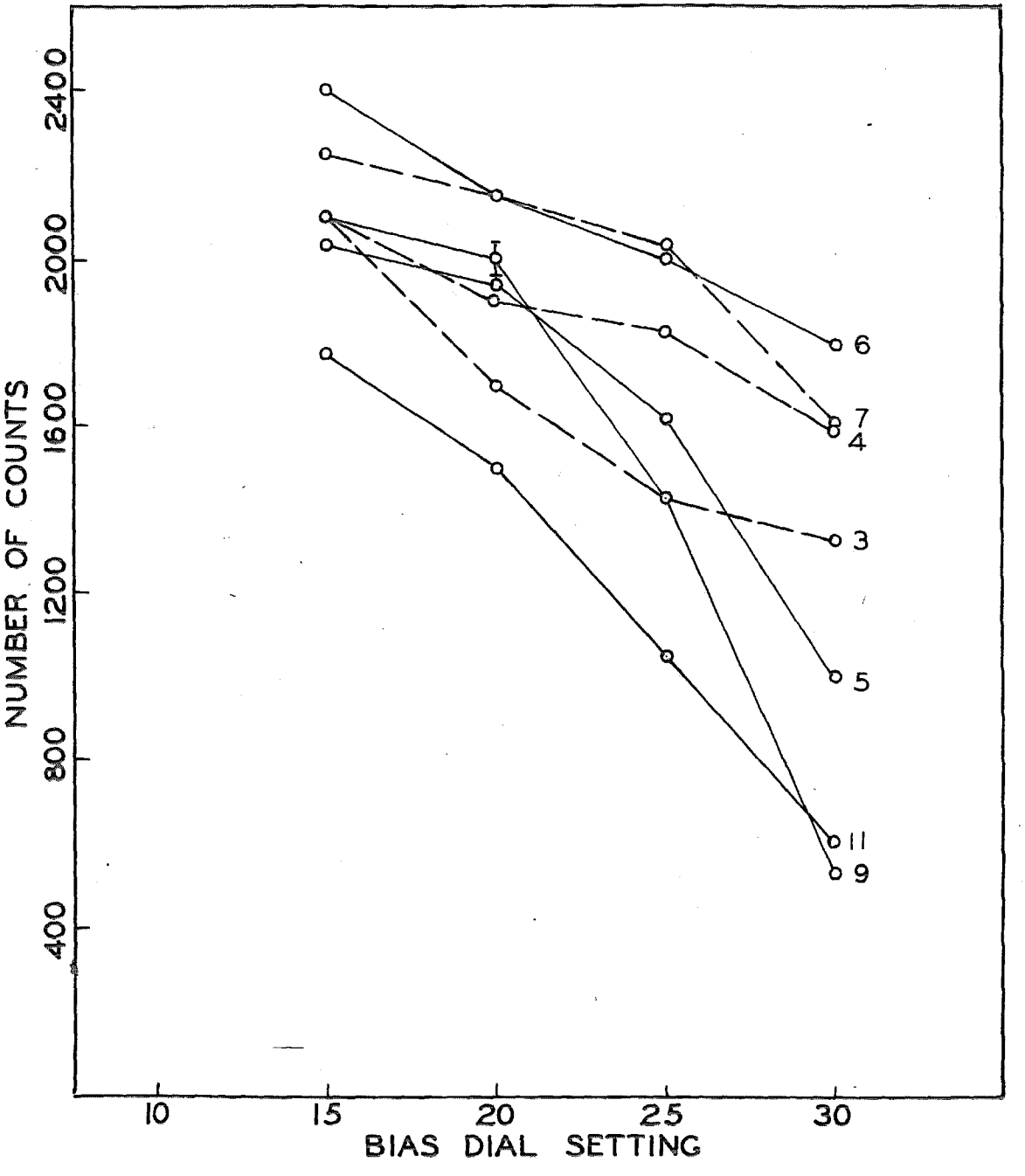

FIGURE 20. 1P28 BIAS "PLATEAU" CURVES

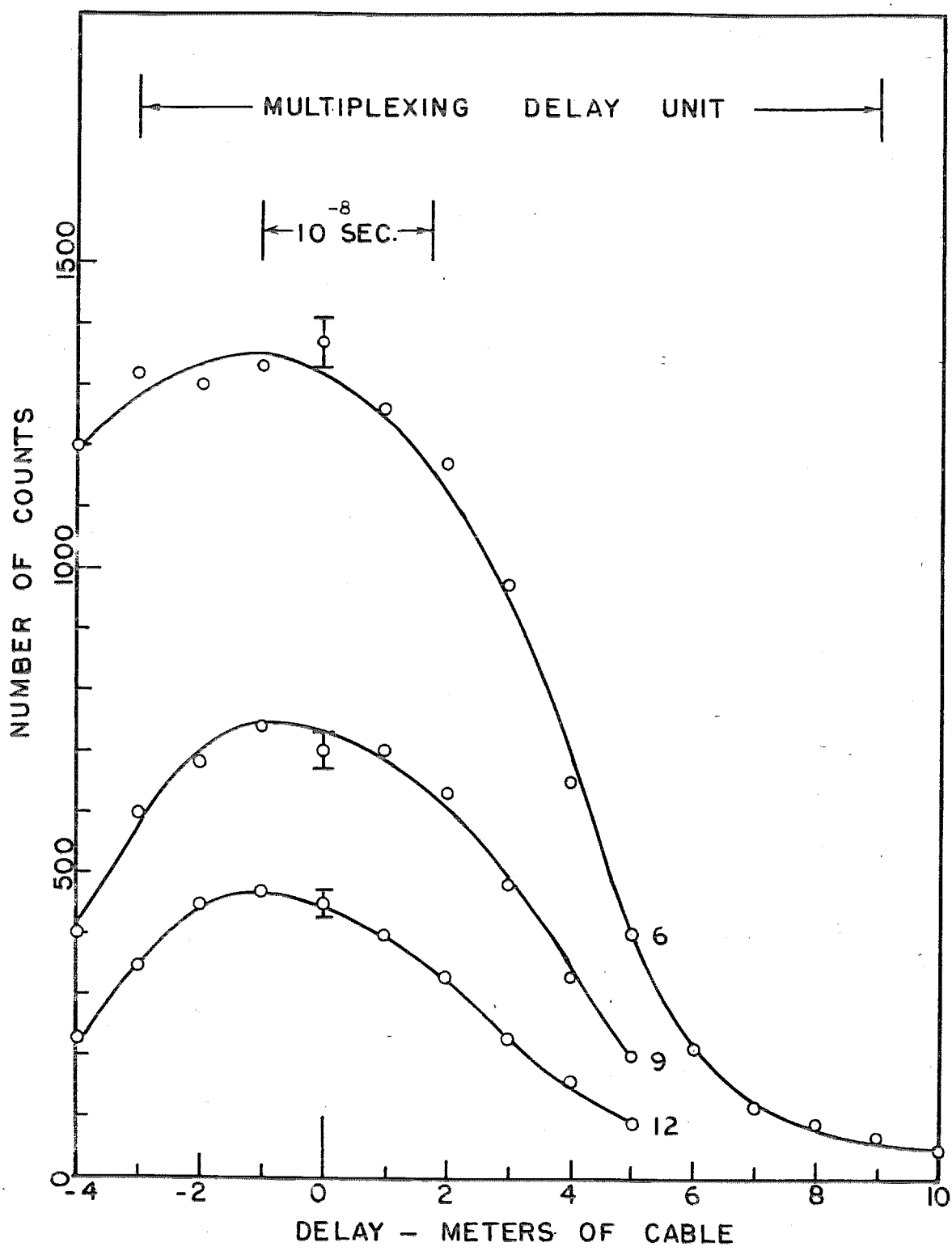

FIGURE 21. COINCIDENCE DELAY CURVES
For these, High Voltage was applied only to Phototube 5 on the left and 1, 4, 7, and 10 on the right.

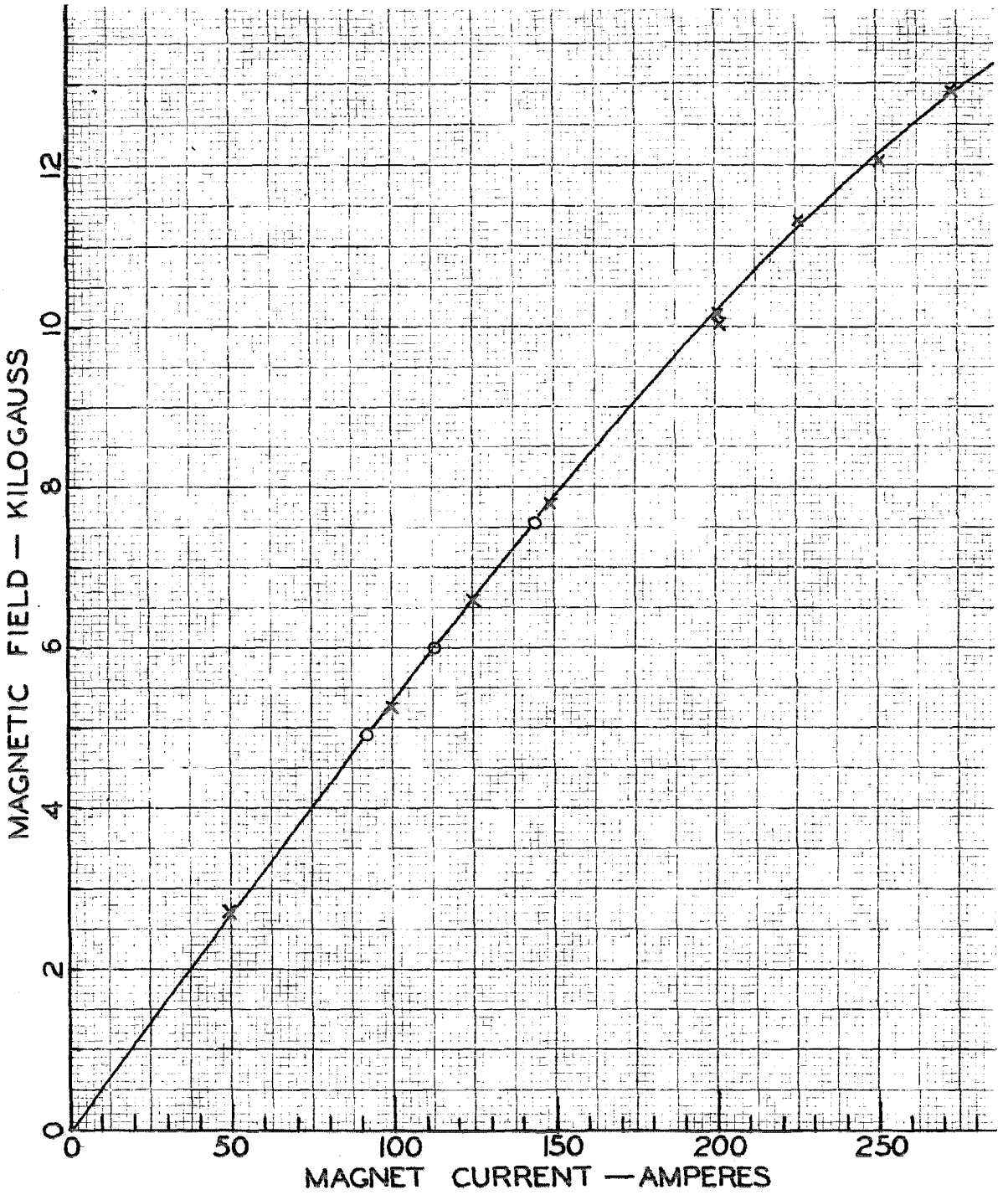

FIGURE 22. MAGNET CALIBRATION
The crosses represent flip-coil data, and the circles represent proton resonance magnetometer data.

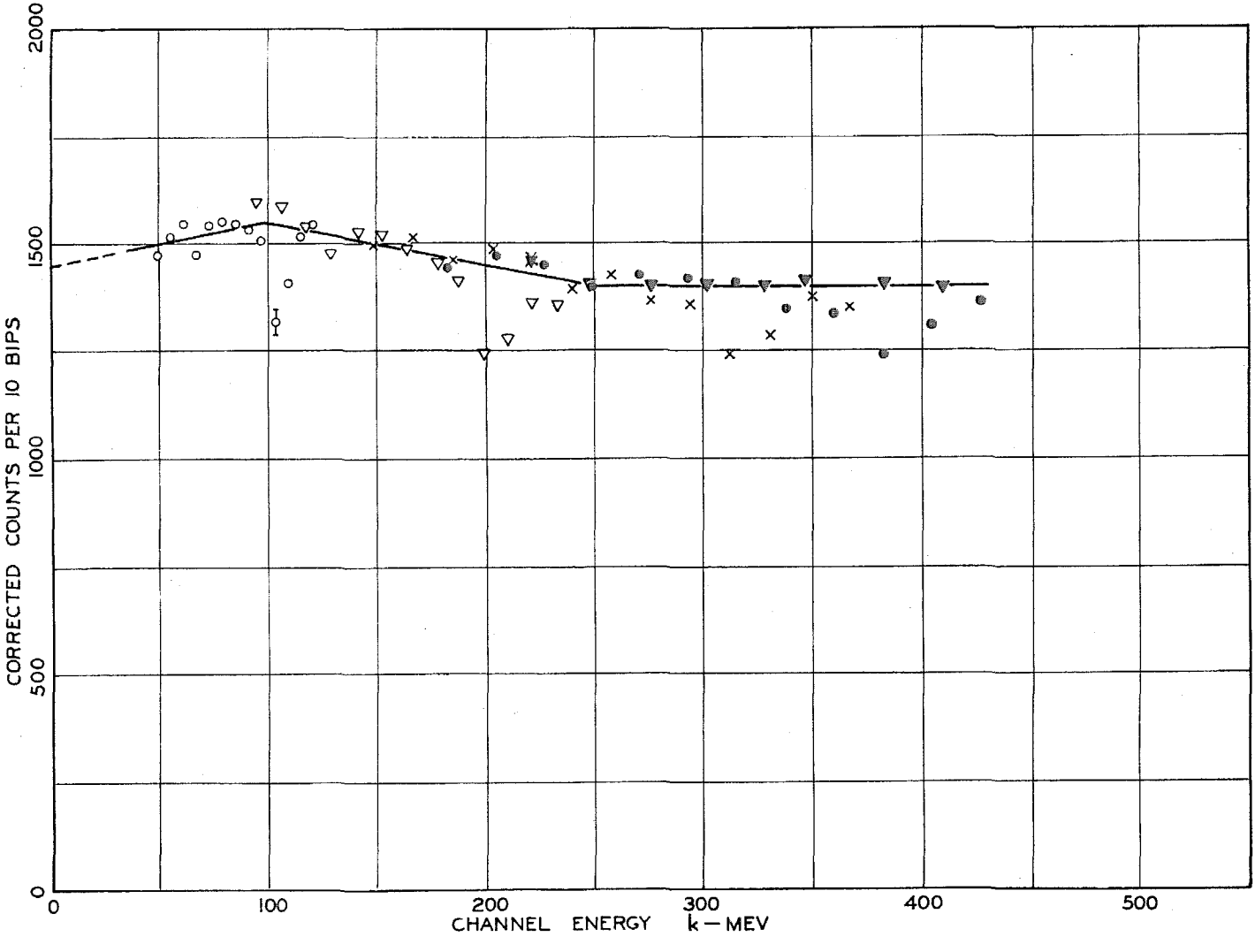

FIGURE 23. DATA FOR BREMSSTRAHLUNG SPECTRUM

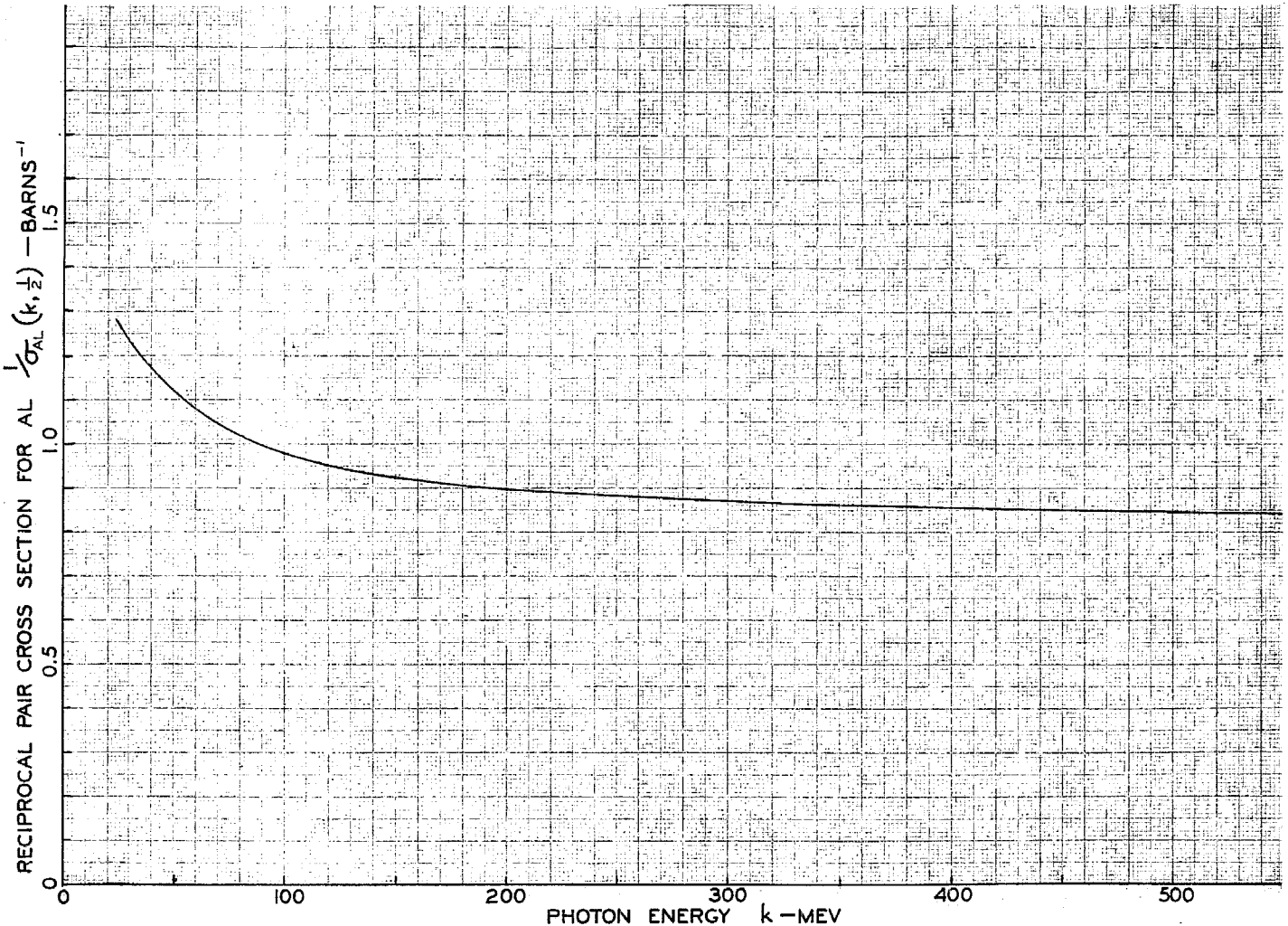

FIGURE 24. RECIPROCAL PAIR CROSS SECTION FOR ALUMINUM
This is for equipartition and includes the correction to the Born approximation and the contribution from the atomic electrons.

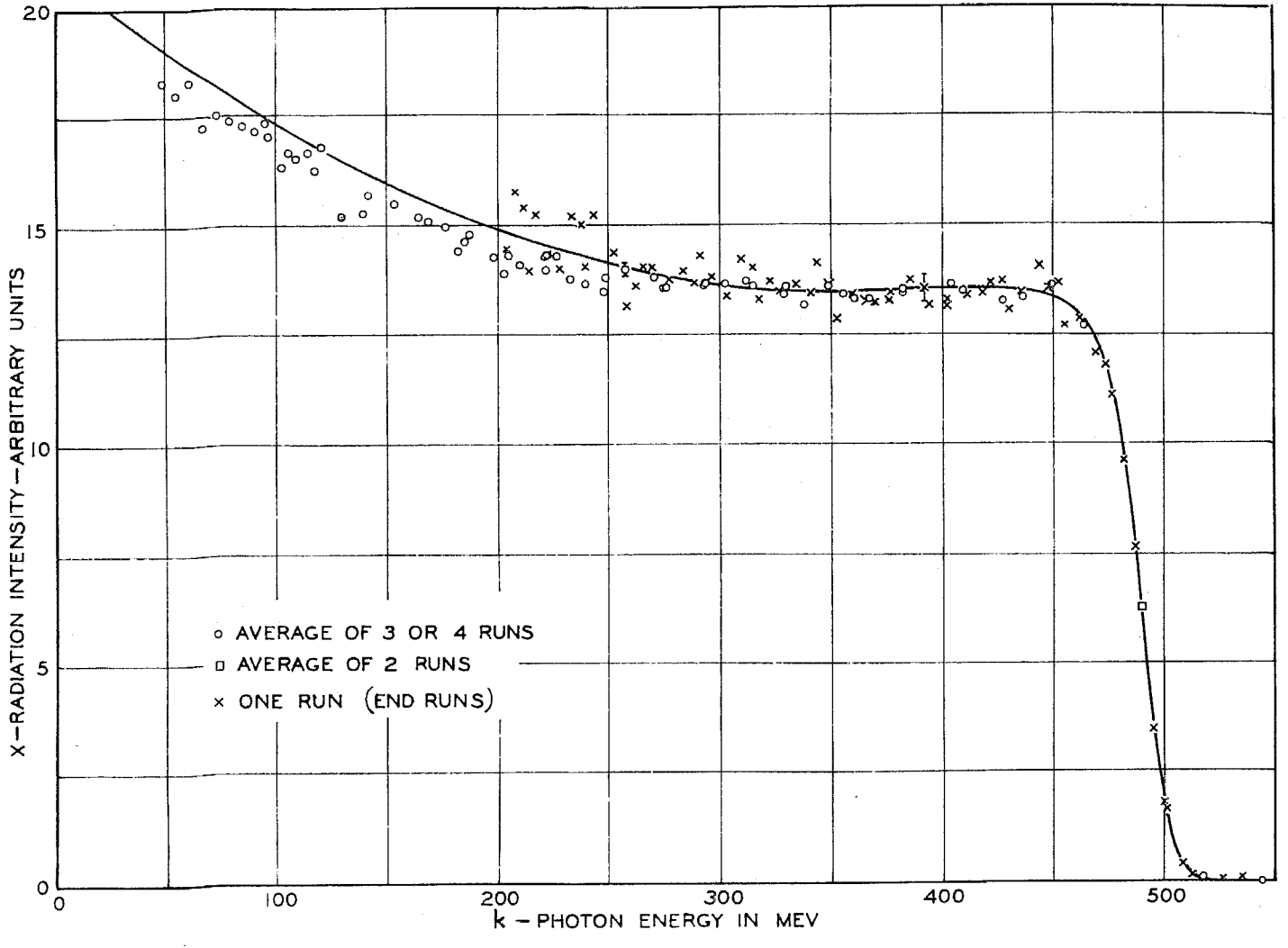

FIGURE 25. ADJUSTED BREMSSTRAHLUNG DATA
The curve is a theoretical prediction.

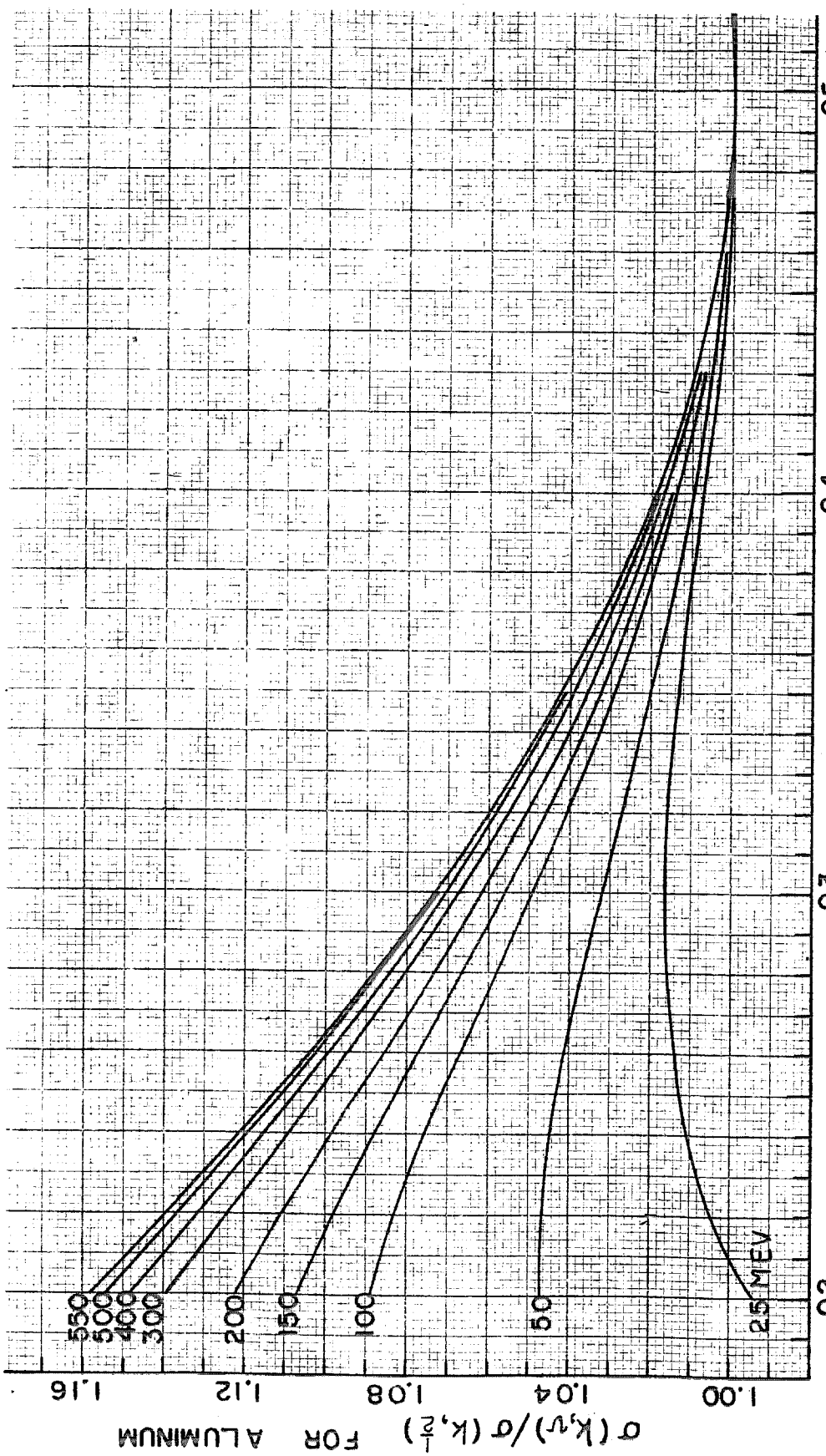

FIGURE 26. VARIATION OF PAIR PRODUCTION WITH PARTITION
These have been divided by the equipartition value. This is for aluminum. The correction to the Born approximation and the contribution from the atomic electrons have been included.

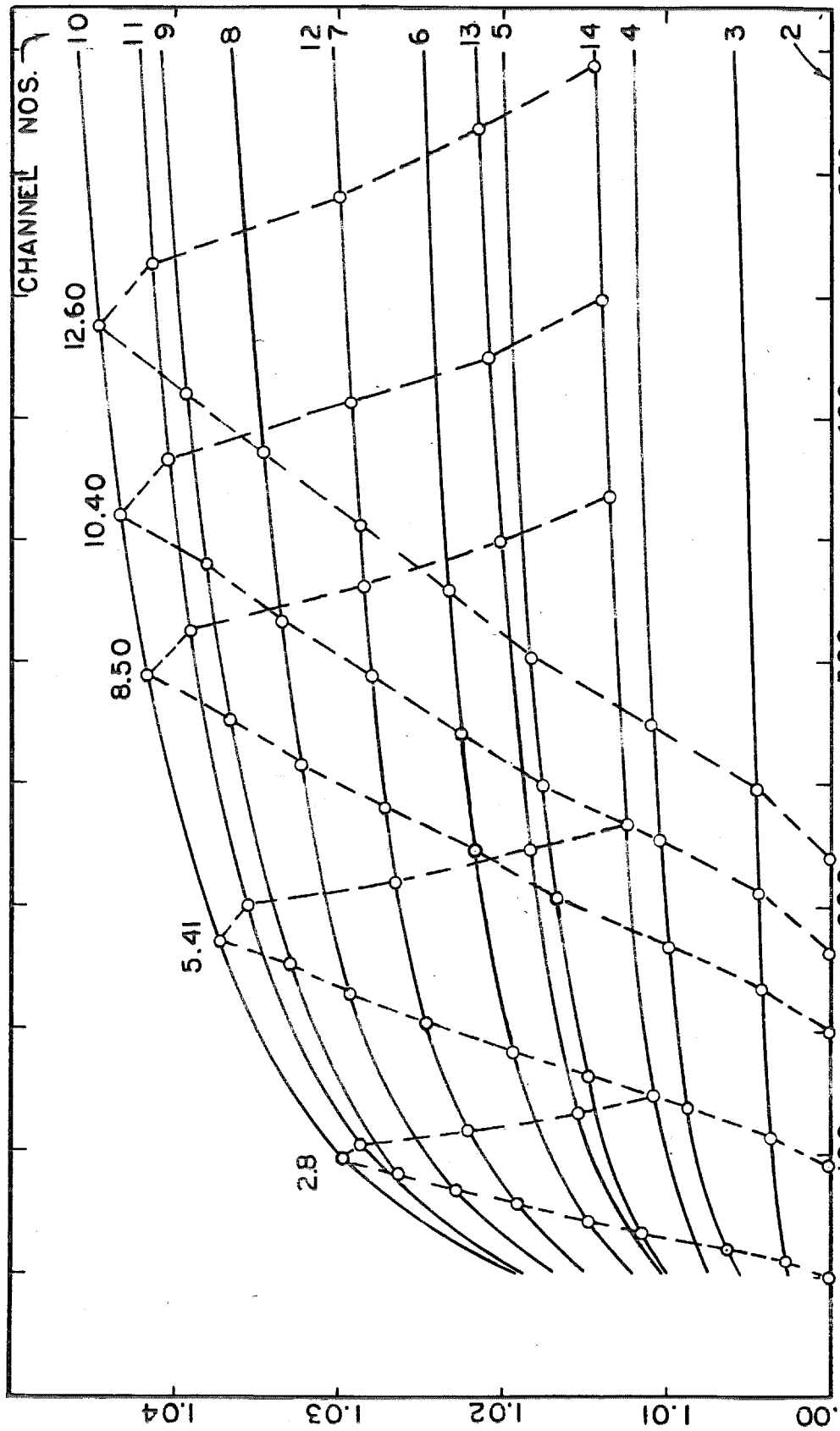

FIGURE 27. CHANNEL PARTITION CORRECTIONS

These are to multiply the equipartition cross sections for aluminum. They are computed for one number 10 phototube being inoperative. The points mark some of the places where data was taken. The dashed lines are intended to connect points belonging to one run. These sets of points are labelled with field values in units of kilogauss.

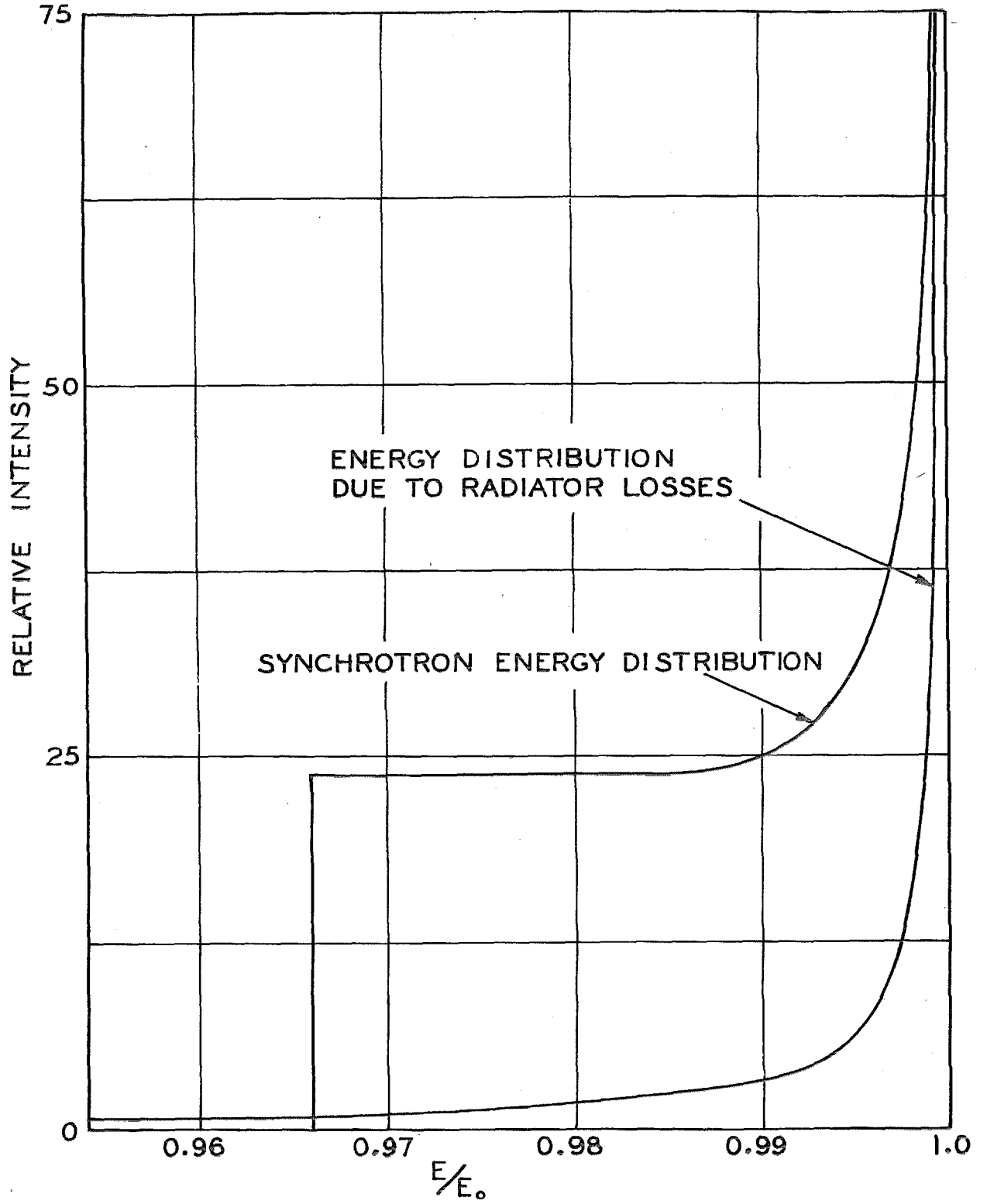

FIGURE 28. ELECTRON ENERGY DISTRIBUTIONS
These curves are each normalized to unit area and are drawn for E_0 = 500 Mev.

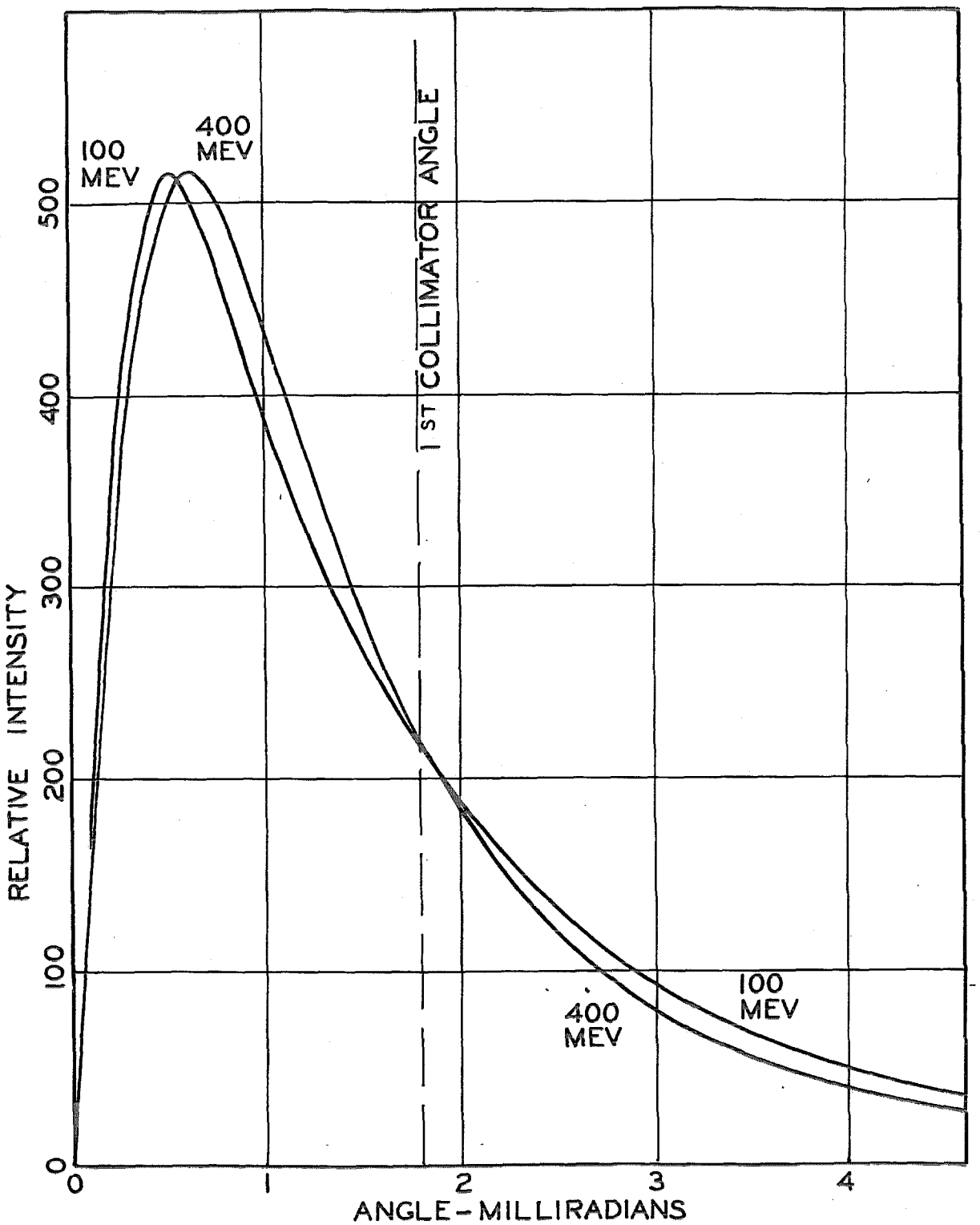

FIGURE 29. BREMSSTRAHLUNG ANGULAR DISTRIBUTIONS
These are for an ideally thin copper radiator and an incident electron energy of E_o = 500 Mev. The curves are each normalized to unit area.

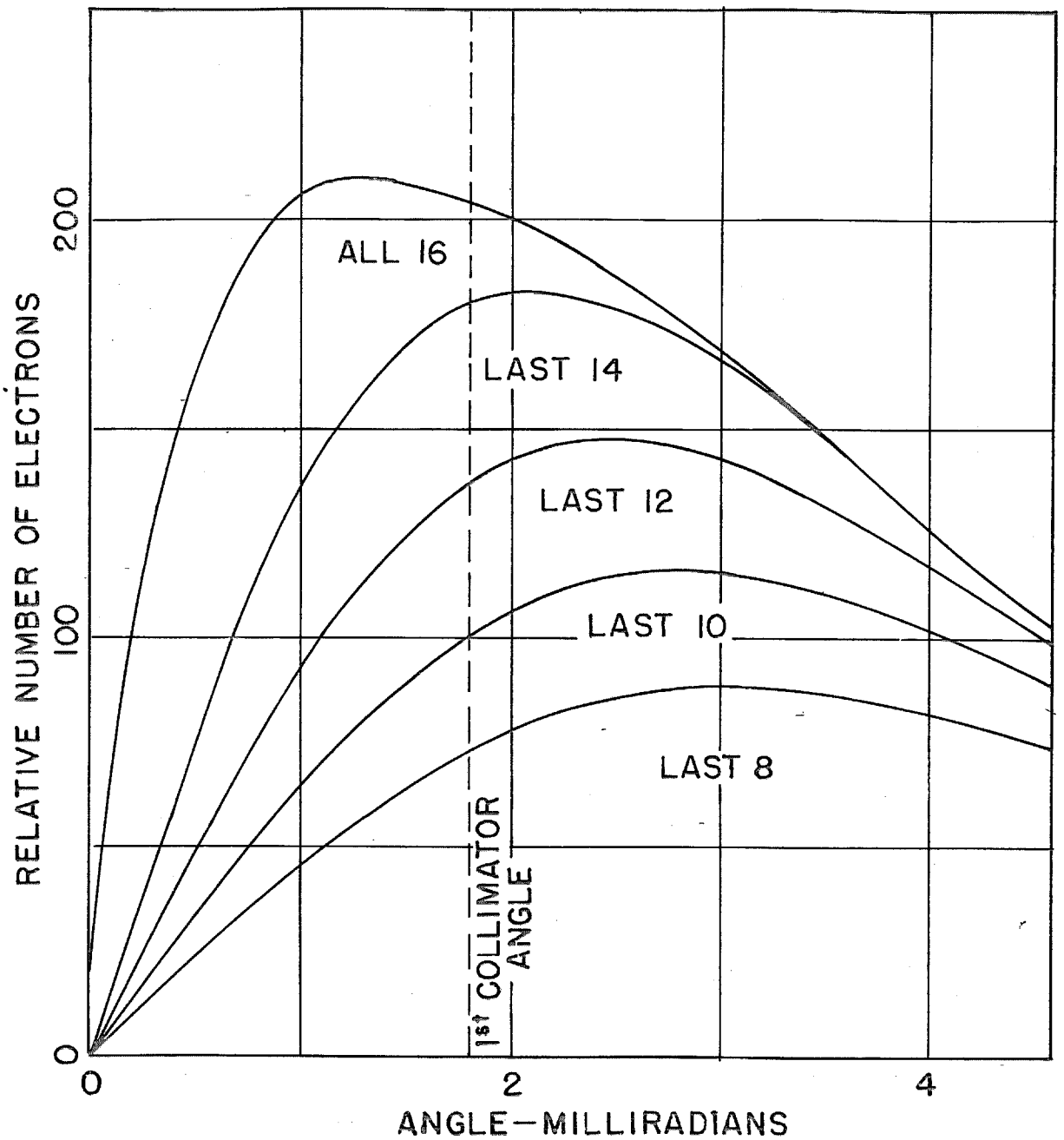

FIGURE 30. MULTIPLE SCATTERING ANGULAR DISTRIBUTIONS
These are for a copper radiator and an incident electron energy of E_0 = 500 Mev. The curve marked "last 14" gives the total number of electrons going in the angular direction θ, in the interval $d\theta$, for electrons moving within the last 14 mils of radiator thickness, and similarly for the other curves. The radiator is 16 mils thick, and the "All 16" curve is normalized to unit area. The others are proportionately normalized; for instance the "last 8" curve has total area 0.5.

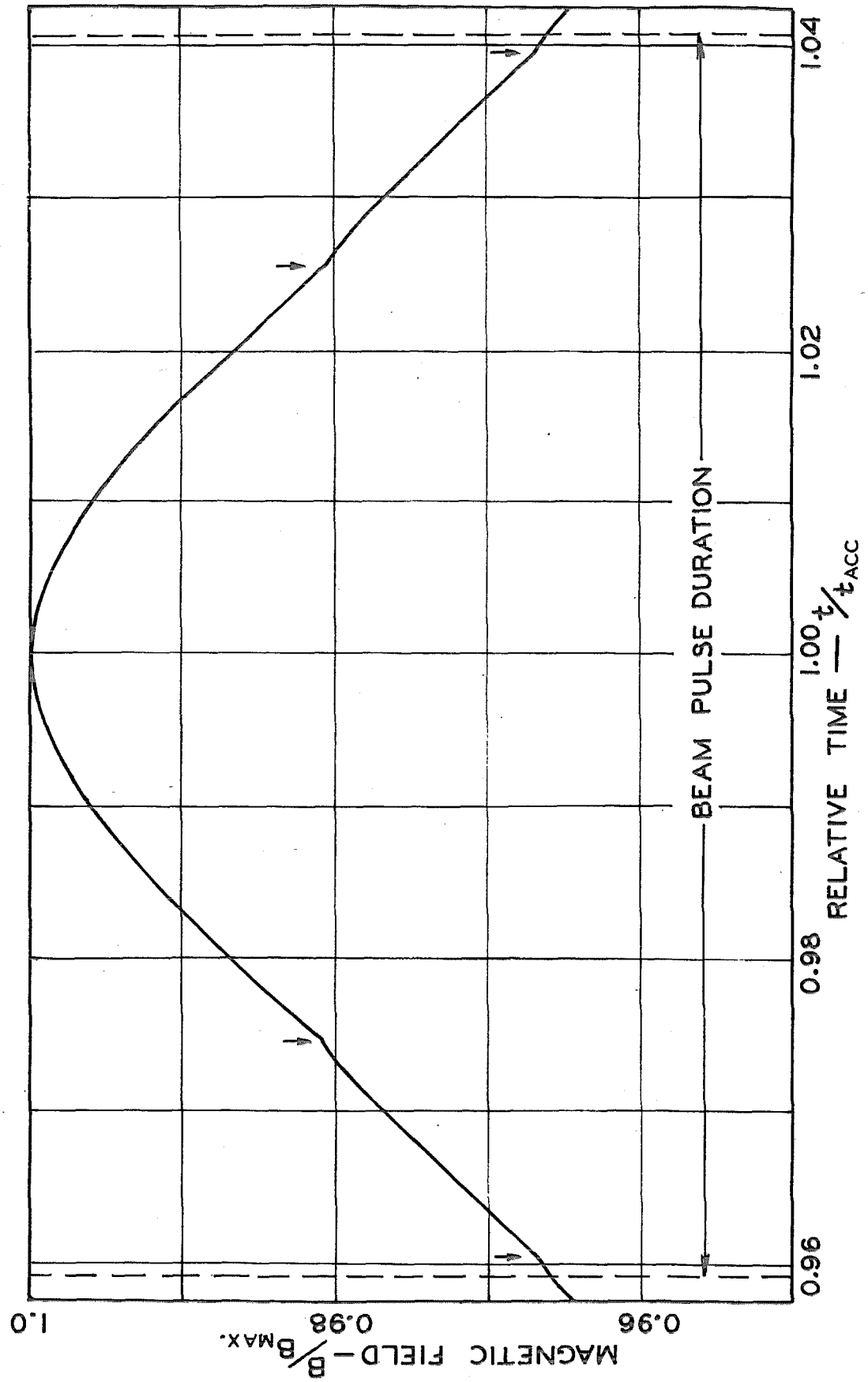

FIGURE 31. TIME VARIATION OF SYNCHROTRON MAGNETIC FIELD
Arrows mark location of ripples.

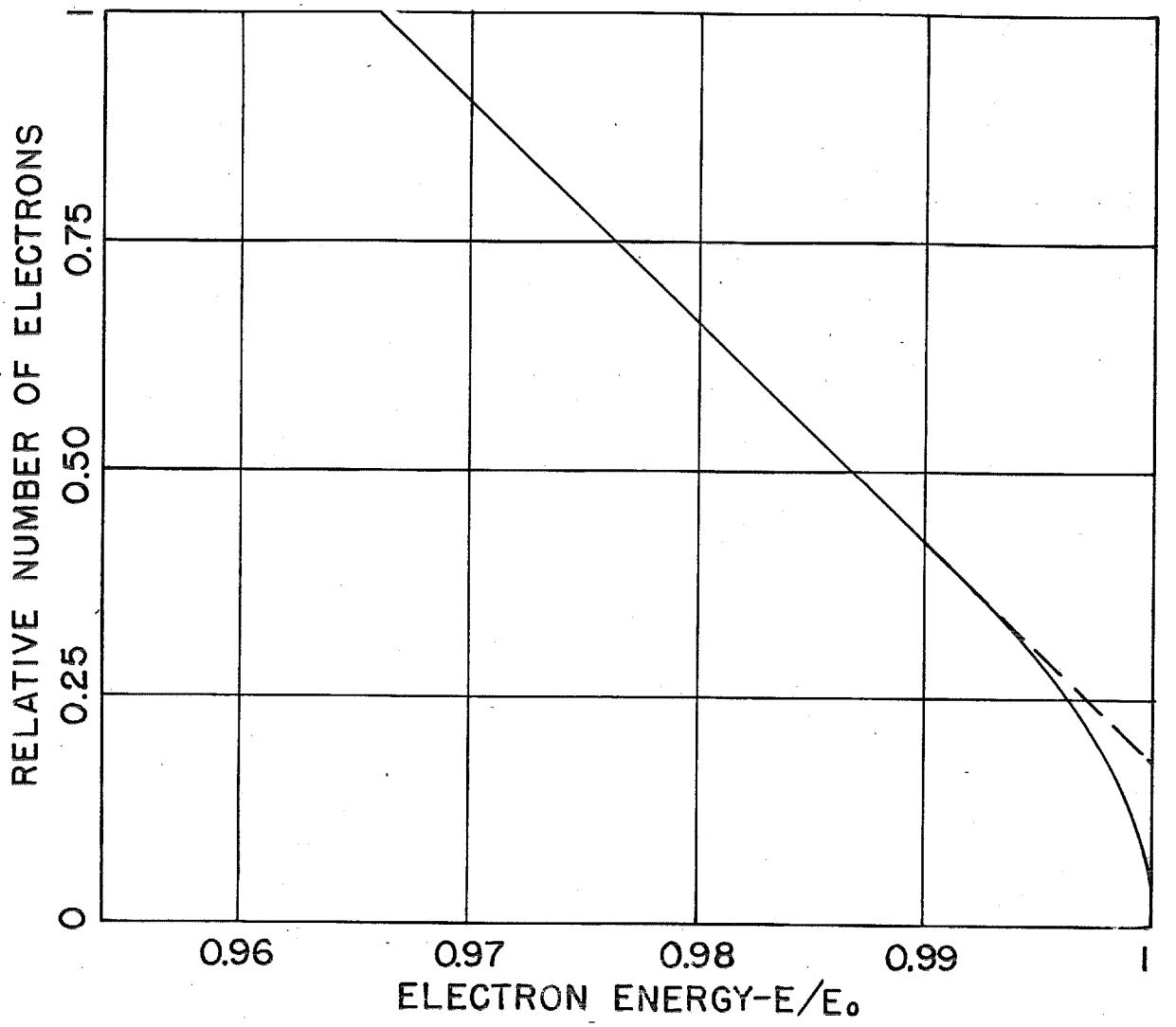

FIGURE 32. INTEGRAL ELECTRON ENERGY DISTRIBUTION

This shows the fraction of the total number of electrons having energy greater than E/E_0, as supplied to the radiator. With the aid of the dashed extension to the "straight" portion, we see that the differential distribution (Fig. 28) is fairly well represented by a rectangle of width 3.4% and integral weight 80%, together with a delta-function of integral weight 20%, located at E_0.

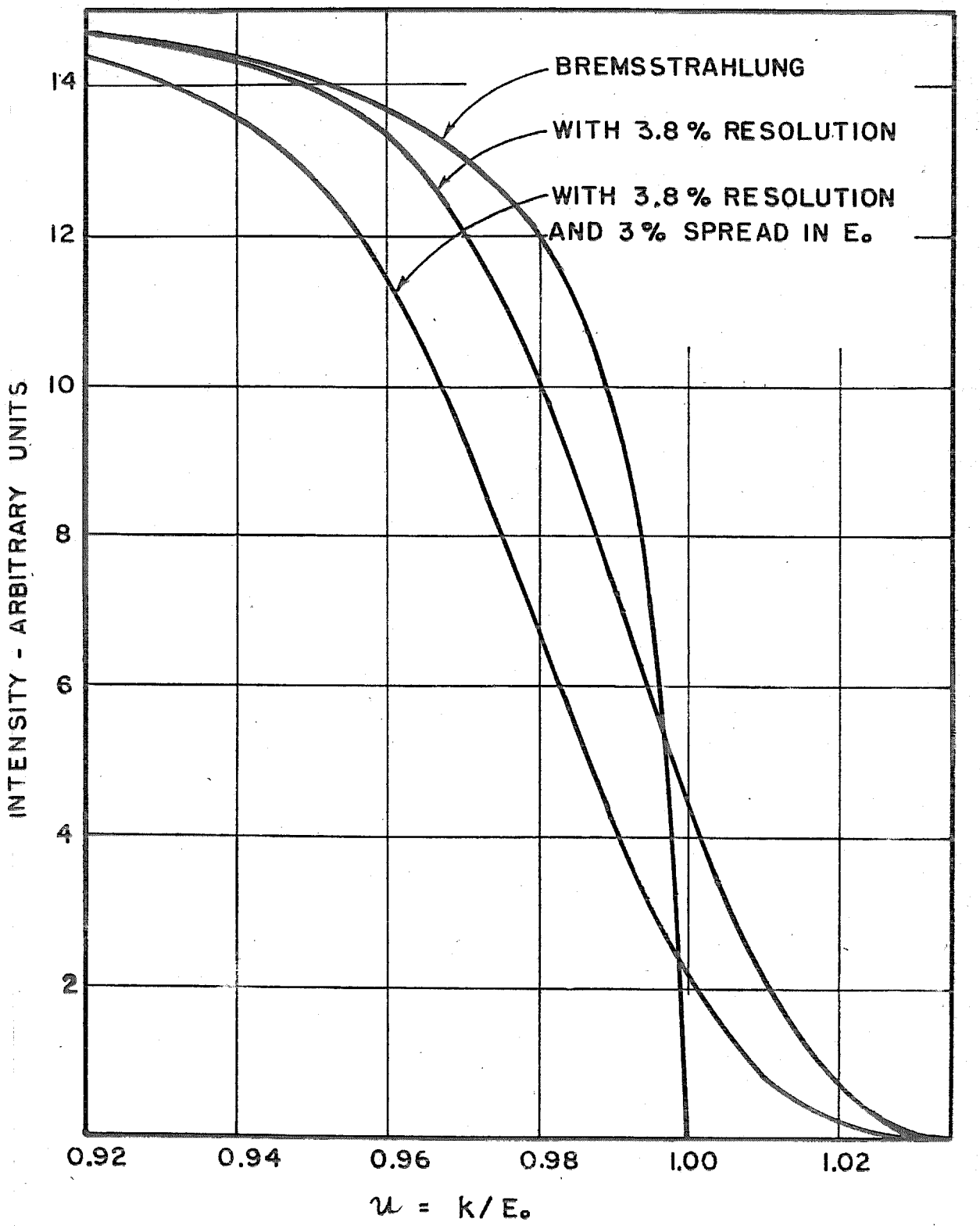

FIGURE 33. CORRECTIONS TO BREMSSTRAHLUNG
This shows the effect of viewing the upper end of the spectrum with finite resolution and a machine energy spread.

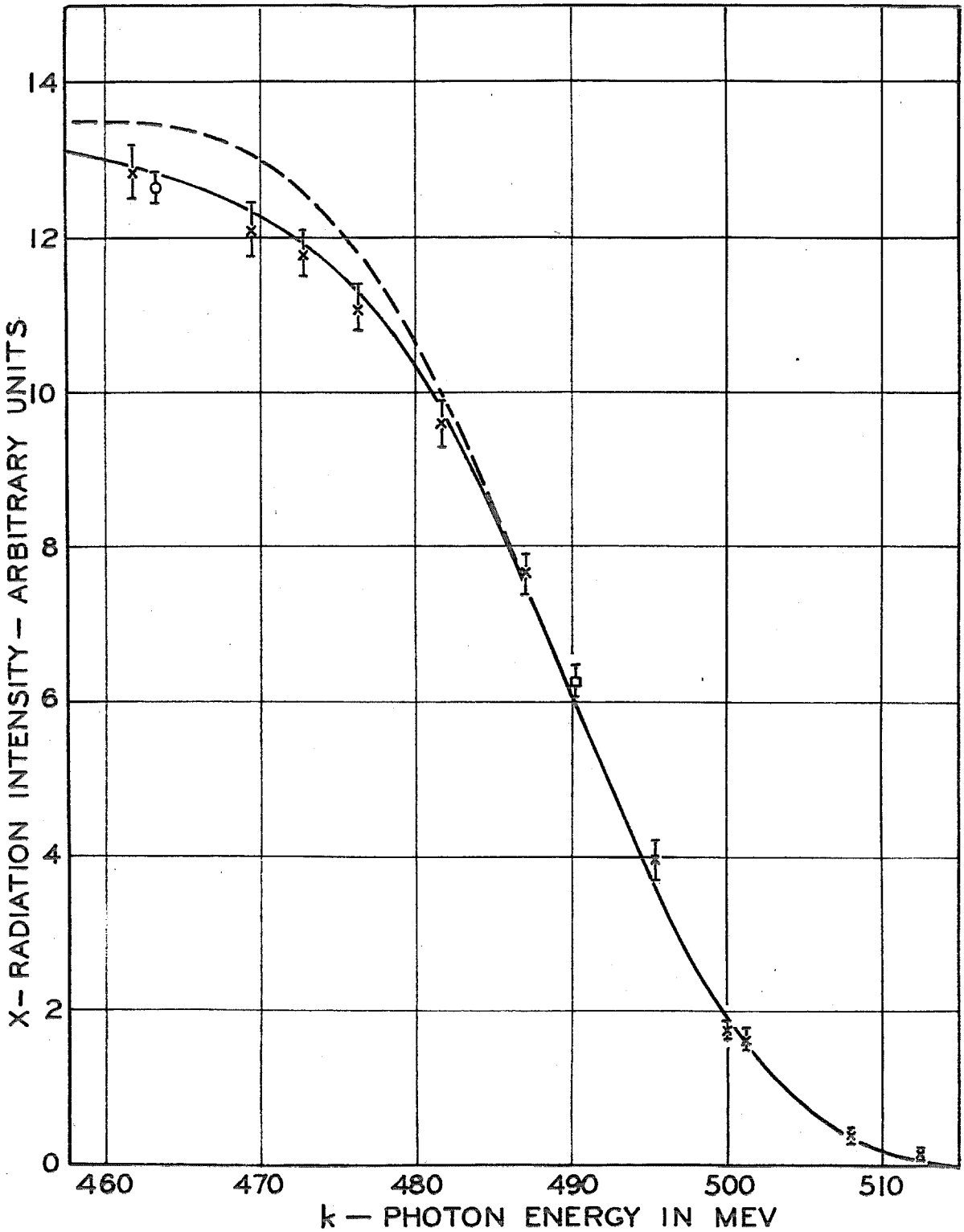

FIGURE 34. SPECTRUM DATA
The curve is theoretical involving the spectrometer resolution and machine energy spread as applied to the bremsstrahlung spectrum. The dashed curve is for a discontinuity in the spectrum at the upper limit.

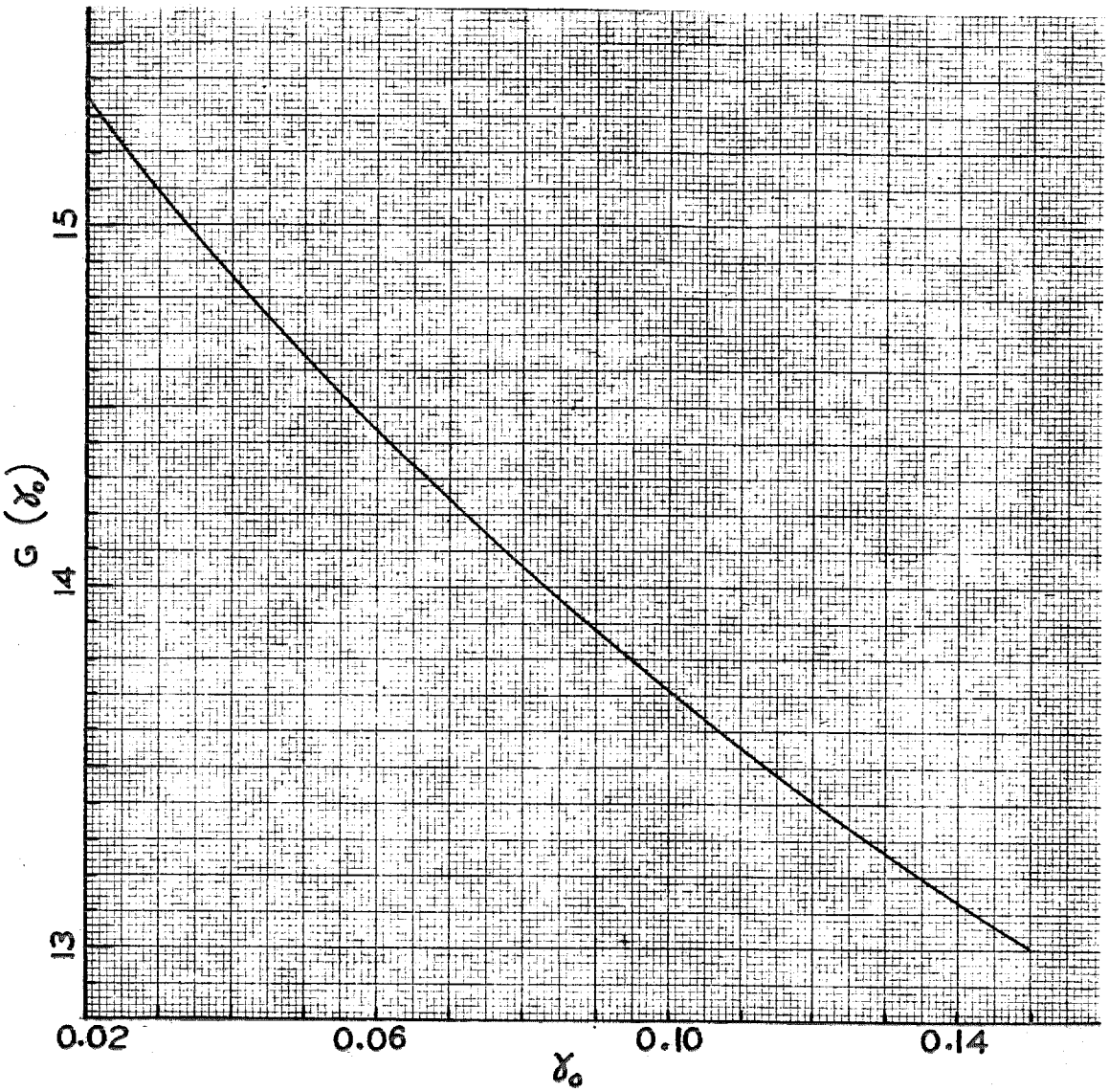

FIGURE 35. SCREENING FUNCTION FOR THE NUCLEAR CONTRIBUTION TO TOTAL PAIR CROSS SECTIONS

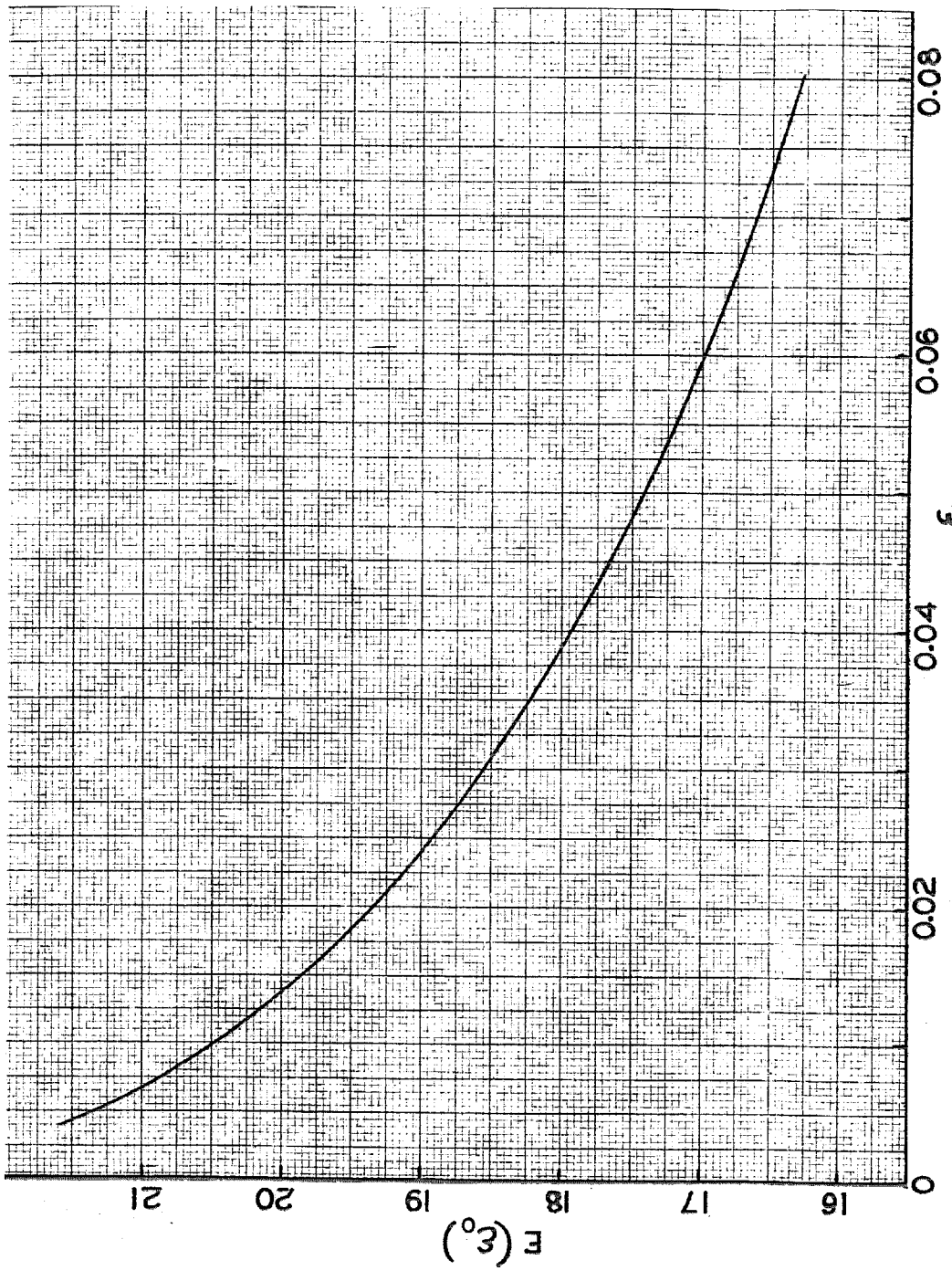

FIGURE 36. SCREENING FUNCTION FOR THE ELECTRONIC CONTRIBUTION TO TOTAL PAIR CROSS SECTIONS

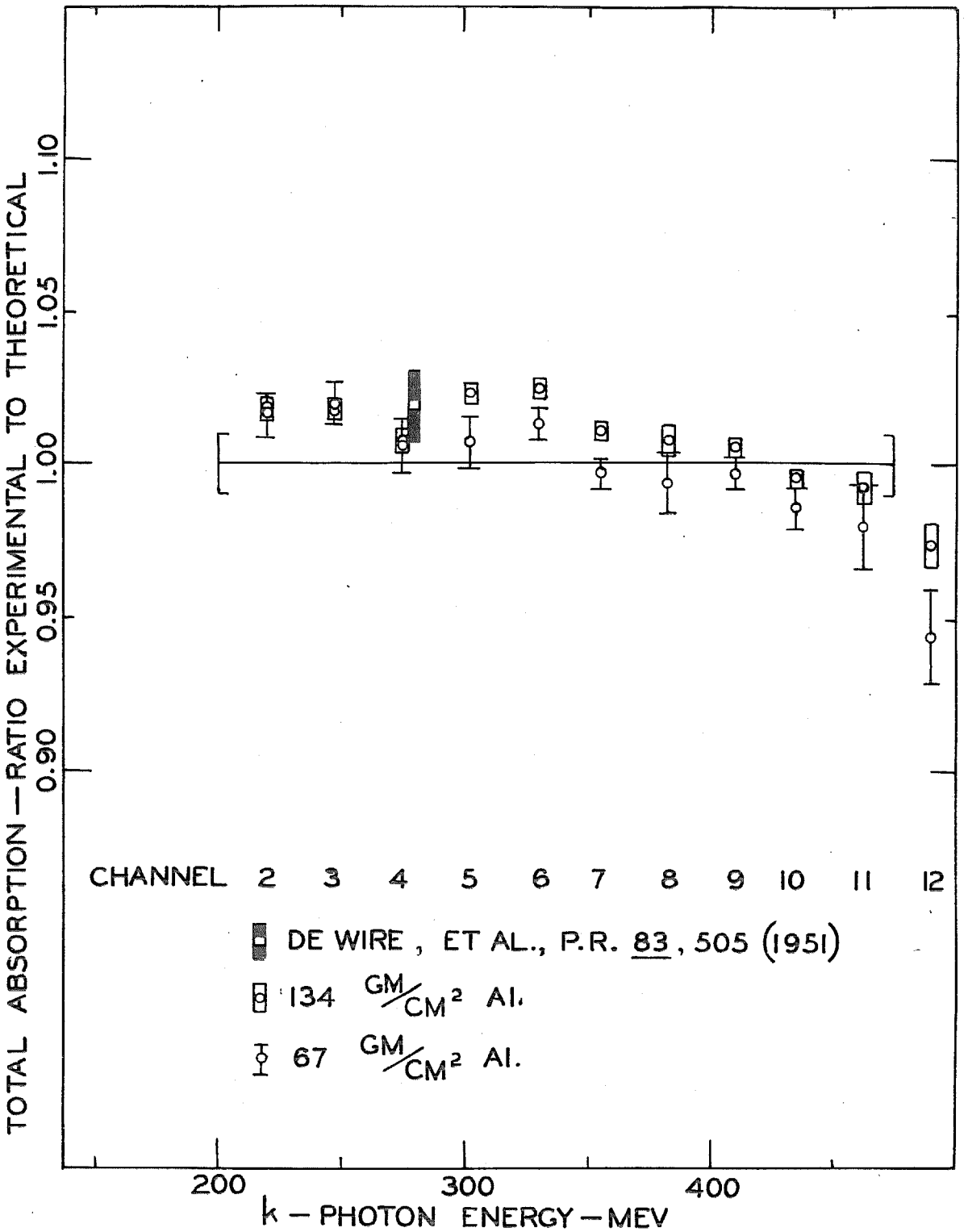

FIGURE 37. TOTAL ABSORPTION IN ALUMINUM
The brackets on the horizontal line show the error to be expected in the screening calculations.

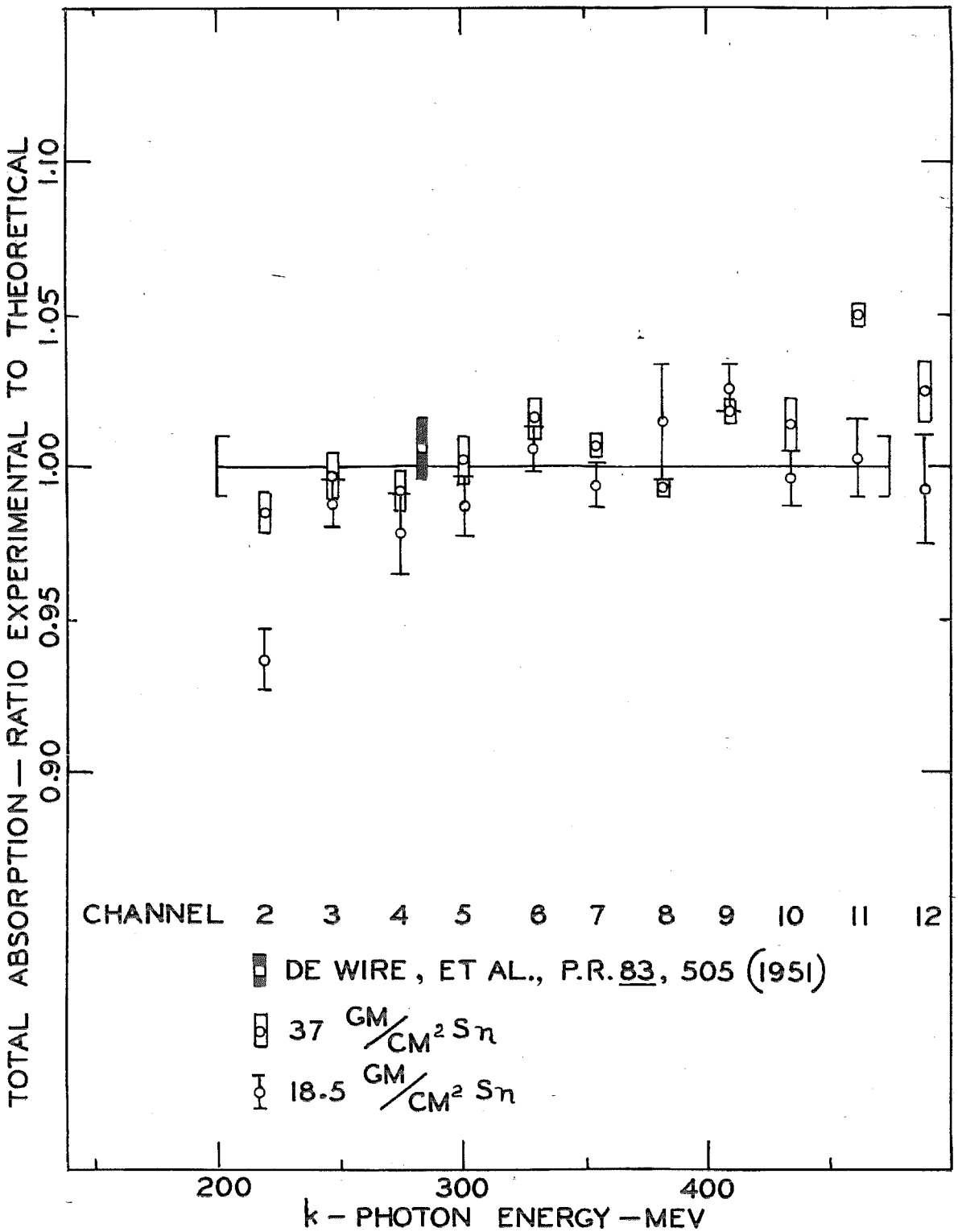

FIGURE 38. TOTAL ABSORPTION IN TIN
The brackets on the horizontal line show the error to be expected in the screening calculations.

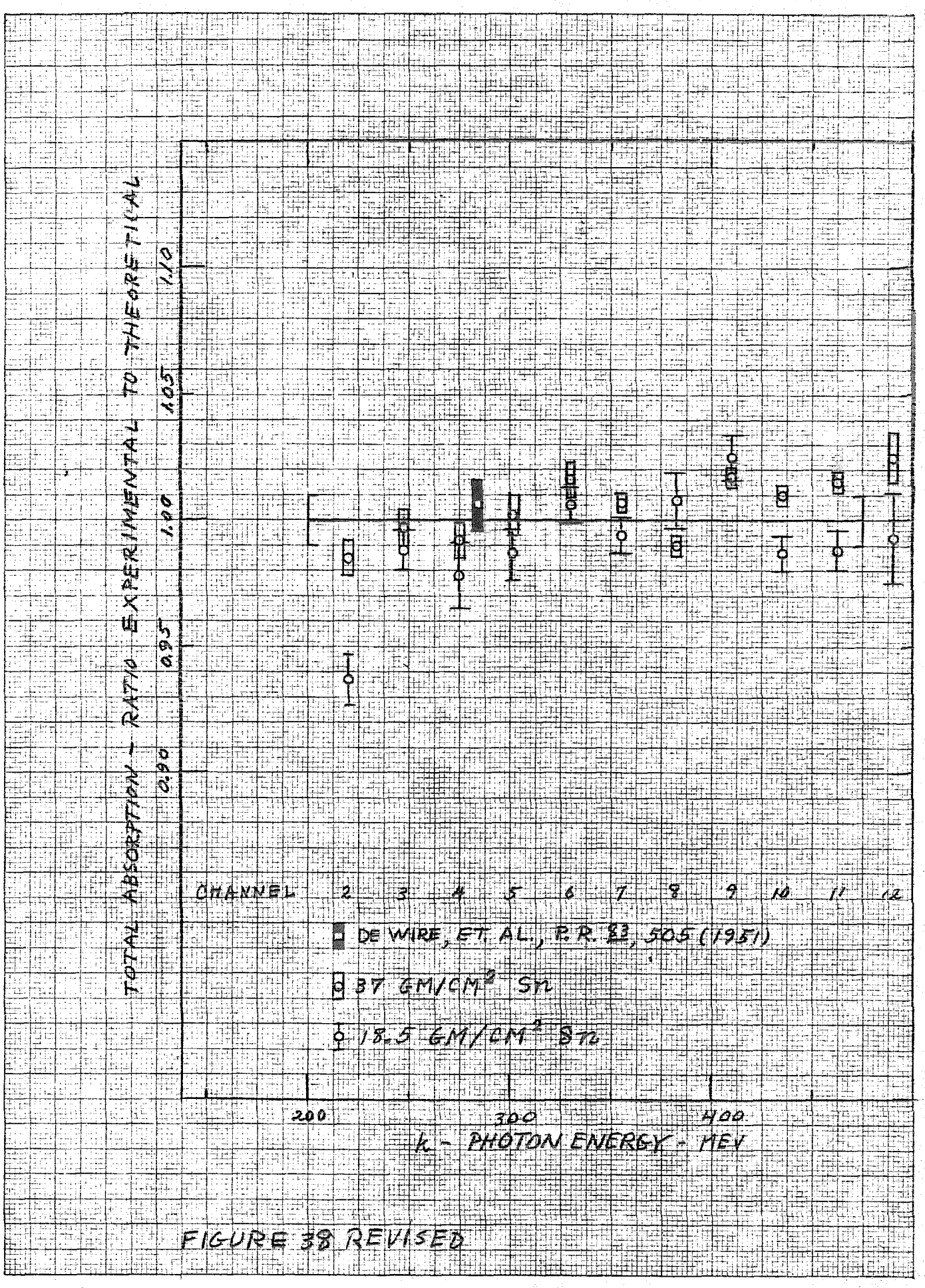

FIGURE 38 REVISED

D.M. Corbett 7/23/54

TABLE 1. SPECTROMETER RESPONSE DATA

Channel (n)	Energy (Mev/kilogauss)	$(\Delta k/k)_n^{-1}$	m_n	$\left[(\Delta k/k)_n^2 m_n\right]^{-1}$	m_n'	$\left[(\Delta k/k)_n^2 m_n'\right]^{-1}$
2	17.53	11.5	1	132.25	1	132.25
3	19.66	12.9	2	83.20	2	83.20
4	21.80	14.3	3	68.16	3	68.16
5	23.93	15.7	4	61.62	4	61.62
6	26.06	17.1	5	54.48	5	58.48
7	28.20	18.5	6	57.04	6	57.04
8	30.33	19.9	7	56.57	7	56.57
9	32.47	21.3	8	56.71	8	56.71
10	34.60	22.7	9	57.25	9	57.25
11	36.73	24.1	10	58.08	9	64.53
12	38.87	25.5	9	72.25	8	81.28
13	41.00	26.9	8	90.45	7	103.37
14	43.14	28.3	7	119.32	6	133.48
15	45.27	29.7	6	147.02	5	176.42
16	47.40	31.1	5	193.44	4	241.80
17	49.54	32.5	4	264.06	3	352.08
18	51.67	33.9	3	383.07	2	574.6
19	53.81	35.3	2	623.0	1	1246.1
20	55.94	36.7	1	1346.9	—	———

TABLE 2. CHANNEL PAIR PARTITIONS

Channel	Weight One	Weight Two				
2	0.5000					
3		0.4457				
4	0.5000	0.4021				
5		0.4544	0.3622			
6	0.5000	0.4181	0.3363			
7		0.4622	0.3865	0.3108		
8	0.5000	0.4296	0.3593	0.2889		
9		0.4671	0.4041	0.3357	0.2700	
10	0.5000	0.4385	0.3767	0.3150	0.2533	
11		0.4710	0.4129	0.3548	0.2967	0.2386
12	0.5000	0.4451	0.3902	0.3353	0.2804	
13		0.4740	0.4218	0.3699	0.3178	
14	0.5000	0.4505	0.4011	0.3516		
15		0.4764	0.4293	0.3821		
16	0.5000	0.4550	0.4100			
17		0.4785	0.4354			
18	0.5000	0.4587				
19		0.4802				
20	0.5000					

TABLE 3. TOTAL ABSORPTION CROSS SECTIONS

(Quoted probable errors do not include errors in the screening calculations.)

Element	Energy (Mev)	Thickness (g/cm^2)	Cross Section (Barns) Exp.	Exp/Theory	Thickness (g/cm^2)	Cross Section (Barns) Exp.	Exp/Theory	Average
Carbon	383	51	0.323	1.002 ± 0.011	128	0.322	1.000 ± 0.005	0.322 ±0.5%
	409	51	0.320	0.989 ± 0.011	128	0.322	0.997 ± 0.005	0.322 ±0.5%
	436	51	0.328	1.011 ± 0.022	128	0.325	1.002 ± 0.008	0.325 ±0.8%
Aluminum	383	67	1.290	0.994 ± 0.010	134	1.308	1.008 ± 0.006	1.304 ±0.6%
	409	67	1.304	0.997 ± 0.005	134	1.316	1.006 ± 0.004	1.313 ±0.4%
	436	67	1.302	0.986 ± 0.007	134	1.316	0.996 ± 0.004	1.314 ±0.4%
Copper	383	20	5.75	1.006 ± 0.009	42	5.79	1.013 ± 0.006	5.78 ±0.6%
	409	20	5.73	0.998 ± 0.009	42	5.80	1.009 ± 0.006	5.78 ±0.6%
	436	20	5.88	1.020 ± 0.009	42	5.83	1.011 ± 0.006	5.84 ±0.6%
Tin	383	18.5	15.84	1.015 ± 0.010	37	15.50	0.993 ± 0.004	15.53 ±0.4%
	409	18.5	16.07	1.026 ± 0.008	37	15.95	1.018 ± 0.005	15.97 ±0.5%
	436	18.5	15.67	0.996 ± 0.009	37	15.96	1.014 ± 0.009	15.82 ±0.8%
Lead	376	15	36.8	0.981 ± 0.009	29	36.9	0.984 ± 0.006	36.9 ±0.6%
	402	15	37.5	0.991 ± 0.014	29	37.0	0.978 ± 0.006	37.1 ±0.6%
	429	15	37.1	0.976 ± 0.010	29	37.2	0.979 ± 0.006	37.2 ±0.6%

CALIFORNIA INSTITUTE OF TECHNOLOGY
Synchrotron Laboratory
July 30, 1954

The following table, while not a part of Duane H. Cooper's thesis "Pair Spectrometer Measurements in 500 Mev Bremsstrahlung", may be interpreted as a revision of his Table 3.

TOTAL ABSORPTION CROSS SECTIONS

(Quoted probable errors do not include errors in the screening calculations)

Element	Energy (Mev)	Thickness (g/cm^2)	Cross Section (Barnes) Exp.	Exp/Theory	Thickness (g/cm^2)	Cross Section (Barnes) Exp.	Exp/Theory	Average
Carbon	383	51	0.323	1.002 ± 0.011	128	0.316	0.981 ± 0.005	0.318 ± 0.5%
	409	51	0.320	0.989 ± 0.011	128	0.322	0.997 ± 0.005	0.322 ± 0.5%
	436	51	0.328	1.011 ± 0.022	128	0.325	1.002 ± 0.008	0.325 ± 0.8%
	463	51	0.331	1.015 ± 0.016	128	0.329	1.008 ± 0.005	0.329 ± 0.5%
Aluminum	383	67	1.290	0.994 ± 0.010	134	1.308	1.008 ± 0.006	1.304 ± 0.6%
	409	67	1.304	0.997 ± 0.005	134	1.316	1.006 ± 0.004	1.313 ± 0.4%
	436	67	1.302	0.986 ± 0.007	134	1.316	0.996 ± 0.004	1.314 ± 0.4%
	463	67	1.306	0.980 ± 0.014	134	1.324	0.993 ± 0.005	1.322 ± 0.5%
Copper	383	20	5.76	1.007 ± 0.009	42	5.79	1.013 ± 0.006	5.78 ± 0.6%
	409	20	5.73	0.999 ± 0.009	42	5.80	1.009 ± 0.006	5.78 ± 0.6%
	436	20	5.88	1.019 ± 0.009	42	5.83	1.011 ± 0.006	5.84 ± 0.6%
	463	20	6.00	1.035 ± 0.014	42	5.94	1.025 ± 0.006	5.95 ± 0.6%
Tin	383	18.5	15.74	1.008 ± 0.019	37	15.46	0.990 ± 0.004	15.48 ± 0.4%
	409	18.5	16.06	1.025 ± 0.009	37	15.94	1.017 ± 0.004	15.96 ± 0.4%
	436	18.5	15.53	0.987 ± 0.007	37	15.90	1.010 ± 0.004	15.85 ± 0.4%
	463	18.5	15.61	0.988 ± 0.008	37	16.03	1.015 ± 0.004	15.98 ± 0.4%
Lead	376	15	36.8	0.980 ± 0.009	29	36.9	0.982 ± 0.006	36.9 ± 0.6%
	402	15	37.5	0.991 ± 0.014	29	37.0	0.978 ± 0.006	37.1 ± 0.6%
	429	15	37.1	0.976 ± 0.010	29	37.2	0.979 ± 0.006	37.2 ± 0.6%
	455	15	35.4	0.929 ± 0.026	29	36.7	0.962 ± 0.007	36.7 ± 0.7%

TABLE 4. RELATIVE PAIR PRODUCTION

Equipartition Pair Cross Sections from Assumed Theoretical Values for Aluminum
(Barns per atom. Average yields quoted relative to Al. Quoted probable errors do not include errors in the screening calculations.)

Channel	Energy (Mev)	Al 29.3mg/cm^2 yield 1.000	Cu 18.2mg/cm^2 yield 1.15 Exp.	Cu 18.2mg/cm^2 yield 1.15 Exp/Theory	Pb 33.2mg/cm^2 yield 4.28 Exp.	Pb 33.2mg/cm^2 yield 4.28 Exp/Theory
2	221	1.121	4.89	0.973 ± 0.023	31.6	0.962 ± 0.023
3	248	1.132	5.06	0.998 ± 0.025	32.2	0.974 ± 0.018
4	275	1.142	5.03	0.986 ± 0.021	32.7	0.983 ± 0.019
5	302	1.149	5.07	0.990 ± 0.020	32.4	0.969 ± 0.025
6	329	1.156	5.06	0.983 ± 0.018	33.0	0.984 ± 0.018
7	356	1.161	5.12	0.992 ± 0.019	32.8	0.977 ± 0.028
8	383	1.165	5.09	0.983 ± 0.018	33.9	1.010 ± 0.032
9	409	1.169	5.33	1.025 ± 0.018	34.2	1.015 ± 0.029
10	436	1.172	5.29	1.016 ± 0.018	35.0	1.035 ± 0.023

Comparison Among Copper Yields (Ratio to measured thickness)

		10.1mg/cm^2	18.2mg/cm^2	40.1mg/cm^2	104.5mg/cm^2
8	383	1.040 ± 0.018	1.000	1.016 ± 0.018	0.998 ± 0.019
9	409	1.006 ± 0.018	1.000	0.992 ± 0.018	0.951 ± 0.018
10	436	1.005 ± 0.018	1.000	0.990 ± 0.018	0.974 ± 0.018

Comparison Among Aluminum Yields (Ratio to measured thickness)

		29.3mg/cm^2	6.14mg/cm^2
5,6	315	1.000	1.042 ± 0.015
8	383	1.000	1.039 ± 0.021
9	409	1.000	1.052 ± 0.017
10	436	1.000	1.018 ± 0.017